INTERNATIONAL JOURNAL OF
ENGINEERING
SCIENCES AND MANAGEMENT

A Bi-annual Research Journal of

DRONACHARYA
GROUP OF INSTITUTIONS
GREATER NOIDA, U.P., INDIA

INTERNATIONAL JOURNAL OF ENGINEERING SCIENCES AND MANAGEMENT

INTERNATIONAL JOURNAL OF
ENGINEERING, SCIENCES AND MANAGEMENT

Editorial Information:
For details please write to the Executive Editor, International Journal of Engineering, Sciences and Management, Dronacharya Group of Institutions, # 27, Knowledge Park-III, Greater Noida – 201308 (U.P.), India.

Telephones:
Landline: +91-120-2323854, 2323855, 2323856, 2323857
Mobile: +91-8826006878

Telefax:
+91-120-2323853

E-mail:
advisor.r&d@gnindia.dronacharya.info
director@gnindia.dronacharya.info
info@dronacharya.info

Website:
www.dronacharya.info
www.ijesm.in

The Institute does not take any responsibility about the authenticity and originality of the material contained in this journal and the views of the authors although all submitted manuscripts are reviewed by experts.

ADVISORY BOARD
MEMBERS

FROM THE DESK OF
EXECUTIVE EDITOR...

Dear Readers,

The qualitative and timely publication of Vol. V / Issue I (Jan-Jun 2015) of our esteemed International Journal of Engineering, Sciences and Management (ISSN: 2231-3273) has brought great joy and happiness to the entire fraternity of the journal and honorable members of the Editorial and Advisory Board. The board members rich experience and varied expertize is providing immense succour in propelling the journal to attain an envious position in areas of research and development and accentuate its visibility. The distinctive feature is indexing of the journal by Jour Informatics, Index Copernicus, Google Scholar and DOAJ. It is a matter of great pride and honor that the journal has been viewed by researchers from 103 countries across the globe. The aim of journal is to percolate knowledge in various research fields and elevate high end research. The objective is being pursued vigorously by providing the necessary eco-system for research and development.

Large number of research papers were received from all over the globe for publication and we thank each one of the authors personally for soliciting the journal. We also extend our heartfelt thanks to the reviewers and members of the editorial board who so carefully perused the papers and carried out justified evaluation. Based on their evaluation, we could accept thirteen research papers for this issue across the disciplines. We are certain that these papers will provide qualitative information and thoughtful ideas to our accomplished readers. We thank all the readers profusely who conveyed their appreciation on the quality and content of the journal and expressed their best wishes for future issues. We convey our deep gratitude to the Editorial Board, Advisory Board and all office bearers who have made possible the publication of this journal in the planned time frame.

We invite all the authors and their professional colleagues to submit their research papers for consideration for publication in our forthcoming issue i.e. Vol. V | Issue II | Jul-Dec 2015 as per the "Scope and Guidelines to Authors" given at the end of this issue. Any comments and observations for the improvement of the journal are most welcome.

We wish all readers meaningful and quality time while going through the journal.

Wg Cdr (Prof) TPN Singh
Executive Editor
International journal of Engineering, Sciences and Management (IJESM)
A bi-annual Research journal of Dronacharya Group of Institutions,
Greater Noida, UP, India.

Jan 2015

CONTENTS

SPEED, POWER AND AREA PERFORMANCE OF ALU IMPLEMENTATIONS IN THE NANOSCALE DOMAIN

Megha Cheboli

Former Graduate Student
Department of Electrical & Computer Engineering
University of Texas at San Antonio,
San Antonio, TX 78249, USA

Pradeep Nair*

Computer Engineering Program
California State University, Fullerton CA 92831, USA
Phone: +1-657-278-3375
E-mail: pnair@fullerton.edu
*Corresponding author

Eugene John

Department of Electrical & Computer Engineering
University of Texas at San Antonio,
San Antonio, TX 78249, USA

ABSTRACT

The Arithmetic and Logic Unit (ALU) is one of the most important components in a computer. All computations are performed in the ALU, which makes it a very busy as well as a power-hungry component of the processor. In this work, nine different 32-bit nanoscale ALU topologies were designed and realized, and their performance was investigated from a speed, power and area standpoint at the 65 nm CMOS technology node. The ALU topology using a carry-lookahead adder unit and a multiplier unit based on carry-save addition with last-stage ripple carry addition was found to occupy the least area. This topology was also found to consume the least amount of power. ALU topologies employing the Kogge-Stone adder occupied the highest area. The ALU topology using the Kogge-Stone adder unit and the traditional array multiplier unit based on ripple carry addition had the highest power consumption. The ALU topology with a Kogge-Stone adder unit and multiplier unit based on carry-save addition with last-stage carry-lookahead addition was the fastest. ALU topologies that employed the traditional array multiplier unit were the slowest.

Keywords - Arithmetic logic unit, speed, power, area, CMOS, adders, multipliers

1. INTRODUCTION

The quest for achieving higher speed performance and smaller form factors through transistor scaling has continued consistently in the semiconductor industry in accordance with the famous *Moore's law*[1, 2]. As more and more transistors are packed on to a given area of an integrated circuit (IC) chip such as a microprocessor, parameters such as IC heat density, power dissipation and battery life remain as major concerns and new circuit-level and system-level low-power techniques continue to be explored in order to address them[3,4,5]. The Arithmetic and Logic Unit (ALU) forms one of the most important components in a computer and is the part of the processor responsible for performing arithmetic and logical operations[6]. The arithmetic unit of a computer was described as early as 1945 by John von Neumann[7, 8, 9], which was soon followed by a description of the logical organization of the arithmetic unit by Burks et al.[10]. During the time that a processor is active, the ALU is kept busy most of the time due to the fact that all computations are performed in the ALU[11].

This makes the ALU a very power-hungry component of the processor[11]. This could lead to the build-up of hotspots in the processor and, therefore, power reduction in the ALU becomes a very significant issue[12]. In this work, the performance of several different versions of a 32-bit nanoscale ALU, based on various adder structures, is investigated from a speed, power and area standpoint at the 65 nm CMOS technology node. The adder structures that were employed in the ALU included the Carry Save Adder (CSA)[7], Ripple Carry Adder (RCA)[13], Carry Lookahead Adder (CLA)[14], Carry Select Adder (CSLA) [15, 16], and Kogge Stone Adder (KSA)[17]. The functional units within the arithmetic part of the ALU consisted of an adder, a multiplier and a divider. The logical part was comprised of circuits capable of performing the shift operation and the rotate operation. The remainder of this article is organized as follows: Related work from the literature is summarized in section 2. Section 3 briefly describes the design of various ALU structures such as the multiplier, subtractor, divider and shifter that are employed in this work. The methodology and tools adopted in this work are presented in section 4. Results are presented in section 5 and conclusions are stated in section 6.

RELATED WORK Due to the fact that the adders are the fundamental unit of computation in the ALU and other processor structures such as the floating-point unit[18, 19], several adder designs have been developed over the years in order to address the challenges related to delay, power and area[7, 13, 14, 15, 16, 17]. Also, recognizing the frequency with which multiplication operations occur in computer arithmetic and the need for fast execution of these operations, several multiplier algorithms and circuits have been developed in the past with an aim to achieve one or more of these following goals: High-speed, low-power, low-area and ease of layout[13, 20, 21, 22, 23, 24, 25, 26]. An analysis of the delays of the Wallace multiplier and the Dadda multiplier was carried out by Townsend et al. at the gate-level[27]. They compared the delays of Dadda and Wallace multipliers of various sizes and concluded that a Dadda multiplier is not only faster than the corresponding Wallace multiplier but is also more area efficient. Shah et al. implemented five different 32-bit multiplier designs, namely array multiplier, modified Booth's (Radix-4) multiplier, Optimized Wallace multiplier, Combined modified Booth-Wallace multiplier and Serial-parallel multiplier, on an FPGA platform[28]. As part of this work they found that the Optimized Wallace multiplier and Combined modified Booth-Wallace multiplier were the fastest and also had the best power delay product among the five multipliers. They also found that the combined modified-Booth-Wallace multiplier had the best area -delay^2 (*area-delay-squared*) product. Recent years have also seen a number of research efforts focused on the ALU structures. Shrivastava et al. modeled the effects of process variation and temperature variation on the leakage power dissipation of processor functional units (FUs) and propose microarchitectural architectural methods known as *leakage-aware operation to functional-unit binding* (LA-OFBM) *and leakage-aware power-gating* (LA-PG) [12]. These techniques aim to mitigate the variation in the power dissipation patterns of various functional units and also to achieve reduced power dissipation within the FUs. Ghosh et al. studied the suitability of various adder circuits for voltage scaling and adaptive clock stretching[29]. They propose a hybrid design methodology for adders and use it to achieve low-power multipliers that are process-variation tolerant at reduced supply voltages. Aguirre-Hernandez et al. proposed new full adder topologies based on pass-transistor logic and compared their speed and power performance with that of other full-adder topologies for a 180 nm technology node implementation[30]. More recently, Tung et al. also proposed a15-transistor full-adder topology targeting low-power and high-speed performance and compared it with other full-adders at the 180 technology node[31]. Frustaci et al. proposed an improved data-driven dynamic logic (D3L) technique for achieving low-energy operation without sacrificing speed performance and applied the technique to a Kogge-Stone adder[32]. They found that the Kogge-Stone adder that incorporated their technique resulted in a lower energy-delay product (EDP) than those designed using conventional D3L and clock-precharged domino logic at the 90 nm technology node. Zeydel et al. targeted the growing mismatch between addition algorithms and energy-efficient realizations brought about due to the technology scaling and proposed a design methodology for achieving energy-efficient high-speed 64-bit adders at various technology nodes[33]. Using tradeoffs at various levels such as algorithm, recurrence, wire delay, circuit topology, circuit sizing etc., they developed a 64-bit high-speed low-energy adder and evaluated its performance at various technology nodes. Tu et al. proposed a pipelined reconfigurable Baugh-Wooley multiplier that employs clock gating and zero input techniques in order to achieve low power dissipation[34]. Their multiplier is capable of operating in four operating modes. Kuang et al. proposed a low-power reconfigurable Booth's multiplier that utilizes an operand dynamic-range detection scheme in order to switch off parts that are not needed for the multiplication operation, thereby reducing energy consumption[35]. Zhang et al. proposed and implemented a 32x32 multi-precision reconfigurable multiplier for reduced area and reduced power dissipation[36]. This multiplier utilized techniques such as parallel processing and dynamic voltage scaling.

ALU STRUCTURES In this section, the ALU structures used in this work are described briefly:
Half-Adder (HA): The half-adder is the most basic adder and can add two 1-bit-wide numbers to produce a sum and a carry[37]. It cannot handle the addition of in-coming carry bits. The Boolean equations for the outputs of a half-adder as a function of its inputs are as follows:

Sum $(A, B) = A \oplus B$ (1)

Carry $= A \times B$ (2)

Full-Adder (FA): The full-adder can add up to three 1-bit-wide numbers to produce a sum and a carry-out. One of these three inputs may be a 'carry-in' coming from a less-significant position in the case where addition of multi-bit numbers is being carried out. The Boolean equations for the outputs of a full-adder as a function of its inputs are as follows[37]:

Sum $(A, B, C_{in}) = A \oplus B \oplus C_{in}$ (3)

$C_{out} (A, B, C_{in}) = A \times B + B \times C_{in} + A \times C_{in}$ (4)

Ripple-Carry Adder (RCA): The RCA is a multi-bit adder formed by the cascading of multiple FAs. It accepts two n-bit-wide inputs and am optional 1-bit-wide carry-input and produces an n-bit-wide sum and a 1-bit-wide carry-out by employing 'n' FAs. Internally, the carry-out of a given FA is fed to the carry-in of the FA to its immediate left. The carry-out of the RCA is the carry-out signal from the last FA. The sum of the RCA is formed by the sum bits of the individual FAs within the RCA. Since carry signals ripple through the circuit, the RCA can suffer from significant delays for large input widths.

Carry-Lookahead Adder (CLA): The CLA uses a dedicated logic to speed up the generation of the intermediate carries once the initial carry-in at the least significant position is known. This eliminates the need for the rippling of carries across multiple full-adder stages and, therefore, overcomes the speed drawback associated with the RCA. The basic principle used by the carry-generation circuit of a CLA is as follows: At any given bit-position, a new carry will be *generated* if both the operands in that position are logic '1's. A carry arriving from a less-significant position on the right will be *propagated* to the next position (on the left) if one of the operands at this position is a logic '1'.

Carry-Select Adder (CSLA): The CSLA splits up the operand bits into blocks. Every block, except the right-most (least-significant) block, makes use of two RCAs and a multiplexer (MUX). The first RCA operates under the assumption that the carry-in coming into that block is a '0' while the other The other RCA operates under the assumption that the carry-in coming into that block is a '1'. The MUX is used to select the correct value of sum and carry for the block based on the actual carry-in that eventually arrives into the block. The least-significant block does not need to use two RCAs and a MUX because the carry-in value for this block is known at the start of the addition process.

Kogge-Stone Adder (KSA): The KSA is a type of carry-lookahead adder that aims to speed up the addition of two binary numbers by employing a three-step process: During the first stage, individual '*propagates*' and '*generates*' are formed for each bit position. The second stage contains logic to compute the '*propagates*' and '*generates*' for bit-groups of multiple widths. At the culmination of the second stage, the carries will be known. The third stage involves logic to compute the sum. The KSA provides a high-speed method for the addition of two binary numbers.

Multipliers: Array multipliers were employed in this work. These include the traditional array multiplier as well as the array multiplier that utilizes carry-save addition. In the latter, the carries generated by the full-adders at a certain partial product level are not supplied to the full-adders at the same level. Instead, they are sent to the full-adders corresponding to the next, more significant partial product level[20]. This approach potentially helps reduce delay and power dissipation. In both approaches, there will be remaining carries at the final stage that need to be added in order to obtain the final product. This addition can be accomplished by using a dedicated multi-bit adder circuit at the final stage. A simple but slower choice for this adder would be the ripple carry adder (RCA). A faster choice would be a circuit such as the carry-lookahead adder (CLA). We have considered both the RCA and CLA approaches for the final addition stage of the multiplier.

Subtractor: The subtractor was implemented as a two's complement signed binary adder/subtractor circuit. The subtraction operation is accomplished through the addition of negative numbers. A negative numbers is represented by the two's complement of the binary pattern representing the corresponding positive number.

Divider: The divider was implemented as a restoring divider[13, 38]. In a restoring divider, if the temporary partial remainder obtained after the subtraction of the divisor from the relevant portion of the dividend (stored in a shift register) is found to be negative at any given step, then it is followed by the assignment of a quotient bit of '0'. Furthermore, it is accompanied by the restoration of the value of the temporary partial remainder that existed prior to the subtraction of the divisor. On the other hand, if the temporary partial remainder obtained after the subtraction of the divisor is found to be positive, the corresponding quotient bit will be a '1' and no restoration of the temporary partial reminder takes place.

Shifters: Shift registers were employed for accomplishing various types of shift operations.

2. METHODOLOGY AND TOOLS

The methodology and tools adopted for characterizing the delay, area and power of the arithmetic units used in this work are described in this section. The arithmetic and logic circuits were described using the Verilog HDL. The designs were compiled, functionally verified using the Xilinx ISE Design Suite [39]. Gate-level design netlists were then generated using Cadence Encounter RTL Compiler[40]. The netlist of a design was then used to generate its GDS-II layout for the TSMC 65nm process (TCBN65LPBWP7T). Following this, the power, area and the timing analysis of the layout were captured. The process flow is summarized in figure 1. Figures 2 and 3 show the layouts generated for selected 32-bit adder circuits and multiplier circuits, respectively. Figure 4 shows the layout for the divider. Following the design of various ALU building blocks, nine different ALU topologies based on various combinations of adders and multipliers were developed and analyzed. The attributes of these topologies are summarized in Table 1.While each of these ALU topologies uses a different adder and a multiplier, the divider and subtractor were the same for all of the topologies. Thus the performance difference in speed, power and area of the various ALU topologies can be attributed to that of just the adder and multiplier units employed in the ALU design. The GDS-II format for the various ALU topologies are shown in figures 5, 6 and 7.
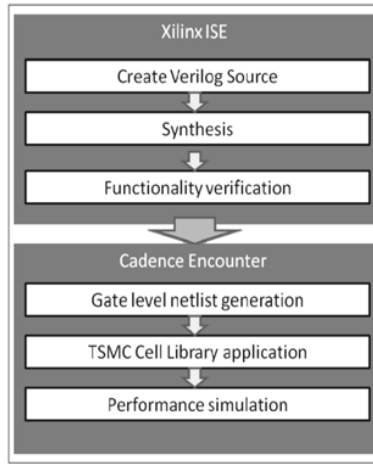
Fig. 1 Summary of the tools and methodology adopted
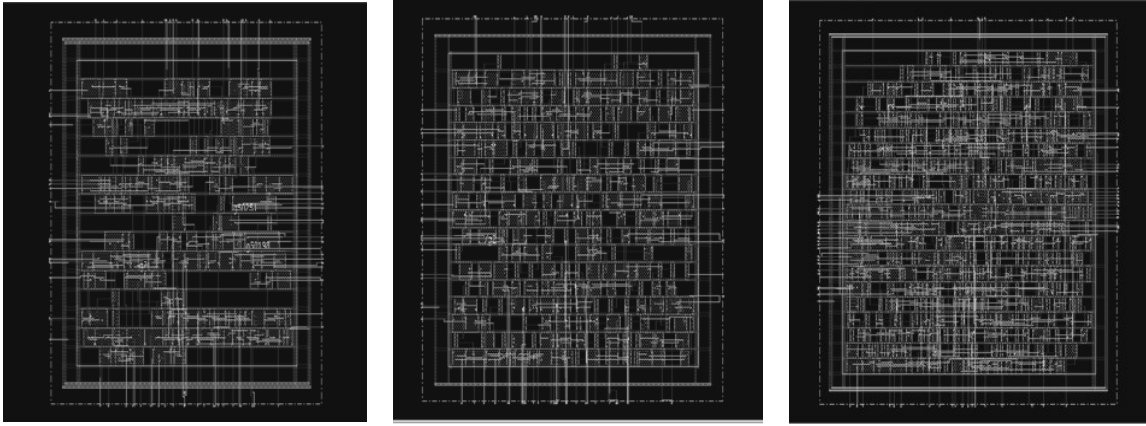
Fig. 2 GDS-II layouts for various 32-bit adders (*left to right*): CLA, CSLA and Kogge-Stone Adder
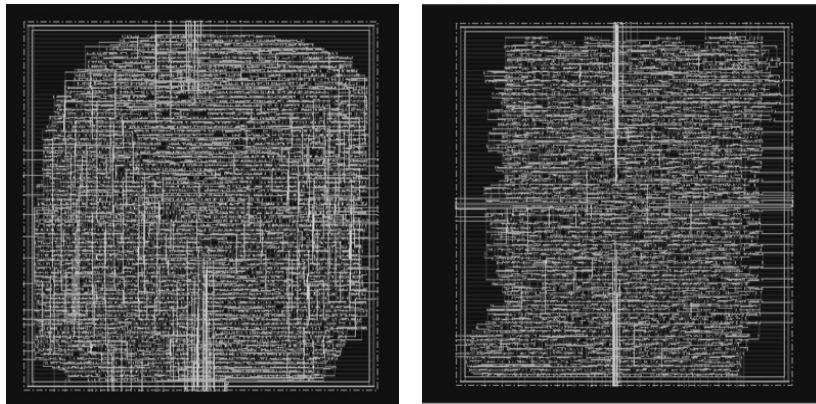
Fig. 3 GDS-II layouts for traditional array multiplier with RCA in the addition final stage (*left*) and CSA-based-array multiplier with CLA in the final addition stage (*right*)
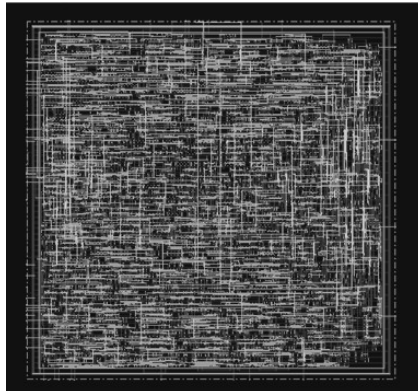
Fig. 4 GDS-II layout for the divider
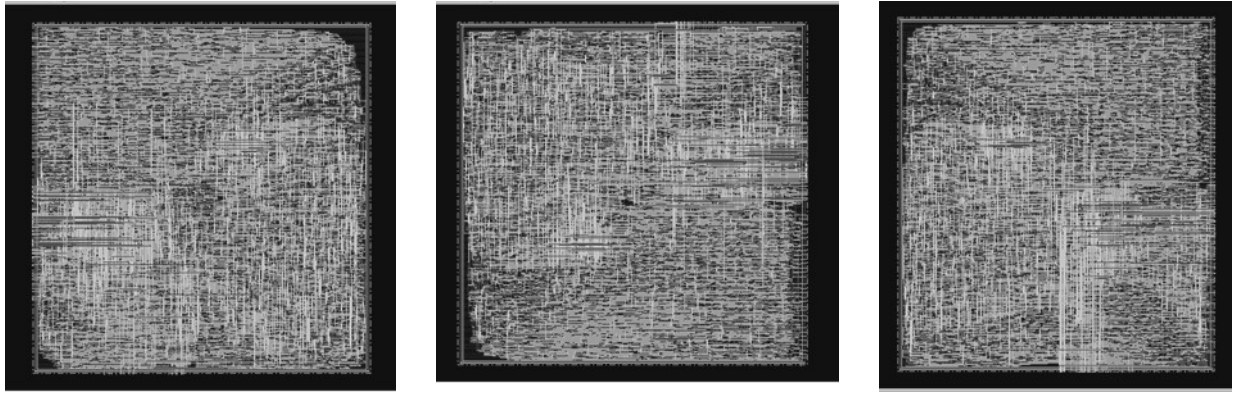
Fig. 5 (*left-right*) GDS-II layouts for ALU topologies #1, #2 and #3
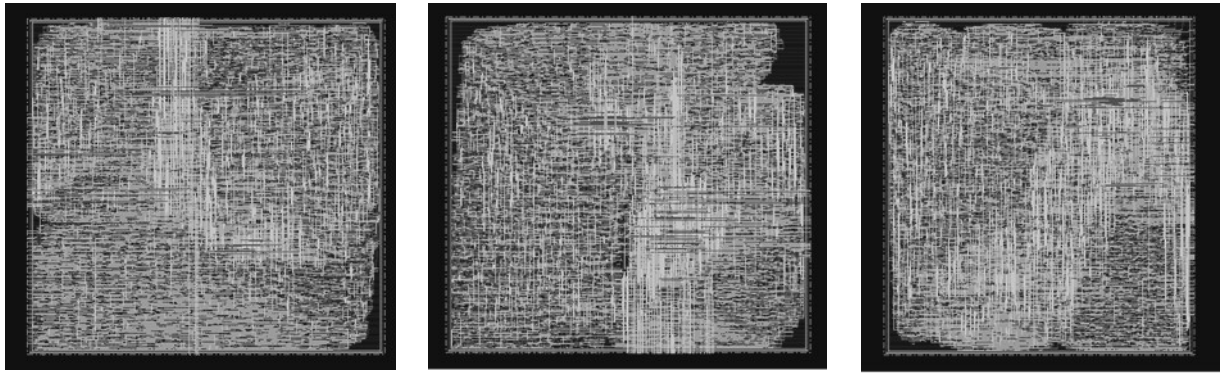
Fig. 6 (*left-right*) GDS-II layouts for ALU topologies #4, #5 and #6
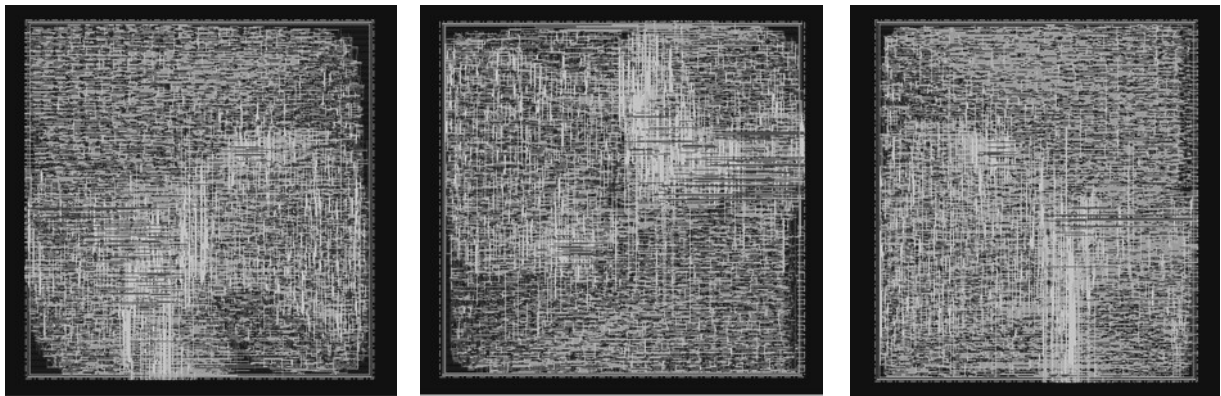
Fig. 7 (*left-right*) GDS-II layouts for ALU topologies #7, #8 and #9

Table 1 Attributes of Various ALU Topologies Analyzed

ALU Topology #	Adder	Multiplier
1	CLA	RCA Array
2	CLA	CSA Array with RCA end adder
3	CLA	CSA Array with CLA end adder
4	CSL	RCA Array
5	CSL	CSA Array with RCA end adder
6	CSL	CSA Array with CLA end adder
7	Kogge-Stone	RCA Array
8	Kogge-Stone	CSA Array with RCA end adder
9	Kogge-Stone	CSA Array with CLA end adder

3. RESULTS

In this section, results pertaining to delay, area and power tradeoffs for various ALU units are analyzed. The area, power dissipation and delay results for the carry-lookahead adder (CLA), carry select adder (CSL) and Kogge-Stone adder (Kogge) are shown in figure 8 for the 65nm CMOS technology node (TSMC).
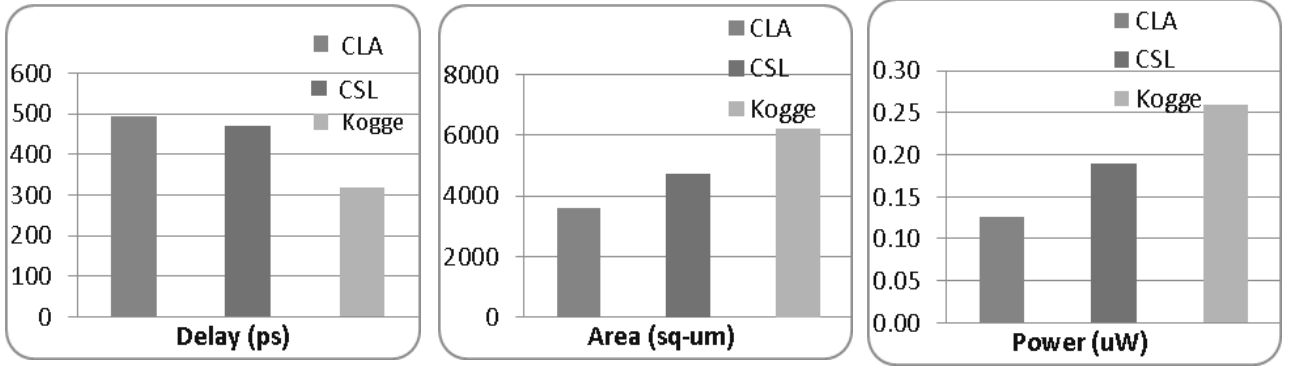
Fig. 8. (*Left-right*) Delay, area and power dissipation for various 32-bit adder units

It can be seen Kogge-Stone adder is the fastest adder but is also the most power-hungry. It is, therefore, suitable for high speed applications. It also consumes the highest area among all the three adders. This can be attributed to its complexity, which necessitates additional circuitry and, therefore, higher power dissipation. The carry lookahead adder (CLA) occupies the least area and dissipates the least amount of power at the cost of increased delay. The carry select adder (CSL) performs two additions for calculating the sum bits - one assuming that the incoming carry bit is equal to 1 and the other assuming the incoming carry bit is equal to 0. This increases its area as compared to the CLA. Figure 9 shows the delay and power results for the various multipliers, namely, the traditional array multiplier based on the ripple carry addition (RCAM), the carry save multiplier based on carry save addition with a ripple carry adder in the last stage (CSA Array-RCA), and the carry save multiplier based on carry save addition with a carry lookahead adder in the last stage (CSA Array-CLA). The traditional array multiplier based on the ripple carry addition (RCAM) has the worst delay. On the other hand, the carry save multiplier structure saves a block of adders when compared to that of RCAM, as addition is performed in parallel without having to wait for the carries from the previous stage. This approach helps reduce delay as well as power dissipation. The speed of these architectures can be further improved using a faster final adder. This can be seen from the delay results for the (CSA Array-CLA) multiplier, which is the fastest design among the ones considered. As far the power is concerned, the traditional array multiplier based on the ripple carry addition (RCAM) has the highest power consumption when compared to carry save multiplication structures (CSA Array-RCA and CSA Array-CLA). The latter structures need a smaller number of iterations for the multiplication operation as compared to the RCAM. Also, fewer logic elements are used in these. The smaller number of interconnections present in the carry save multiplication structures significantly reduces the possibility of glitches occurring in the circuit. The lower power dissipation of the carry save multiplication structures could be attributed to this fact. However, among the two carry save multiplication structures, the CSA Array-RCA multiplier consumes less power owing to the simplicity of its design.
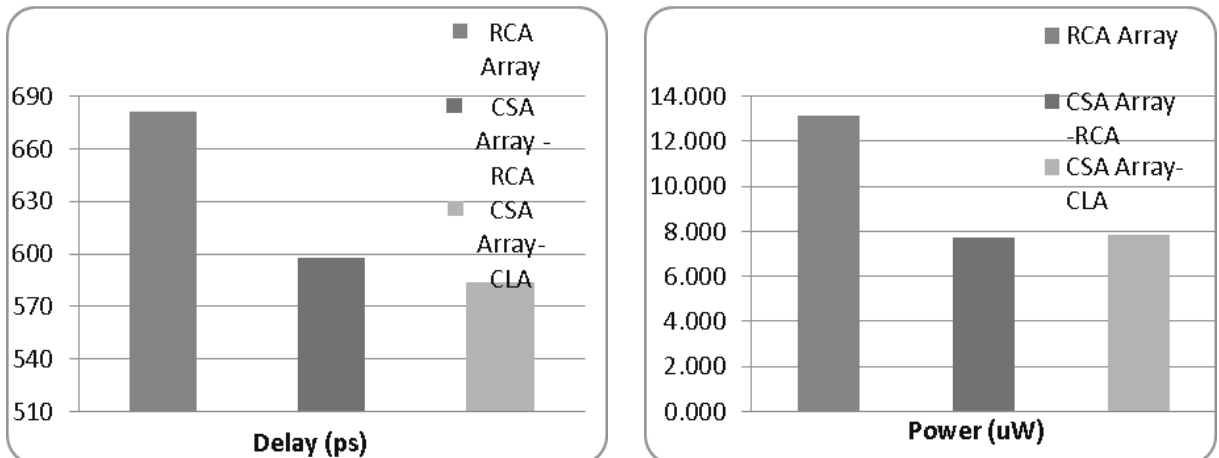
Fig. 9. (*Left-right*) Delay and power dissipation for various multiplier units
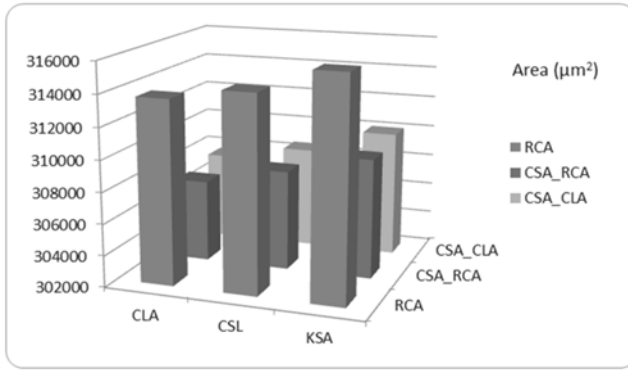
Fig. 10. Area comparison of ALU topologies
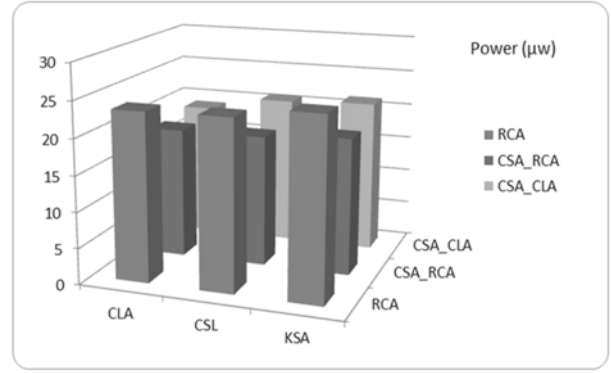
Fig. 11. Power comparison of ALU topologies
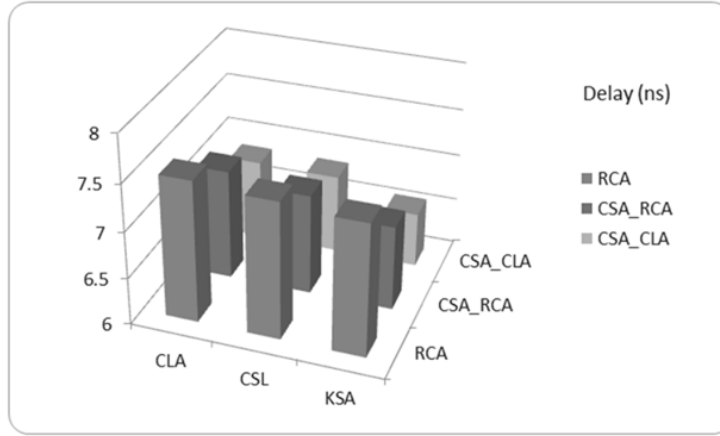
Fig. 12. Delay comparison of ALU topologies

The area, power and delay for the various ALU topologies mentioned in table 1 are shown in figures 10 through 12, respectively. It can be seen that among all other topologies investigated in this work, ALU topologies employing the Kogge-Stone adder occupy the highest area, which can be attributed to the complex interconnect routing of the Kogge-Stone adder. As far as power is concerned, the ALU topology with the KSA and array multiplier based on ripple carry addition (topology #7 of table 1) has the highest power consumption. This can be attributed to the complexity of the KSA and the carry rippling of the array multiplier. However the CLA with the CSA-RCA (topology #2 of table 1) has the least power consumption. From the adder unit perspective, the CLA has the most straight forward design compared to the carry select adder (CSL) where a row of adder computation is wasted, as it calculates the sum twice once with a carry in as 0 and once with a carry-in as 1. From the multiplier perspective the CSA-RCA consumes the least power, as the CSA structure has less number of gates compared to the RCAM structure. It can be seen that the ALU topology with the Kogge Stone Adder and the CSA-CLA has the shortest computation time. This could be attributed to the Kogge Stone Adder which is the fastest adder. The CSA-CLA also contributes to the speed of the design due to the carry-save structure and the faster carry generation and propagation circuit of the CLA. The ALU Topologies with CSL are faster than ALU topologies with the CLA.

4. CONCLUSION

In this work, various 32-bit ALU topologies were designed and realized for the TSMC 65nm technology node, following which their performance was compared from a speed, power and area perspective. The ALU designs were distinguished based on the type of adder circuits used in the addition and multiplication units of the ALU. These adder circuits included the carry lookahead adder (CLA), the carry select adder (CSLA) and Kogge-Stone Adder (KSA). The performance metrics by which the circuits are compared are the silicon area required for the implementation of the algorithm in hardware, the power dissipation during calculation, and the worst case delay in performing the operation. The Kogge-Stone adder has the best performance among all the adders for all the input data width considered. It is widely used in high performance applications and it has the merits of uniform structure and balanced loading in each internal node to get high speed performance. The high performance of the Kogge-Stone adder comes at the cost of increased power consumption. In fact, the power consumption of this adder was the highest among all the adders circuits investigated in this work. The CLA is the slowest compared to other adders. However it compensates for this with its power efficiency and its simpler design. The CSLA is faster than CLA but slower than the Kogge Stone adder. It achieves a balance between power and delay. As far as the performance of entire ALU topologies are concerned, the ALU topology employing a carry-lookahead adder unit and a multiplier unit based on carry-save addition with last-stage ripple carry addition was found to be

the most area-efficient as well as the lowest-power-consuming topology. Topologies employing the Kogge-Stone adder occupied the highest area. Topologies that employed a Kogge-Stone adder unit and the traditional array multiplier unit based on ripple carry addition had the highest power consumption. However, the ALU topology with a Kogge-Stone adder unit and multiplier unit based on carry-save addition with last-stage carry-lookahead addition was the fastest. ALU topologies that employed the traditional array multiplier unit were the slowest.

REFERENCES

1. Moore, G.E. *Cramming More Components onto Integrated Circuits*. Electronics, **38**, 1965, p.114-117.

2. Edwards, C. *The Many Lives of Moore's Law*. Engineering and Technology Magazine, 3, 2008.Available online at http://eandt.theiet.org/magazine/2008/01/moores-law.cfm

3. Rabaey, J. *Low Power Design Essentials*. Springer, 2009.

4. Courtland, R. *Six paths to longer battery life*. IEEE Spectrum, **49**, 2012, p.13.

5. Taylor, C. *Understanding Low-Power IC Design Techniques*. Electronic Design. Website. Available at: http://electronicdesign.com/power/understanding-low-power-ic-design-techniques

6. Sun, J. & Jiang, A. "*The power dissipation comparison of different ALU architectures*", Presented at the IEEE 2nd International Conference on Mechanical and Electrical Technology (ICMET), 10-12 Sept. 2010, p. 430 – 433.

7. von Neumann, J. *First Draft of a Report on the Edvac*. IEEE Annals of the History of Computing, **15**, 1993, p. 27-75.

8. Godfrey, M.D. & Hendry, D.F. "*The Computer as von Neumann Planned it*", IEEE Annals of the History of Computing, **15**, 1993, p.11 -21.

9. Aspray, W., "*John von Neumann's Contributions to Computing and Computer Science*", IEEE Annals of the History of Computing, **11**, 1989, p. 189 – 195.

10. Burks, A.W.; Goldstine, H.H. & von Neumann, J. "*Preliminary Discussion of the Logical Design of an Electronic Computing Instrument*" Available at the Institute of Advanced Study (IAS) Libraries and Archives website. Available at: http://library.ias.edu/files/Prelim_Disc_Logical_Design.pdf

11. Ghosh, S. & Roy, K. *Exploring high-speed low-power hybrid arithmetic units at scaled supply and adaptive clock-stretching*. Presented at the Asia and South Pacific Design Automation Conference, ASPDAC 2008. March 21-24, 2008, p. 635 – 640.

12. Shrivastava, A.; Kannan, D.; Bhardwaj, S. & Vrudhula, S. *Reducing Functional Unit Power Consumption and its Variation Using Leakage Sensors*. IEEE Transactions on Very Large Scale Integration (VLSI) Systems, **18**, 2010, p. 988 – 997.

13. Vladutiu, M. *Computer Arithmetic: Algorithms and Hardware Implementations*. Springer, 2012.

14. Weinberger, A. & Smith, J. L. *A Logic for High Speed Addition*. National Bureau of Standards, Circulation 591, p. 3-12, 1958.

15. O.J. Bedrij, Carry-select adder," IRE Transaction on Electronic Computers, **EC-11**, 1962, p. 340 – 346.

16. J. Sklansky, Conditional-sum addition logic," IRE Transaction on Electronic Computers, **EC-9**, 1960 p. 226-231.

17. Kogge, P. M. & Stone, H. S. *A Parallel Algorithm for the Efficient Solution of a General Class of Recurrence Equations*. IEEE Transactions on Computers, **C-22**, 1973, p. 786-793.

18. Ko, U; Balsara, P.T .& Lee, W. *Low-power design techniques for high-performance CMOS adders*. IEEE Transactions on Very Large Scale Integration (VLSI) Systems, **3**, 1995, p. 327 – 333.

19. Kamp, W.; Bainbridge-Smith, A. & Hayes, M. *Efficient Implementation of Fast Redundant Number Adders for Long Word-Lengths in FPGAs*. Presented at the International Conference on Field-Programmable Technology, 2009, p. 239- 246.

20. Rabaey, J. M.; Chandrakasan, A. & Nikolic, B. *Digital Integrated Circuits, A Design Perspective*. Pearson Education Inc., NJ, 2nd edition, 2003.

21. Booth, A. D. *A Signed Binary Multiplication Technique*. The Quarterly Journal of Mechanics and Applied Mathematics, **4**, 1951, p. 236-240,.

22. Robertson, J. E. *Two's Complement Multiplication in Binary Parallel Digital Computers*. IRE Transactions on Electronic Computers, **EC-4**, 1955, p. 118 – 119.

23. Wallace, C.S. *A Suggestion for a Fast Multiplier*. IEEE Transaction on Electronic Computers, **EC-13**, 1964, p. 14 – 17.

24. Dadda, L. *Some Schemes for Parallel Multipliers*. Alta Frequenza, **34**, 1965, p. 349–356.

25. Baugh, C. R. & Wooley, B.A. *A Two's Complement Parallel Array Multiplication Algorithm*. IEEE Transactions on Computers, **C-22**, 1973, p. 1045 – 1047.

26. Mahant-Shetti, S.S. ; Balsara, P.T. & Lemonds, C. *High Performance Low Power Array Multiplier Using Temporal Tiling*. IEEE Transactions on Very Large Scale Integration (VLSI) Systems, **7**, 1999, p. 121- 124.

27. Townsend, W.J.; Swartzlander Jr., E.E. & Abraham, J.A. *A Comparison of Dadda and Wallace Multiplier Delays*. Presented at SPIE, Advanced Signal Processing Algorithms, Architectures, and Implementations XIII, 2003, p. 552 -560.

28. Shah, S.; Al-Khalili, A.J. & Al-Khalili, D. *Comparison of 32-Bit Multipliers for Various Performance Measures*. Presented at the 12th International Conference on Microelectronics, 2000, p.75- 80,.

29. Ghosh, S.; Mohapatra, D.; Karakonstantis, G. & Roy, K. *Voltage Scalable High-Speed Robust Hybrid Arithmetic Units Using Adaptive Clocking*. IEEE Transactions on Very Large Scale Integration (VLSI) Systems, **18**, 2010, p. 1301 – 1309.

30. Aguirre-Hernandez, M. & Linares-Aranda, M. *CMOS Full-Adders for Energy-Efficient Arithmetic Applications*. IEEE Transactions on Very Large Scale Integration Systems, **19**, 2011, p. 718-721.

31. Tung, C.-K.; Shieh, S.-H. & Cheng, C.-H. *Low-Power High-Speed Full Adder for Portable Electronic Applications*. Electronics Letters. **4**, 2013, p. 1063-1064.

32. Frustaci, F.; Lanuzza, M.; Zicari, P.; Perri, S. & Corsonello, P. *Designing High-Speed Adders in Power-Constrained Environments*. IEEE Transactions on Circuits and Systems—II: Express Briefs, **56**, 2009, p. 172-176.

33. Zeydel, B. R; Baran, D. & Oklobdzija, V. G. *Energy-Efficient Design Methodologies: High-Performance VLSI Adders*. IEEE Journal of Solid-State Circuits, **45**, 2010, p. 1220-1233.

34. Tu, J-H & Van, L-D. *Power-Efficient Pipelined Reconfigurable Fixed-Width Baugh-Wooley Multipliers*. IEEE Transactions on Computers, **58**, 2009, p. 1346 – 1355.

35. Kuang, S-R & Wang, J-P. *Design of Power-Efficient Configurable Booth Multiplier*. IEEE Transactions on Circuits and Systems—I: Regular Papers, **57**, 2010, p. 568-580.

36. Xiaoxiao Zhang, Farid Boussaid, & Amine Bermak. *32 Bit×32 Bit Multiprecision Razor-Based Dynamic Voltage Scaling Multiplier With Operands Scheduler*. IEEE Transactions on Very Large Scale Integration Systems, **22**, 2014, p.759-770.

37. Roth, Jr, C. H. *Fundamentals of Logic Design. 5th edition*. Brooks/Cole, Thomson Learning Inc., 2004.

38. Parhami, B. *Computer Arithmetic: Algorithms and Hardware Designs*. Oxford University Press, New York, 2000.

39. Xilinx ISE Design Suite. Website. Available at http://www.xilinx.com/products/design-tools/ise-design-suite/

40. Cadence Encounter. Website. Available at http://www.cadence.com/products/di/edi_system/pages/default.aspx

A RECTANGULAR PROBE FED MICROSTRIP PATCH ANTENNA FOR FIXED WIRELESS ACCESS (FWA)

Dr. Sanjay Kumar*
Former Principal Advisor
Defence Avionics Research Establishment (DARE)
C V Raman Nagar, Bangalore-560093
M: 9890045917
tnksk@yahoo.co.in
*Corresponding author

Saurabh Shukla
Defence Avionics Research Establishment (DARE)
C V Raman Nagar, Bangalore-560093
Tel.No. 080-25047607
saurabh.dare@gmail.com

ABSTRACT

A compact Microstrip Patch Antenna has been designed for 5725 to 5875 MHz. This band is used for Fixed Wireless Access (FWA) services. FWA operating at C-band can be used to provide broadband services where such services can't be provided through standard delivery platforms. The designed antenna is fed through a standard 50Ω coaxial line and matching is obtained at the centre frequency of band 5.725-5.875 GHz i.e. 5.80 GHz. The physical dimensions of the antenna have been derived using the standard design equations. The microstrip patch antenna is modeled and simulated using CST Microwave Studio 2011. Optimum antenna feed location is obtained through simulations to achieve the desired antenna characteristics as well as the impedance matching with coax feed. The antenna parameters like return loss, beamwidth and gain have been presented and discussed in this paper.

Keywords— Microstrip Patch Antenna, Fixed Wireless Access and Impedance Matching.

1. INTRODUCTION

Microstrip Patch Antenna is a planar antenna in which a metal patch is etched out on a substrate of specific thickness. It represents a three layer sandwich structure which has many advantages like light weight, low profile, low cost, ease of fabrication with conformal shapes. Some of the important properties of microstrip patch antennas are moderate gain with dual frequency operation, linear & circular polarization and omnidirectional patterns. Due to its compactness; Microstrip patch antennas are used widely for RFID tags, cordless telephony and short & medium distance communications like Blue tooth, Wi-Fi and cellular telephony. Microstrip Patch Antenna works as a resonant antenna and provides a return loss better than -15 dB for a narrow band near its resonant frequency. That's why the microstrip patch antennas are mainly designed and used for narrow band applications like RADARS and other microwave communication and detection system [1].

2. ANTENNA CONFIGURATION

The Microstrip patch Antenna has three main components. These components are:

- A planar geometrical metal patch on the top of the substrate (generally rectangular or circular).
- A dielectric substrate with finite height in the middle.
- A thin metallic metal layer bottom to the substrate (known as ground plane).

A rectangular Microstrip Patch Antenna is shown in Fig. 1. Due to the planar configuration and easy integration with microwave planar transmission lines, the microstrip patch antenna is most widely used antenna as compared to other conventional antennas.
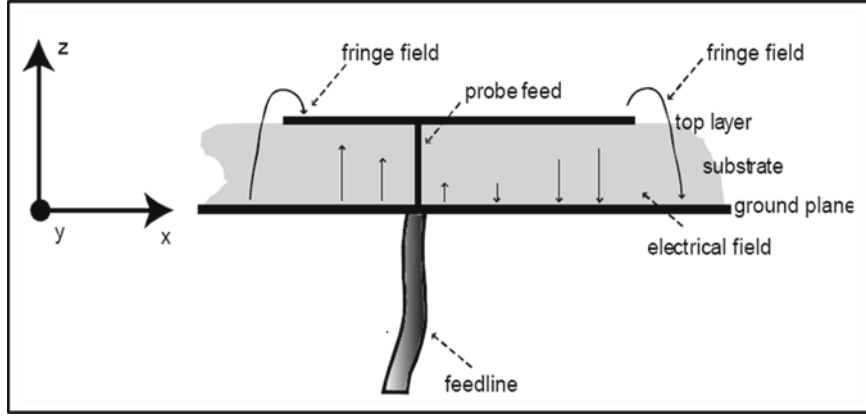
Fig. 1 Patch Antenna Configuration

3. DESIGN PARAMETERS

The design of the Microstrip Patch Antenna is based on three essential parameters namely [2]:

1. Resonant frequency: As the designated ISM band is 5.725-5.85 GHz, the resonant frequency must be the centre frequency of the band. Hence

$$f_0 = \frac{5.725 + 5.875}{2} = 5.8 \text{ GHz}$$

2. Dielectric Constant: A substrate with high dielectric constant reduces the physical dimensions of the antenna but provides less bandwidth. In this design the bandwidth is 150 MHz and our prime aim is to design a compact antenna at centre frequency i.e. 5.8 GHz hence **RT Duroid 6010 LM** substrate is chosen which has dielectric constant of 10.9.

3. Substrate Thickness/Height: The substrate height decides the weight of the Antenna hence in order to have a low weight antenna, 75 mil (1.905 mm) thick RO 3010 substrate is chosen for our Microstrip Patch Antenna [3].

Other important parameters required for the rectangular Microstrip Patch Antenna Design are:
a) Patch Width (W): The width of the rectangular Patch for f_0= 5.8 GHz is defined as:

$$W = \frac{c}{2f_0} \times \frac{1}{\sqrt{\frac{(\varepsilon_r + 1)}{2}}} = 10.6 \text{ mm}$$

b) Effective Dielectric Constant (ε_{eff}): The effective dielectric constant for W = 26 mm and h = 1.27 mm is defined as:

$$\varepsilon_{reff} = \frac{(\varepsilon_r + 1)}{2} + \frac{(\varepsilon_r - 1)}{2}) \times (1 + 12 \times \frac{h}{W})^{-\frac{1}{2}} = 8.45$$

c) Effective Length (L_{eff}): The effective Length for ε_{reff}= 8.45 is defined as:

$$L_{eff} = \frac{c}{2f_0} \times \frac{1}{\sqrt{\varepsilon_{reff}}} = 8.9 \text{ mm}$$

d) Length Extension (ΔL) for L_{eff}= 8.9 mm, W=10.6 mm, h = 1.905 mm and ε_{reff} = 8.45, the Length extension is defined as:

$$\Delta L = 0.412 \times h \times \frac{(\varepsilon_{reff} + 0.3) \times (\frac{W}{h} + 0.264)}{(\varepsilon_{reff} - 0.258) \times (\frac{W}{h} + 0.8)} = 0.767 \text{ mm}$$

e) Actual Length (L): Actual Length of the rectangular patch is defined as:

$$L = L_{eff} - 2 \times \Delta L = 7.36 \text{ mm}$$

f) Ground Plane Dimensions: The transmission line model is applicable to infinite ground planes only but for practical considerations, it is essential to have a finite ground plane. It has been shown that if the size of the ground plane is greater

than the patch dimensions by approximately six times of the substrate thickness then similar results for finite and infinite ground plane can be obtained. Hence, for this design, the ground plane dimensions would be given as:

$$L_g = 6h + L = 18.79 \text{ mm}$$

$$W_g = 6h + W = 22.03 \text{ mm}$$

The physical dimensions of a rectangular microstrip patch antenna are shown in Fig.2.
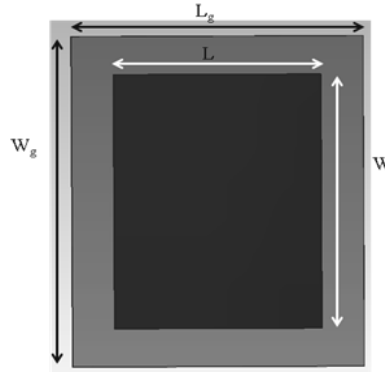
Fig.2 Physical Dimensions of a Patch Antenna

4. COAXIAL FEEDING

The rectangular patch Antenna can be fed directly from coaxial probe at any point except the centre (as shown in Fig. 3) because electric field is always zero at the centre of the patch and the patch will not radiate at all [4].
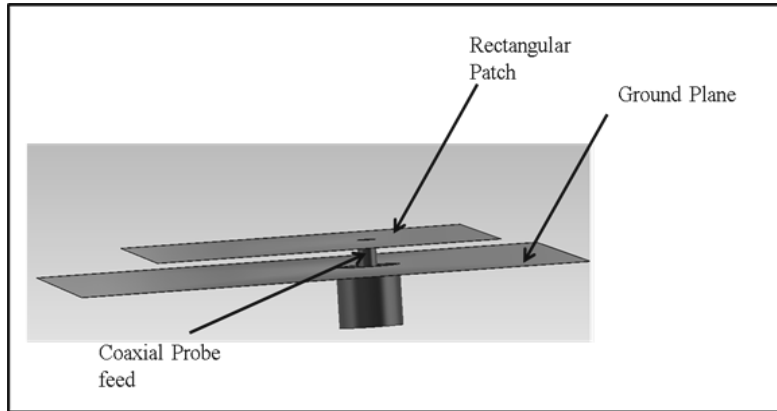
Fig.3 Coaxial Feeding in a Patch Antenna

Now we aim to get return loss better than -10 dB for the centre frequency of band of 5.725 - 5.875 GHz with the dimensions tabulated below:

Table 1: Design Parameters for Simulation	
Parameter	**Value**
Resonant frequency (f_0)	5.8 GHz
Dielectric Constant (ε_r)	10.9
Substrate height (h)	1.905 mm
Patch Width (W)	10.6 mm
Patch Length (L)	7.5 mm
Ground Plane Width (W_g)	22.1 mm
Ground Plane Length (L_g)	18.8 mm

To find out the optimum feed location coordinates; we use Cartesian coordinate system with origin at the centre of the patch as shown in Fig. 4. Position of the feed in terms of Cartesian coordinates (x_f, y_f) is varied to obtain the desired response at resonant frequency. As per the theory, the Return Loss will be minimum along the length of the patch antenna hence $y_f = 0$ [5]. Thus only x_f is varied over the patch to get 50 Ω impedance at resonant frequency.

The Feeding technique plays an important role in impedance matching. To feed the patch antenna with coax probe, a coaxial probe with 1mm diameter has been designed. The direct matching is obtained by varying the position of probe along the length of the patch. This type of feeding gives impedance matching for a very narrow band and used especially for matching at centre frequency [6]. To achieve broadband performance several techniques like microstrip line feeding and feeding through slot are used.

Matching at a particular frequency helps in the excellent rejection of signals lying outside the band of interest. The ISM band is occupied by several other devices and hence for some specific applications it is required that the device should operate at a specific frequency instead of a band.
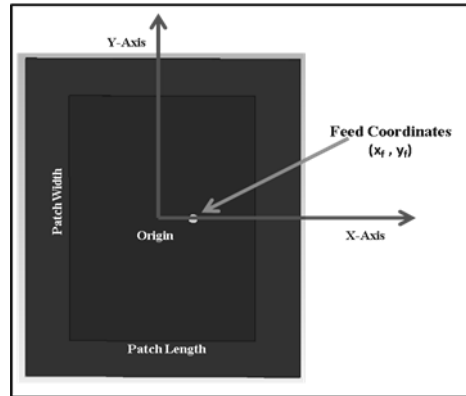
Fig. 4 Coaxial Feed position relative to the origin

5. SIMULATION SET-UP

The Antenna is simulated in CST Microwave Studio 2011 with frequency range from 5.7 to 5.9 GHz. The other physical dimensions used are:

L = 8.1 mm; W = 11.2 mm
L_g = 19.2 mm; W_g = 22.5 mm

The boundary conditions are set as "Open (with add space)" to obtain the free space condition with finite ground. The Broadband Farfield monitor is set at f = 5.8 GHz to check the radiation pattern of the antenna at its resonant frequency. While selecting the plot mode, the plot view is kept in realized gain mode instead of directivity to get the approximate value of gain.

The Microstrip Rectangular Patch Antenna optimized model is shown in Fig.5.
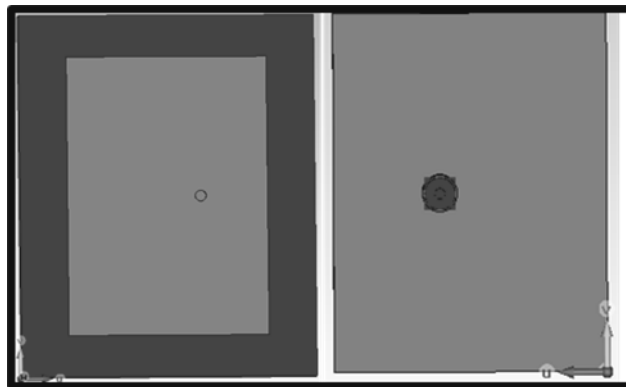
Fig. 5 Simulated Probe fed Patch Antenna

The optimization is done for probe location and the optimized feed location is found at x = 3mm. The optimized results for reflection coefficient, radiation pattern & 3-dB beamwidth are presented in Fig.6 and Fig.7 respectively. The results are matching with the theoretical calculations and a further study can be done on enhancing the bandwidth of the antenna.
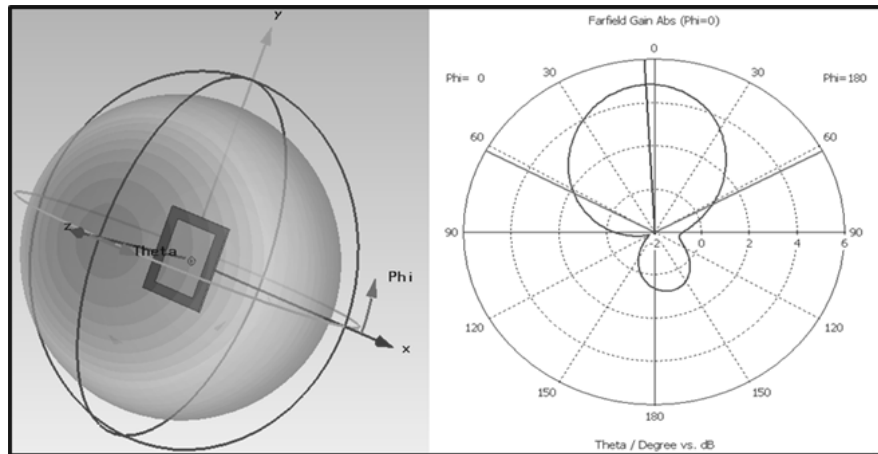
Fig. 6 Simulated Radiation Pattern at f = 5.8 GHz
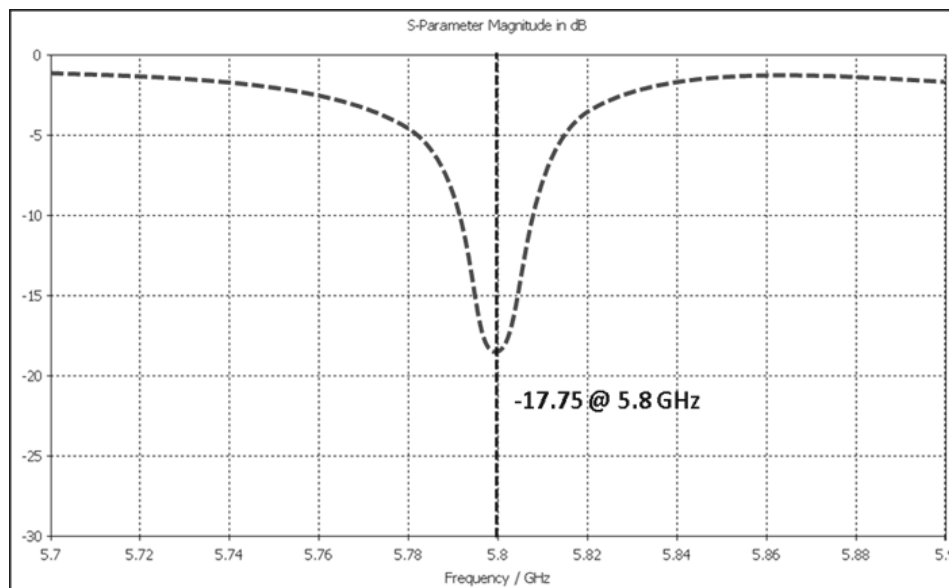
Fig. 7 Simulated S_{11} for Patch Antenna

6. CONCLUSION

On the basis of the simulated results presented here, it can be concluded that the Patch antenna works optimally in ISM band for 5.8 GHz frequency. The ISM band is extremely useful in low power short range communications like Bluetooth, Wi-Fi and cordless phones. To avoid interference with other radio communications, ISM band is unlicensed only for low power applications. The Antenna is showing a moderate gain of 3.5 dB which makes it very useful for low power short range communication. FWA operating at band C can be used to provide broadband services to a range of business, private and public users.

This Antenna can be used for receiving purpose for FWA. The compact size and less weight are other advantages which makes it an important element that can be integrated with cordless telephone and personal computers.

The design equation and the simple coaxial feeding technique presented in this paper allows the researchers and fabricators to design patch antenna in different frequencies for various applications ranging from Global Positioning System (GPS) to antenna arrays used in high power electronic beam scanning. The simplified geometry suggested in this paper reduces the chances of manufacturing defects and improves the yield of production. The further improvement in bandwidth for this type of Antenna can be achieved by using feeding techniques like microstrip feeding or slot feeding.

ACKNOWLEDGEMENTS

REFERENCES

1. Chang, F. S. & Wong, K. L. (2001), A broadband probe-fed patch antenna with a thickened probe pin, *Proceedings of Asia-Pacific Microwave Conference*, (1247-1250), ISBN: 0-7803-7138-0, Taipei, China, Dec. 2001

2. R. Garg, P. Bhartia, I. Bahl, and A. Ittipiboon, "Microstrip Antenna Design Handbook" London: Artech House, 2001

3. Lee , K. F. & Chen, W. (1997). *Advances in Microstrip and Printed Antennas*, John Wiley, ISBN: 0-471-04421-0, New York.

4. Michael Paul Civerolo, "Aperture Coupled Microstrip Antenna Design and Analysis" Thesis, California Polytechnic State University; June 2010

5. Marzall, L. F., Nascimento D.C., Schildberg, R. & Lacava, J. C. S. (2010), An effective strategy for designing probe-fed linearly-polarized thick microstrip arrays with symmetrical return loss bandwidth, *PIERS Online*, Vol. 6, No. 8, (July 2010) (700-704), ISSN:1931-7360.

6. Antenna Theory, C.Balanis, Wiley,2nd edition Chapter 14. ISBN 0- 471-59268-4.

STRENGTH EVALUATION OF PHYLLITE AGGREGATES AS CONCRETE MATERIAL

Prince Appiah Owusu[*]
Department of Civil Engineering,
P. O. Box 854, Kumasi Polytechnic, Kumasi, Ashanti, Ghana
Email: princeappiahus@gmail.com
Tel:00233245885748
[*]Corresponding author

Emmanuel Kwesi Nyantakyi
Department of Civil Engineering,
P. O. Box 854, Kumasi Polytechnic, Kumasi, Ashanti, Ghana
Email: emmanuelkwesinyantakyi@yahoo.com.
Tel: 00233268289250

Julius Kwame Borkloe
Department of Civil Engineering,
P. O. Box 854, Kumasi Polytechnic, Kumasi, Ashanti, Ghana
Email: juliusborkloe1@yahoo.com
Tel: 0208163906/0276377093

ABSTRACT

The availability of construction materials is a major factor affecting housing delivery in Ghana. This has necessitated research into alternative materials for construction. This research presents the results of an investigation carried out on the comparative analysis of strength characteristics of concrete produced using crushed phyllites as substitutes for conventional coarse aggregate. Five mix ratios (1:1:2, 1:1.5:3, 1:3:6, 1:2:3 and 1:2:4) with constant water cement ratio were used for the research. A total of 120 concrete cubes of size 100×100×100mm, 30 prisms of size 100×100×500mm and 6 cylinders of size 150×300mm were cast using both phyllites and granite aggregates as a control. The samples were tested to determine their physical and mechanical properties. Concrete made of phyllite was realized to be of heavy density concrete with values ranging between 2200-2600 kg/m^3. Both compressive and tensile strengths of phyllite concrete showed increase with age with a higher compressive strength of 6% more than concrete produced by granite; with tensile strength of 17.15% less than that produced by granite aggregate. The 1:2:4 mix ratio was found to be the most appropriate design, since it gives a steady increase in strength. The tensile strength obtained from phyllite was found to be in a range of be between 19% and 21% of the compressive strength. The tangent modulus of elasticity was found to be in the range of 33.8KN/mm^2 to 82.6KN/mm^2. Considering the above, it was realized that phyllite aggregates are suitable when used as substitutes for conventional aggregates in concrete production.

Keywords: Tensile strength, compressive strength, flexural modulus of elasticity, aggregate properties, concrete slump

1. INTRODUCTION

The compressive strength of concrete depends on the water to cement ratio, degree of compaction, ratio of cement to aggregate, bond between mortar and aggregate, and grading, shape, strength and size of the aggregate [13, 8]. Concrete can be visualized as a multi-phase composite material made up of three phases; namely the mortar, mortar/aggregate interface, and the coarse aggregate phase. The coarse aggregate in normal concrete are mainly from rock fragments characterized by high strength. Therefore, the aggregate interface is not a limiting factor governing the strength requirement [2]. The onset of failure is manifested by crack growth in the concrete. For normal concrete the crack growth is mainly around the cement paste or at the aggregate/cement paste interfacial zone. The strength of concrete at the interfacial zone essentially depends on the integrity of the cement paste and the nature of the coarse aggregate. The effect of using crushed quartzite, crushed

granite, limestone, and marble as coarse aggregate on the mechanical properties of high-performance concrete was investigated [14]. The outcome of the study revealed that the strength, stiffness, and fracture energy of concrete for a given water/cement ratio depend on the type of aggregate. Basalt, limestone and gravel have been used as coarse aggregate to produce normal and high-performance concrete [12].

Concrete which is the mixture of cement, coarse aggregate, fine aggregate and water each weighed in their right proportions, is the most widely used material in the construction industry in Ghana. The availability of its constituents accounts for its acceptance and usage as building material in the country. Coarse aggregate as a product of natural rock accounts for about 70% of the end product and as such plays a very significant role in the building industry. This material is the focus of the research. The material is made available as a result of blasting in a quarry, which reduces the rock mass to acceptable workable sizes for the production of concrete. The kinds of rock which are mostly used in industry include; granite, basalt, sandstones, limestone, etc are gradually getting depleted over the years. This as a matter of fact has given rise to high cost of building. The industry has resorted to the use of other alternative materials as crushed rocks which are obtained from mining pits and other available sources to get the industry going forward. Even though laboratory tests have shown that some of these materials perform satisfactorily, a greater number of them have raised certain public concerns about their structural integrity. This research seeks to investigate into the physical properties of one of such acceptable coarse aggregate, phyllite which is obtained from Anglo Gold Mine in Ashanti region, Ghana. The research investigates structural performance of phyllite aggregates when used in lieu of granite aggregates in concrete production.

SCOPE OF WORK The investigation was based on series of experiments which were performed in the laboratory on the phyllite aggregate and compared with that of normal granite obtained from a commercial quarry. Particle size distribution was performed to determine the grading patterns of phyllite aggregates. Thirty six (36) modulus of rapture beams of size 100×100×500mm, six (6) concrete cylinders of size 150×300mm, together with one hundred and twenty (120) 100×100×100mm concrete cubes were prepared at the laboratory using the mix ratios of 1:1:2, 1:1.5:3, 1:2:4, 1:2:3, and 1:3:6, with constant water cement (w/c) ratio of 0.5 to investigate the concrete tensile strength and compressive strength characteristics at 7th, 14th, 28th, and 56th days and young's modulus of elasticity (stress-strain relationship) at 28th day.

OBJECTIVE The objective of the research was to determine the characteristic strength of concrete made with phyllite at different age periods as stated above. This characteristic strength would be compared with that of granite aggregate used as control to come out with a relationship between the two different aggregates at the different age periods. Finally, to establish the stress-strain relationship for both aggregates.

JUSTIFICATION In the construction industry, the use of aggregates is the most important material in the concrete mix. Granite as aggregate in the construction industry has reliable strength characteristics however the product is not evenly distributed across the geological setting. As a result different rocks with limited or none existing research on strength characteristics are resorted to in lieu of granite to overcome haulage and the rise in aggregate cost of the product which makes cost of construction high in recent history. Again the uncertainty in the strength characteristic of the various rocks borders on the structural integrity of the aggregates. The study was therefore carried out to establish the strength characteristics patterns of the phyllite aggregates which will help designers in the industry of its suitability or otherwise.

2. MATERIALS AND METHODS

MATERIALS The materials used for this research include commercially available Ordinary Portland Cement. This cement has a specific gravity of 3.15. Two types of coarse aggregates; crushed granite, and crushed phyllite were used. The fine aggregate is normal sand obtained from a borrow pit. Preliminary laboratory investigation was conducted to ascertain the suitability of the aggregates for construction work. Potable drinking water suitable for concrete work [6] was used for this work.

WATER ABSORPTION Water absorption is used to determine the amount of water absorbed under specific conditions. Factors affecting water absorption include temperature and length of exposure. The process involves weighing a quantity of the aggregate and soaking it in water over a 24 hour period. The samples were collected from water and kept in oven for 24 hours at 105^{0}C. The material samples were removed from the oven and kept in desiccators to cool. The difference between the wet weight and the oven dry weight of the sample gives the water absorption.

DENSITY Phyllite aggregates has a density which is relatively higher than the usual range (2200-2600kg/m^3). The concrete made with phyllite therefore is classified as heavy density concrete. However the density increases with the age in days.

MIX PROPORTIONING A nominal mix ratios of 1:2:4, 1:1:2, 1:1.5:3, 1:2:3, and 1:3:6 (Cement: Fine Aggregate: Coarse Aggregate) were adopted for the purpose of this work and a water-cement ratio of 0.5 was used. The mix composition was computed using the absolute volume method from equation (1).

$$\frac{W_W}{1000} + \frac{W_C}{1000SG_C} + \frac{W_{FA}}{1000SG_{FA}} + \frac{W_{CA}}{1000SG_{CA}} = 1 (m^3) \qquad (1)$$

Where:
W = Weight of water (Kg)
C = Weight of cement (Kg)
FA = Weight of fine aggregate (Kg)
FA = Weight of coarse aggregate (Kg)
SG_C = Specific gravity of cement (3.15)
SG_{FA} = Specific gravity of sand
SG_{CA} = Specific gravity of coarse aggregate

CASTING, CURING AND TESTING OF SPECIMEN There are three sets of mix ingredients; cement, fine aggregates and coarse aggregates. The required volumes of mix ingredient were measured and mixing was done thoroughly to ensure that homogenous mix is obtained. Before casting, the slump of the concrete is measured in accordance to [3]. For both types of coarse aggregates 120 concrete cubes of size 100×100×100mm, 36 MOR beams of 100×100×500mm and 6 cylindrical samples of size 150×300mm were cast in accordance to [4]. After one day of casting, the concrete cubes were removed from the mould and were transferred to a water tank for curing until the time of test. The curing of the specimen was done according to [5]. The concrete samples were tested for compressive and tensile strength at 7, 14, 28 and 56 days and then tensile and compressive modulus at 28th day. Three cubes were crushed using the compressive testing machine and the average taken as the compressive strength of the concrete.

TENSILE TEST The tensile strength considered in this study was the flexural tensile strength or the modulus of rapture (MOR). The beams were loaded on a system of third point loading support until rapture as shown in Figure 1. The test was in accordance with ASTM C78 (third-point loading) and BS: 1881, parts 3&4. The tensile load at failure was used to determine the ultimate tensile strength.

YOUNG'S MODULUS OF ELASTICITY Both cylindrical and MOR beams were used to determine the modulus of elasticity. A total of 6 cylindrical samples and 6 MOR beams were loaded in compression and in flexure. In each case the strain gauge was used to record the incremental deflections until failure. A graph of stress verses strain was plotted and tangent of the straight portion gives the young's modulus.

THEORY OF THE TENSILE STRENGTH ANALYSIS Considering the system of loading Figure 1 next,

Maximum moment at the mid-span $M = \dfrac{PL}{6}$ \qquad (1)

From the analysis of the section, moment capacity of the section $M = \delta Z$ \qquad (2)

The elastic modulus $= \dfrac{bd^2}{6}$, where b and d denotes the breadth and thickness of the beam.
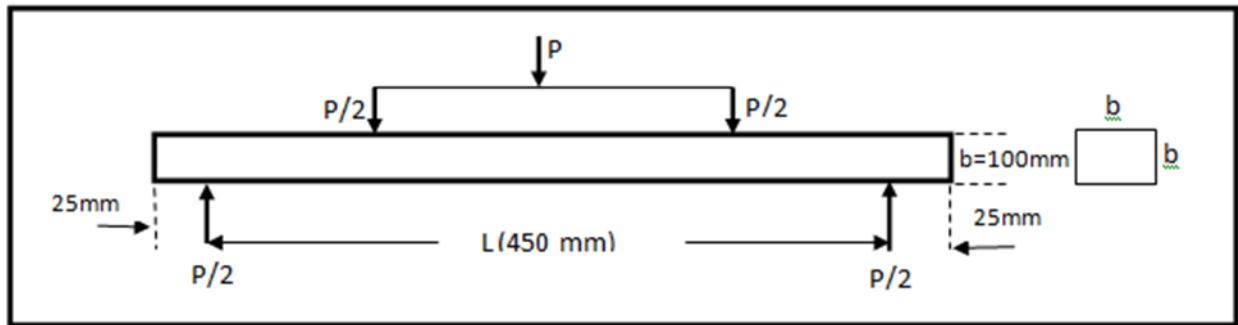
Fig. 1. System of third point loading support

Substitution the elastic modulus into Eq. 1 gives the maximum moment as

$$M = \frac{f_{tc}bd^2}{6} \qquad (3)$$

Where f_{tc} is the tensile strength of the beam in bending, b and d are the breadth and thickness of the beam respectively.

3. RESULT AND DISCUSSION

The experimental results are discussed as follows:

PROPERTIES OF AGGREGATES The results for the grading analysis on the aggregates are shown in Figures 2. The grading curve for the granite aggregates falls partly within the lower and upper limit and partly outside the limits. However, the grading curve for phyllite aggregate reasonably falls out from the gradation limit and a significant portion of the curve is below the lower limit requirement. Such aggregate may require greater fines to achieve reasonable workability.

The values of the specific gravities of the aggregates are from 2.60 to 2.70 (Table 1). These values are within the ranges for the specific gravity of aggregates from rock fragments [11, 10]. This further buttresses the point that the aggregates can be used for construction work.
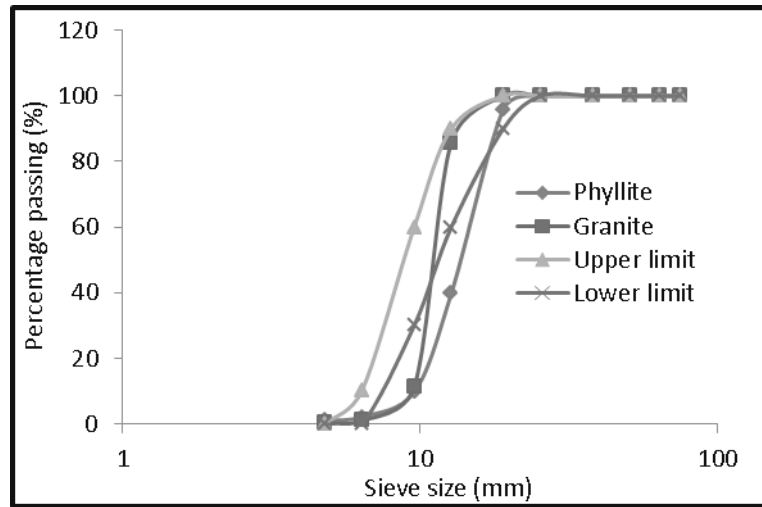
Fig. 2. Sieve analysis for crushed granite and phyllite aggregates

SLUMP. The result for the slump test of the fresh concrete is shown in Figure. 3. The slumps obtained are in the medium range (12–70mm) and (10-138) for phyllite and granite aggregate respectively. The highest slump was obtained with concrete mix of 1:1:2 for both cases and decreases with increasing aggregate content. This is due to the fact that there is reduced cement content which forms paste around the aggregates. Both types of aggregates require more amount of paste to coat their surfaces to improve on their slump and make them workable but due to increasing volume of aggregates there is less amount of paste for lubrication leading to increasing interaction between aggregates during mixing [9]. Phyllite and granite aggregates are crushed from rock fragments and this gives the aggregate a characteristic rough and fairly angular in shape. Aggregate of this nature requires more amount of water when used for concrete work to provide for aggregate coating and lubrication [1]. The concrete containing crushed phyllites and granite aggregates therefore shows lower workability.
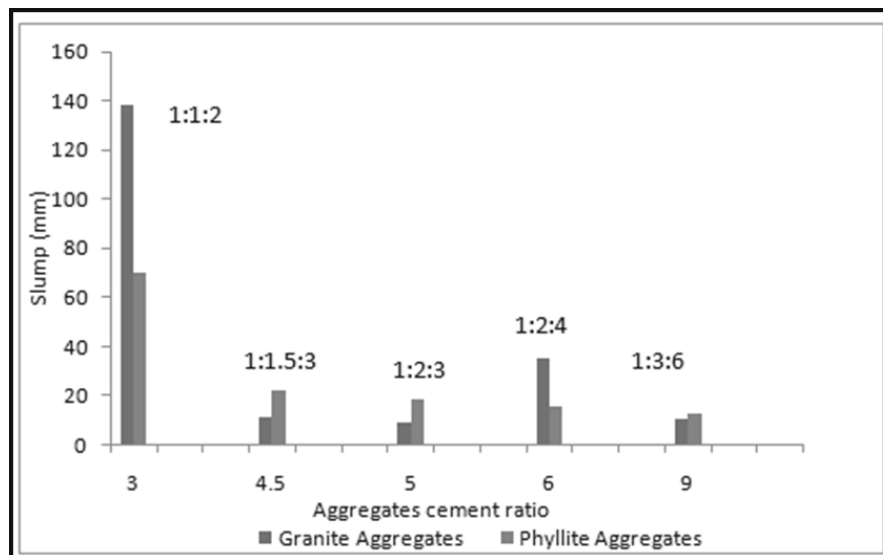
Fig. 3. Slump of concrete mix

Water Absorption limits are rare in British Standards, although BS 8007:1987 does include recommendation that the aggregate absorption should not generally be greater than 3% with maximum value of 2.5% often specified in some cases. Phyllite aggregate has seemingly insignificant water absorption rate which makes it suitable for construction.

Table 1. Water absorption of aggregates

Water Absorption				
Aggregate	Weight of wet Sample (g)	Weight of dry Sample (g)	Weight of Water (g)	Water Absorption (%)	Average Absorption (%)
Granite	123.26	120.93	2.33	1.93	
	154.07	151.6	2.47	1.63	1.75
	141.95	139.58	2.37	1.7	
Phyllite	189.64	186.91	2.73	1.46	
	188.1	185.5	2.6	1.4	1.47
	189.88	186.99	2.89	1.55	

STRENGTH PROPAGATION WITH DAYS. The results for the compressive strength test on the concrete are shown in Figure 4. For both types of concrete, it was observed that the compressive strength increases with age at curing. For all the ages at curing, the highest strength was obtained from concrete made with crushed phyllite aggregates with the highest registered by mix ratio 1:2:4. The significant portion of the gradation curve for the phyllite aggregate as earlier mentioned, falls outside the recommended range and it is lower than the lower limit. This implies that the coarse aggregate has greater voids to be occupied by mortar. This may affect the workability of the concrete, unless mixture proportioning adjustment is carried out to improve on the rheology. This produces concrete with relatively lower workability where the paste is not necessarily sufficient to coat the aggregate and provide the necessary lubrication. However, the strength mobilization of the phyllite aggregates, in 1:2:4 mix ratio, is derived from the disintegration of the phyllite aggregates into column type fragments as the cracks formed approximately parallel to the applied load with majority of cracks formed at an angle to the applied load and normal to the direction to the applied load. This type of failure is synonymous to uni-axial compression. The parallel cracks are caused by a localized tensile stresses in a direction normal to the compressive loads. The included cracks occur due to collapsed caused by the development of shear planes. Similarly, strength analysis of the tensile strength of both crushed phyllite and granite registered similar characteristics as that of compressive strength with curing. The strength propagation increases progressively with age. The phyllite aggregate still shows much stronger in tensile strength than crushed granite Figure 5.
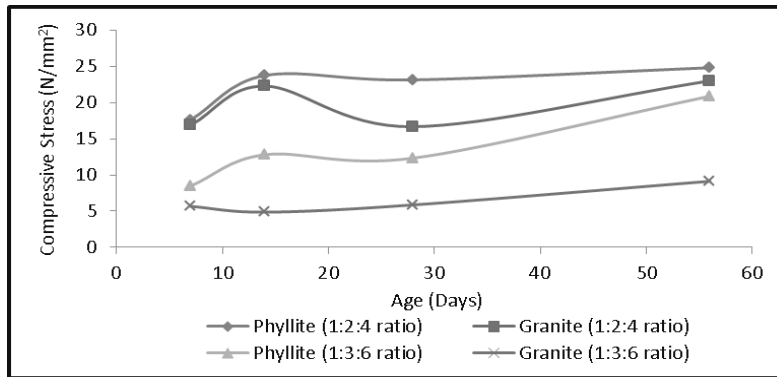
Fig. 4. Compressive Stress against days
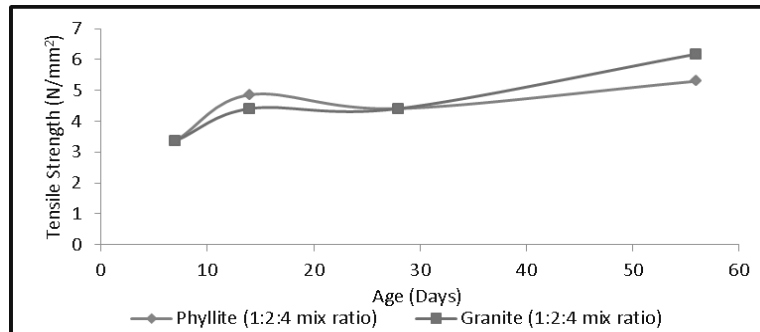
Fig. 5. Tensile strength of phyllite and granite aggregates for mix ratio of 1:2:4

STRENGTH DEVELOPMENT WITH AGGREGATE CEMENT RATIO. Both compressive strength and tensile strength of the aggregates behaved as anticipated. The stress development in each case decreases with increasing aggregate content as showed in Figure 6. This is due to the fact that with the increase in the quantity of the aggregate there is a tearing effect on the bonding effect from the binder leading to an easier disintegration of the concrete. From the study, the compressive strength of the phyllite aggregate decreases by 32.4% from the mix designs of 1:1:2 to 1:3:6. As the phyllite aggregate registers gradual decline in strength for compressive strength the opposite is true for the granite aggregates. For the case of tensile strength the 7th day strength showed a deviation from the 28th day with much lower values compared with the compressive strength as showed in Figure 7. This buttresses the fact that concrete is weak in tension and with the increase in aggregate content the tensile strength shows very poor performance.
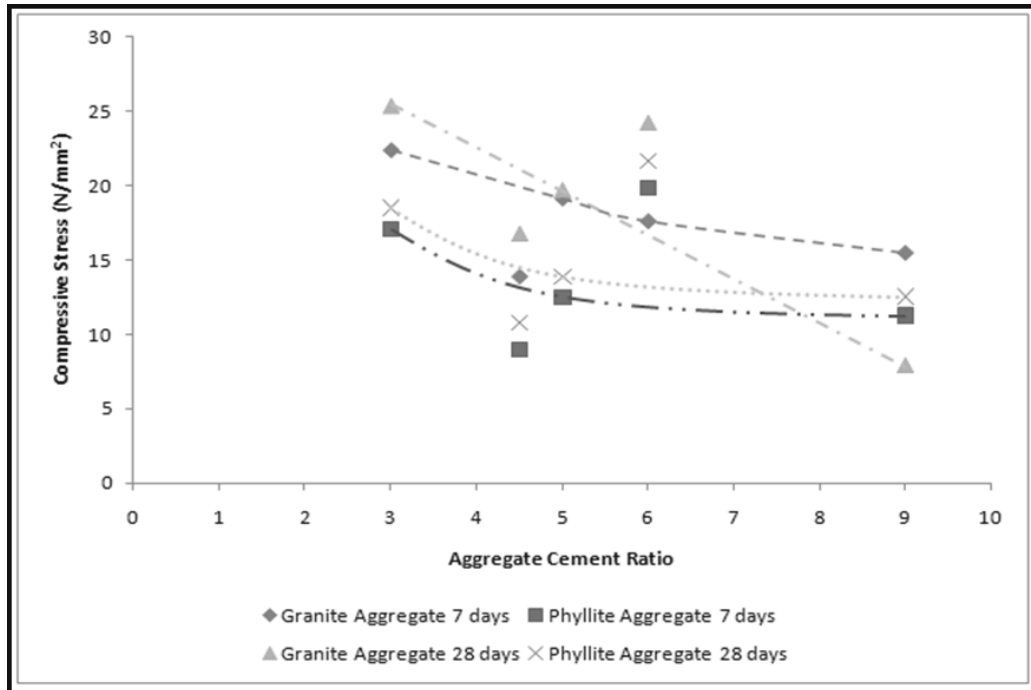
Fig. 6. Compressive strength against aggregate cement ratio
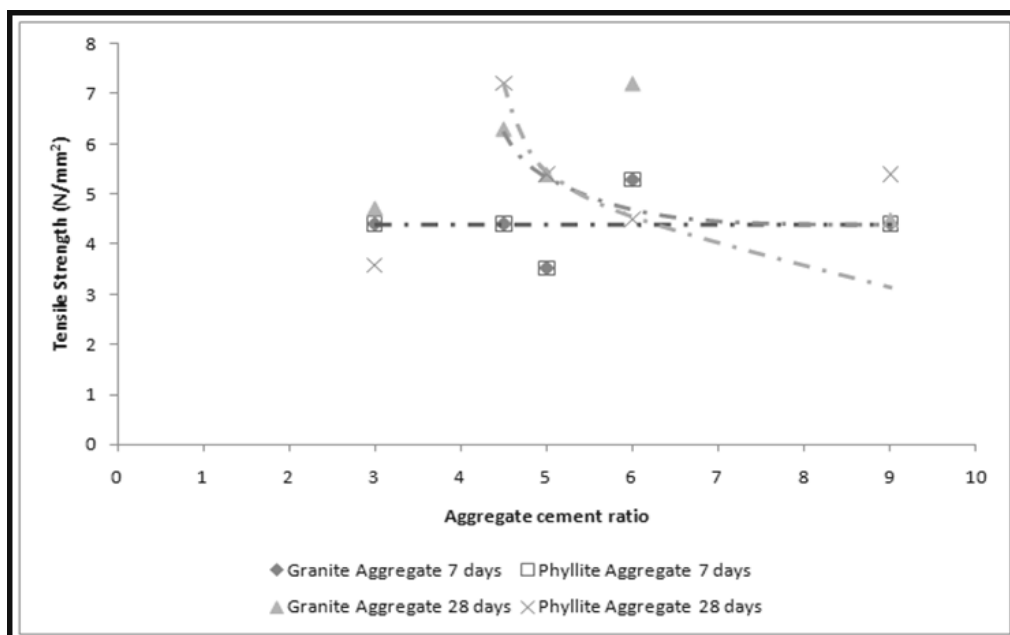
Fig. 7. Tensile strength against aggregate cement ratio

MODULUS OF ELASTICITY. The analysis of the modulus of elasticity confirmed the predicted behavior. As a trend both the compressive and tensile modulus consists of an initial straight elastic portion in which the stress and strain are closely proportional and then begin to approximate a horizontal reaching the maximum stress. The phyllite concrete shows a better brittleness in nature compared to the counterpart in granite. This is seen in the fact that at strength value of 15 N/mm^2, the fracture of the phyllite concrete occurs at a much larger strain of 0.00187 which is better than the counterpart. The phyllite concrete PH1 gave a tangent modulus of elasticity value of 82.6 KN/mm^2 at compressive strength of 12.79N/mm2

whiles the counterpart of granite GR A and GR B gave a tangent modulus of 181.2 KN/mm^2 and 46.16 KN/mm^2 at compressive strength of 16.48N/mm2 and 14.34 N/mm^2 respectively as shown in Figure 8. This shows that the modulus of elasticity depends on the compressive strength and that the nature of aggregate decisively affects the value of elasticity. The phyllite concrete showed typical structural behavior in modulus of elasticity from the tensile modulus perspective as seen in Figure 9. Again the phyllite concrete exhibits less brittleness than the granite concrete with significant influence of the aggregate type on the modulus of elasticity.
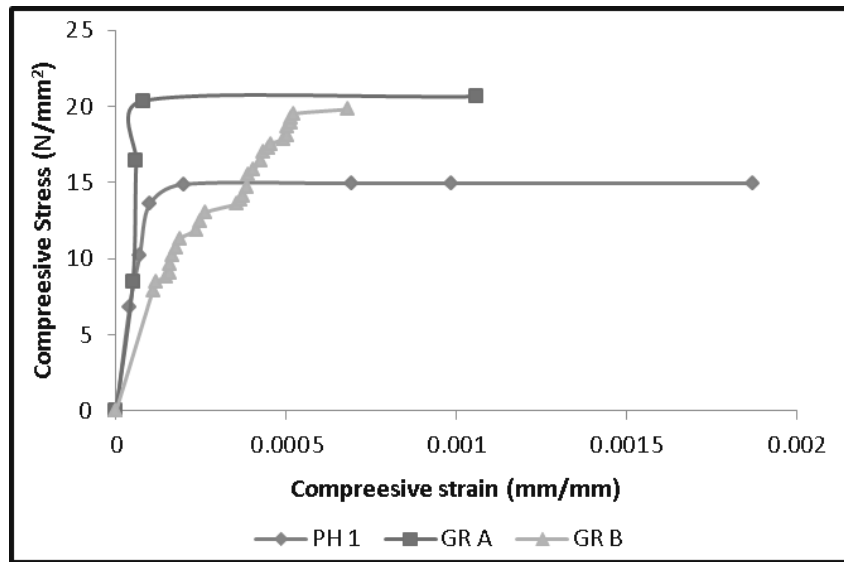
Fig. 8. Compressive modulus using cylindrical samples
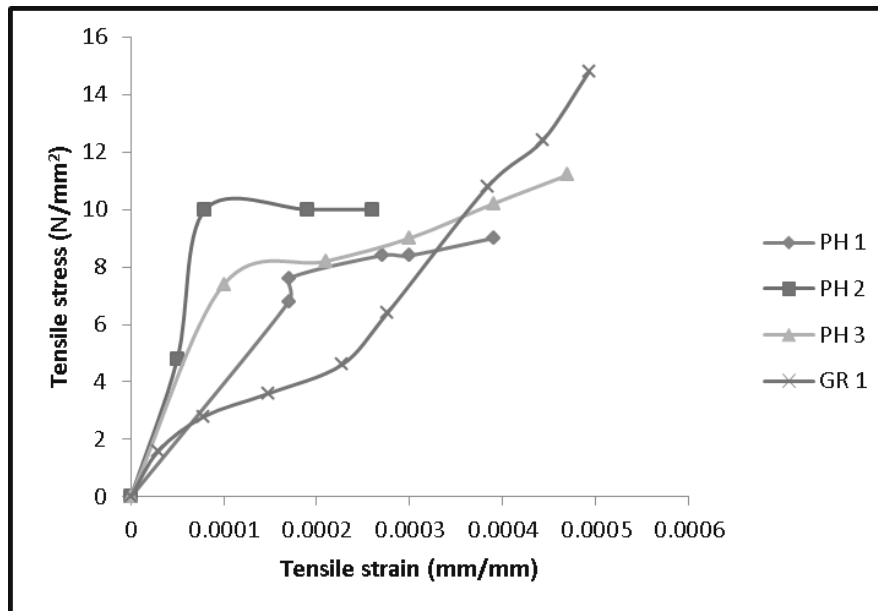
Fig. 9. Tensile modulus using prismatic samples

SIGNIFICANCE OF OBTAINED MODE OF FAILURE OF CONCRETE CUBES. For mix ratios 1:1:2 and 1:2:3, the cubes were still intact after failure, with little broken particles. There were inherent micro-cracks which aligned themselves in path normal to the direction of applied load but closed to 45° the type of failure is suggested to be uni-axial.

For 1:1.5:3 and 1:2:4 mix ratios, the aggregates in the cubes were disintegrated into column type fragments with the cracks formed approximately parallel to the applied load but some cracks formed were at an angle to the applied load and normal to the direction to the applied load. This type of failure is synonymous to uni-axial compression. The parallel cracks are caused by a localized tensile stresses in a direction normal to the compressive loads. The included cracks occur due to collapsed caused by the development of shear planes. The later mix ratio showed a cube failure which acquires the form of two truncated pyramids joined at their bases. The last mix ratio 1:3:6, registered a type of failure that showed disintegrated cubes to a lager extent with cracks inclination from conners of the base and propagated to the top. The cubes failed in a manner with fragments of columns. Collapsed was caused by shear planes with tensile stresses in a direction normal to the

compressive load. The mode of failure discussed above conforms to the standard to some extent as shown in Figures 10 and 11. The failure is however influenced by the compressive strength. It is most probable that the ultimate strain is the criterion of failure but the level of strain varies with the strength of concrete; the higher the strength the lower the ultimate strain.'
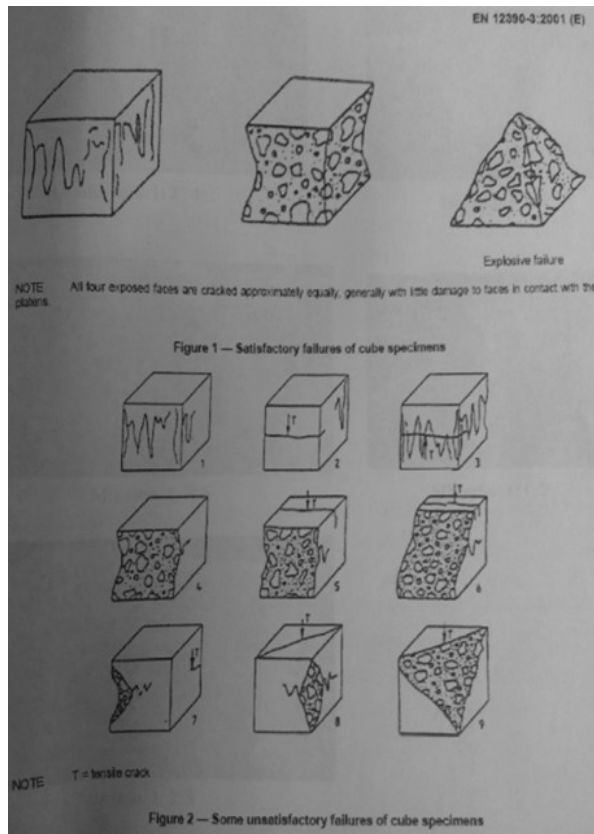
Fig. 10. Standard failures of cube specimen
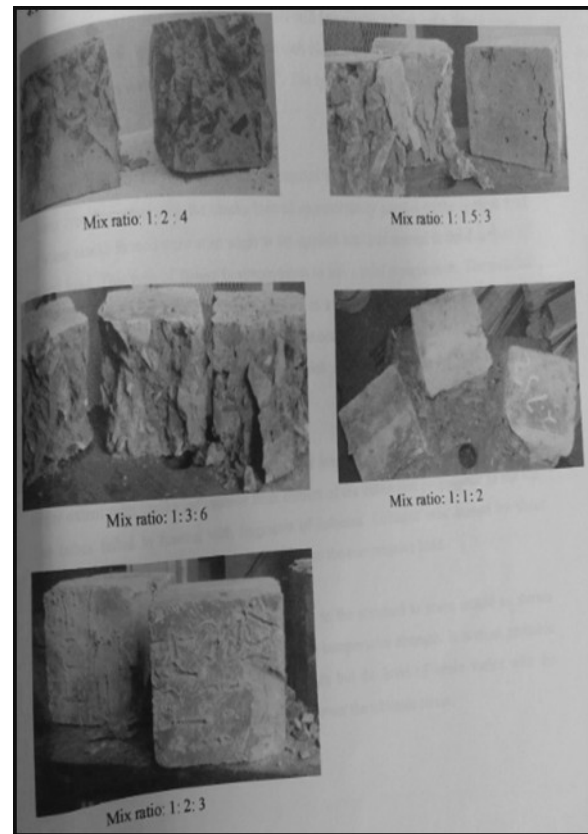
Fig. 11. Observed failure modes of concrete

4. CONCLUSION

It is established from the research that the growth in concrete strength is largely proportional to age, and inversely proportional to the increase in aggregate cement ratio. Both tensile and compressive strength obtained for phyllite concrete exhibited a progressive increase in strength with curing. The tensile strength of phyllite concrete was found to be in the range of 19% to 21% of the compressive strength. From the analysis of the various mix ratios, it was observed that mix ratio 1:2:4 with water cement ratio of 0.5 gives better strength characteristic. Tangent modulus of elasticity of phylite concrete has a range of 33.8 KN/mm^2 to 82.6 KN/mm^2 whiles that obtained for the granite aggregate fell in the range of 30.45 KN/mm^2 to 399.54KN/mm^2.

5. ACKNOWLEDGEMENTS

REFERENCES

1.   ACI Committee 211. *Standard Practice for Selecting Proportions for Normal, Heavyweight and Mass Concrete*. Detroit, American Concrete Institute, 1991, 1- 91.

2.   Beshr, H.; Almusallam, A.A. & and Maslehuddin, M. *Effect of Coarse Aggregate Quality on the Mechanical Properties of High Strength Concrete*, Construction and Building Materials, 17(2), 2003, pp 97-103.

3.   BS 1881: *Method for determination of slump*. British Standards Institution, Her Majesty Stationery Office, London, 1983, Part 102.

4.   BS 1881: *Method for making test cubes from fresh concrete*. British Standards Institution, Her Majesty Stationery Office, London, 1983, Part 108.

5.   BS 1881: *Method of normal curing of test specimen*. British Standards Institution, Her Majesty Stationery Office, London, 1983, Part 111.

6.   BS 3148, *Methods of test for water for making concrete*: British Standards Institution, London 1980.

7.   BS 882, *Specification for aggregates from natural sources for concrete*. British Standards Institution,   London 1992.

8.   Elices, M.; & Rocco, C.G., *Effect of Aggregate Size on the Fracture and Mechanical Properties of a Simple Concrete*, Engineering Fracture Mechanics, 75(13), 2008, pp 3839-3851.

9.   Mindess, S., Young, J.F., & Darwin, D., *Concrete.* Pearson Education, Inc. New Jersey, 2nd ed. 2003.

10.   Neville, A. M. *Properties of concrete*, Addison Wesley Longman, England, 4th ed. 1995.

11.   Olanipekun, E.A.; Olusola, K.O., & Ata, O.A., *Comparative study of concrete properties using coconut shell and palm kernel shell as coarse aggregates*, Building and environment, 41(3), 2006, pp 297 – 301.

12.   Özturan, T., & Çeçen, C., , *Effect of Coarse Aggregate Type on Mechanical Properties of Concretes With Different Strength*, Cement and Concrete Research, Vol 27, Issue 2, 1997, pp 165-170.

13.   Rocco, C.G., & Elices, M., *Effect of Aggregate Shape on the Mechanical Properties of a Simple Concrete*, Engineering Fracture Mechanics, 2009, 76(2), 2009, pp 286-298.

14.   Wu, K-R., Chen, B., Yao, W., & Zhang, D., *Effect of Coarse Aggregate Type on Mechanical Properties of High-Performance Concrete*, Cement and Concrete Research, 31(10), 1997, pp 1421-1425.

REDUCTION OF REAL POWER LOSS BY EARLIGLOW STRAWBERRY PLANT ALGORITHM

Mr.K.Lenin*
Research Scholar, JNTU, Hyderabad 500 085 India
gklenin@gmail.com
*Corresponding Author

Dr. B.Ravindhranath Reddy
Deputy executive engineer, JNTU,
Hyderabad 500 085 India

Dr.M.Surya Kalavathi
Professor of Electrical and Electronics Engineering, JNTU,
Hyderabad 500 085, India.

ABSTRACT

In this paper, Earliglow strawberry plant Algorithm (ESPA) is utilized to solve optimal reactive power dispatch problem. Earliglow strawberry plant progresses runners, roots for promulgation and quest for water resources and mineral deposits. In Earliglow plants, runners, roots are assumed as tools for global and local searches. The planned ESPA algorithm will (i) duplicate the computational agents at all iterations, (ii) exposing all agents to both small and large movements from the start to finish, (iii) data interchange between agents. The proposed EPSA has been tested on standard IEEE 57 bus test system and simulation results show evidently the better performance of the projected algorithm in tumbling the real power loss.

Key words —*Earliglow strawberry plant, optimization, reactive power, Transmission loss.*

1. INTRODUCTION

Reactive power optimization plays an important role in optimal operation of power systems. Numerous arithmetical approaches like the gradient method [1-2], Newton method [3] and linear programming [4-7] have been executed to solve the optimal reactive power dispatch problem. Both the gradient and Newton methods have the difficulty in handling inequality constraints. The problem of voltage stability and collapse play a significant role in power system planning and operation [8]. Evolutionary algorithms such as genetic algorithm have been already proposed to solve the reactive power flow problem [9-11]. Evolutionary algorithm is an exploratory technique used for minimization problems by employing nonlinear and non-differentiable continuous space functions. In [12], Hybrid differential evolution algorithm is offered to upsurge the voltage stability index. In [13] Biogeography Based algorithm is planned to solve the reactive power dispatch problem. In [14], a fuzzy based method is used to solve the optimal reactive power scheduling method. In [15], an enhanced evolutionary programming is used to elucidate the optimal reactive power dispatch problem. In [16], the optimal reactive power flow problem is solved by integrating a genetic algorithm with a nonlinear interior point method. In [17], a pattern algorithm is used to decipher ac-dc optimal reactive power flow model with the generator capability limits. In [18], F. Capitanescu proposes a two-step approach to compute Reactive power reserves with respect to operating constraints and voltage stability. In [19], a programming based methodology is used to solve the optimal reactive power dispatch problem. In [20], A. Kargarian et al present a probabilistic algorithm for optimal reactive power provision in hybrid electricity markets with ambiguous loads. This paper proposes Earliglow strawberry plant algorithm (ESPA) [21-24] to solve optimal reactive power dispatch problem. In the proposed algorithm the capacity of computational agents is not constant from the start to finish. In each iteration the quantity of computational agents is replicated in an appropriate manner and then partial of the weakest agents are lay open to to decease. And computational agent is imperilled to both small and large movements

recurrently from the start to finish, which makes it conceivable to achieve both the local and global explorations synchronously. In the projected approach ESPA the computational agents do not converse with each other, and the above said duplication-elimination procedure united with a kind of sieve that persuades the agents on the road to the global best solution. The proposed ESPA algorithm has been evaluated on standard IEEE 57 bus test system.   The simulation results show   that our projected approach outclasses all the entitled reported algorithms in minimization of real power loss.

2. PROBLEM FORMULATION

The Optimal power Flow problem is measured as a common minimization problem with constraints, and can be written in the following form:

Minimize a (x, u)   (1)
Subject to b (x,u)=0   (2)
And
c (x,u)≤0   (3)

Where a(x,u) is the objective function. b(x,u) and c (x,u) are respectively the set of equality and inequality constraints. x is the vector of state variables, and u is the vector of control variables.

The state variables are the load buses (PQ buses) voltages, angles, the generator reactive powers and the slack active generator power:
$x=(P\_g1,\theta\_2,..,\theta\_N,V\_L1,.,V\_LNL,Q\_g1,..,Q\_gng)^\wedge T$ (4)

The control variables are the generator bus voltages, the shunt capacitors and the transformers tap-settings:
$u=(V\_g,T,Q\_c)^\wedge T$ (5)

or
$u=(V\_g1,...,V\_gng,T\_1,..,T\_Nt,Q\_c1,..,Q\_cNc)^\wedge T$ (6)

Where Ng, Nt and Nc are the number of generators, number of tap transformers and the number of shunt compensators respectively.

3. OBJECTIVE FUNCTION

3.1 Real power loss The objective of the reactive power dispatch is to diminish the Real power loss in the transmission network, which can be mathematically designated as follows:

$$F = PL = \sum_{k \in Nbr} g_k \left(V_i^2 + V_j^2 - 2V_i V_j cos\theta_{ij} \right)$$ (7)

or

$$F = PL = \sum_{i \in Ng} P_{gi} - P_d = P_{gslack} + \sum_{i \neq slack}^{Ng} P_{gi} - P_d$$ (8)

Where g_k : is the conductance of branch between nodes i and j, Nbr: is the total number of transmission lines in power systems. P_d: is the total active power demand, P_{gi}: is the generator active power of unit i, and P_{gsalck}: is the generator active power of slack bus.

3.2 Voltage profile enhancement

For minimizing the voltage deviation in PQ buses, the objective function becomes:
$F=PL+\omega\_v \times VD$ (9)

Where ω_v: is a weighting factor of voltage deviation.
VD is the voltage deviation given by:
$$VD = \sum_{i=1}^{Npq} |V_i - 1|$$ (10)

3.3 Equality Constraint   The equality constraint b(x,u) of the Optimal Reactive Power Dispatch problem is represented by the power balance equation, where the total power generation must cover the total power demand and the power losses:

$P_G = P_D + P_L$ (11)

3.4 Inequality Constraints The inequality constraints c(x,u) replicate the limits on components in the power system as well as the limits created to guarantee system security. Upper and lower bounds on the real power of slack bus, and reactive power of generators:

$$P_{gslack}^{min} \leq P_{gslack} \leq P_{gslack}^{max} \tag{12}$$

$$Q_{gi}^{min} \leq Q_{gi} \leq Q_{gi}^{max} , i \in N_g \tag{13}$$

Upper and lower bounds on the bus voltage magnitudes:

$$V_i^{min} \leq V_i \leq V_i^{max} , i \in N \tag{14}$$

Upper and lower bounds on the transformers tap ratios:

$$T_i^{min} \leq T_i \leq T_i^{max} , i \in N_T \tag{15}$$

Upper and lower bounds on the compensators reactive powers:

$$Q_c^{min} \leq Q_c \leq Q_C^{max} , i \in N_C \tag{16}$$

Where N is the total number of buses, N_T is the total number of Transformers; N_c is the total number of shunt reactive compensators.

4. NATURE OF EARLIGLOW STRAWBERRY

Earliglow strawberry plant (Fig 1) which promulgates through runners will do to augment its survival. If it is in an upright spot of the ground, with enough water, nutrients, and light, then it is sound to undertake that there is no stress on it to leave that spot to promise its survival. So, it will propel numerous short runners that will give new earliglow strawberry plants and inhabit the locality as greatest they can. If, on the other hand, the mother plant is in a spot that is meagre in water, nutrients, light, or any one of these essential for a plant to endure, then it will try to find a healthier spot for its offspring. So, it will propel few runners further afield to explore distant areas. One can also assume that it will propel only a limited, since sending a long runner is a large venture for a plant which is in a meagre spot. We may further assume that the class of the spot (abundance of nutrients, water, and light) is imitated in the development of the plant.
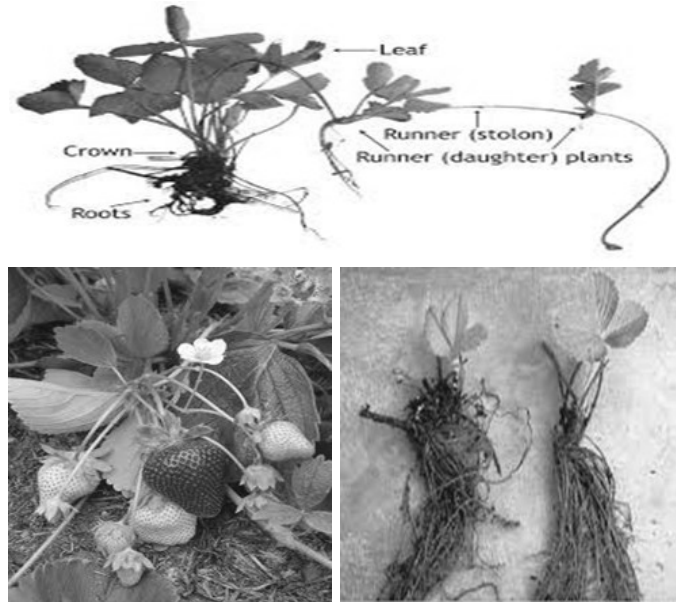
Fig 1. Earliglow strawberry plant

A plant p_i is in spot X_i in dimension n . This means $X_i = \{x_{i,}$ for $j = 1, \ldots, n\}$. Let NP be the number of strawberry plants to be used initially, and the Plant Propagation Algorithm (PPA) [22] trusts on the following policy.

(i)   Strawberry plants which are in noble spots propagate by engendering numerous short runners.

(ii)   Those in poor spots promulgate by producing few long runners.

It is clear that, in the above explanation, exploitation is applied by sending many short runners by plants in noble spots, while exploration is applied by sending few long runners by plants in meagre spots. The parameters used in PPA are the population size NP which is the number of strawberry plants, the maximum number of generation's g_{max}, and the maximum number of possible runner's n_{max} per plant. g_{max} is effectively the stopping criterion in this primary version of PPA. The algorithm uses the objective function value at different plant positions $X_i, i = 1, \ldots, NP$, in a regularized form N_i, to rank them as would a fitness function in a standard genetic algorithm. The number of plant runners, n_α^i calculated according to (17), has length dx^i calculated using the regularized form of the objective value at X_i, each giving a $dx^i \in (-1,1)^n$, as calculated with (18). Afterward all plants in the population have sent out their apportioned runners, new plants are appraised and the whole increased population is sorted. To keep the population continuous, individuals with lower growth are eradicated. The number of runners allocated to a given plant is proportionate to its fitness as in

$$n_\alpha^i = [n_{max} N_i \alpha], \alpha \in (0,1) \qquad (17)$$

Each solution X_i engenders at least one runner and the length of each such runner is contrariwise proportionate to its growth as in (18) below:

$$dx_j^i = 2(1 - N_i)(\alpha - 0.5), for\ j = 1, .., n \qquad (18)$$

where n is the problem dimension.

Having calculated dx_j^i, the extent to which the runner will reach, the exploration equation that finds the next area to discover is as follows

$$y_{i,j} = x_{i,j} + (b_j - a_j) dx_j^i, for\ j = 1, .., n. \qquad (19)$$

If the bounds of the exploration domain are desecrated, the point is accustomed to be within the domain $[a_j, b_j]$, where a_j and b_j are lower and upper bounds demarcating the exploration space for the jth coordinate.

5. EARLIGLOW STRAWBERRY PLANT ALGORITHM PLANT

In application of ESPA, the preliminary population is vital. We run the algorithm number of times from arbitrarily produced populations. The finest individual from each run forms a member of the preliminary population. The amount of runs to produce the preliminary population is NP ; so, the population size is $r = NP$. When this number is greater than a definite threshold, the variables are fixed for the rest of the run. Let pop be a common matrix containing the population of a given run. Its rows correspond to individuals. The following equation is used to produce an arbitrary population for each of the preliminary runs.

$$x_{i,j} = a_j + (b_j - a_j)\alpha, j = 1, .., n \qquad (20)$$

where $x_{i,j} \in [a_j, b_j]$ is the jth entry of solution X_i and a_j and b_j are the jth entries of the lower and upper bounds defining the exploration space of the problem and $\alpha \in (0, 1)$.

In the chief frame of the algorithm, before updating the population we produce a provisional population Φ to clutch new solutions produced from each individual in the population. Then we implement three rules with fixed amendment parameter P_m, chosen here, as $P_m = 0.79$. The first two rules are applied if the population is initialized arbitrarily.

Regulation one uses the following equation to modernize the population:

$$x_{i,j}^* = x_{i,j}(1 + \beta), j = 1, .., n \qquad (21)$$

where $\beta \in [-1, 1]$ and $x_{i,j}^* \in [a_j, b_j]$.

The produced individual X_i^{**} is calculated according to the objective function and is stored in Φ.

In regulation two another individual is produced with the same modification parameter $P_m = 0.79$ as in the following equation:

$$x_{i,j}^* = x_{i,j} + (x_{l,j} - x_{k,j})\beta, j = 1, .., n \qquad (22)$$

where $\beta \in [-1, 1]$, $x_{i,j}^* \in [a_j, b_j]$. l, k are conjointly special indices and are different from i.

The created individual X_i^* is appraised according to the objective function and is stored in Φ. The first two regulations are

valid for $r \leq NP$ the number of runs. For $r > NP$ the algorithm also attempts to identify entries which are settling to their ultimate values through a counter IN. If the jth entry in existing population has a low IN value, then it is adapted by implementing (23); or else it is left as it is. The following equation is used when modification is essential:

$$x_{i,j}^* = x_{i,j} + \left(x_{i,j} - x_{k,j}\right)\beta \, , j = 1,..,n \qquad (23)$$

where $\beta \in [-1, 1], x_{i,j}^* \in [a_j, b_j]$, and k is different from i. To preserve the size of the population constant, the extra plants at the bottom of the organized population are eradicated.

ESPA FOR SOLVING OPTIMAL REACTIVE POWER PROBLEM

Initialization: $g_{\max}, \text{NP}, r$

if $r \leq \text{NP}$ at that juncture

(iii)   Produce an arbitrary population of plants $pop = \{Xi \mid i = 1, 2, \ldots, \text{NP}\}$, using (20) and collect the best solutions.

end if

while $r > \text{NP}$ do

Use population pop_g formed by congregation all best solutions from preceding runs. Compute IN_j value for each column j of pop_g

end while

Estimate the population. In case of pop_g the algorithm does not need to estimate the population,

Set number of runners

while $(ngen < g\max)$ do

Generate Φ:

for $i = 1$ to NP do

for $k = 1$ to n_r do

if $r \leq \text{NP}$ then

if rand $\leq P_m$ then

Produce a new-fangled solution $x_{i,j}^*$ according to (21);

Calculate it and store it in Φ;

end if

if rand $\leq P_m$ then

Produce a new-fangled solution $x_{i,j}^*$ according to (22);

Estimate it and store it in Φ;

end if

else

for $j = 1 : n$ do

if (rand $\leq P_m$) then

Modernize the j th entry of X_i, $i = 1,2,..,\text{NP}$, according to (23);

end if

Calculate new-fangled solution and store it in Φ;

end for

end if

end for

end for

Augment Φ to existing population;

Arrange the population in uphill order of the objective values;

Modernize current best;

end while

Return: Modernised population.

6. SIMULATION RESULTS

The projected ESPA algorithm for solving ORPD problem is tested in standard IEEE-57 bus power system. The IEEE 57-bus system data consists of 80 branches, 7 generator-buses and 17 branches under load tap setting transformer branches. The probable reactive power compensation buses are 18, 25 and 53. Bus 2, 3, 6, 8, 9 and 12 are PV buses and bus 1 is nominated as slack-bus. In this case, the exploration space has 27 dimensions, i.e., the seven generator voltages, 17 transformer taps, and three capacitor banks. The system variable limits are given in Table 1. The prime conditions for the IEEE-57 bus system are given as follows:

P_{load} = 12.425 p.u. Q_{load} = 3.339 p.u.

The complete primary generations and power losses are obtained as follows:

$\sum P_G$ = 12.7728 p.u. $\sum Q_G$ = 3.4559 p.u.

P_{loss} = 0.27447 p.u. Q_{loss} = -1.2243 p.u.

Table 2 shows the various system control variables i.e. generator bus voltages, shunt capacitances and transformer tap settings acquired after ESPA based optimization which are within their satisfactory limits. In Table 3 a comparison of optimum results attained from proposed ESPA with other optimization techniques for optimal reactive power dispatch (ORPD) problem.

TABLE 1: VARIABLES LIMITS FOR IEEE-57 BUS POWER SYSTEM (P.U.)

REACTIVE POWER GENERATION LIMITS							
BUS NO	1	2	3	6	8	9	12
Q_{GMIN}	-1.1	-.010	-.01	-0.01	-1.1	-0.02	-0.2
Q_{GMAX}	1	0.1	0.1	0.23	1	0.01	1.50
VOLTAGE AND TAP SETTING LIMITS							
V_{GMIN}		V_{GMAX}		V_{PQMIN}	V_{PQMAX}	T_{KMIN}	T_{KMAX}
0.5		1.0		0.91	1.01	0.5	1.0
SHUNT CAPACITOR LIMITS							
BUS NO		18		25		53	
Q_{CMIN}		0		0		0	
Q_{CMAX}		10		5.1		6.2	

Table 2: control variables obtained after optimization by ESPA method for IEEE-57 bus system (p.u.).

Control Variables	ESPA	Control Variables	ESPA	Control Variables	ESPA
V1	1.1	T4-18	1.019	T13-49	1.057
V2	1.068	T21-20	1.053	T11-43	0.919
V3	1.056	T24-25	0.968	T40-56	0.908
V6	1.049	T24-26	0.939	T39-57	0.969
V8	1.064	T7-29	1.076	T9-55	0.975
V9	1.038	T34-32	0.938		
V12	1.044	T11-41	1.019		
Qc18	0.0847	T15-45	1.052		
Qc25	0.333	T14-46	0.926		
Qc53	0.0626	T10-51	1.034		

Table 3: Comparative optimization results for IEEE-57 bus power system (p.u.)

S.No.	Optimization Algorithm	Best Solution	Worst Solution	Average Solution
1	NLP [25]	0.25902	0.30854	0.27858
2	CGA [25]	0.25244	0.27507	0.26293
3	AGA [25]	0.24564	0.26671	0.25127
4	PSO-w [25]	0.24270	0.26152	0.24725
5	PSO-cf [25]	0.24280	0.26032	0.24698
6	CLPSO [25]	0.24515	0.24780	0.24673
7	SPSO-07 [25]	0.24430	0.25457	0.24752
8	L-DE [25]	0.27812	0.41909	0.33177
9	L-SACP-DE [25]	0.27915	0.36978	0.31032
10	L-SaDE [25]	0.24267	0.24391	0.24311
11	SOA [25]	0.24265	0.24280	0.24270
12	LM [26]	0.2484	0.2922	0.2641
13	MBEP1 [26]	0.2474	0.2848	0.2643
14	MBEP2 [26]	0.2482	0.283	0.2592
15	BES100 [26]	0.2438	0.263	0.2541
16	BES200 [26]	0.3417	0.2486	0.2443
17	Proposed ESPA	0.22338	0.23457	0.23103

7. CONCLUSION

In this paper, the ESPA has been successfully implemented to solve Optimal Reactive Power Dispatch problem. The proposed algorithm has been tested on the standard IEEE 57 -bus system. Simulation results indicate the toughness of projected ESPA approach for providing better optimal solution in reducing the real power loss. The control variables obtained after the optimization by ESPA is within the limits.

REFERENCES

1. O.Alsac,and B. Scott, "Optimal load flow with steady state security",IEEE Transaction. PAS -1973, pp. 745-751.

2. Lee K Y ,Paru Y M , Oritz J L –A united approach to optimal real and reactive power dispatch , IEEE Transactions on power Apparatus and systems 1985: PAS-104 : 1147-1153

3. A.Monticelli , M .V.F Pereira ,and S. Granville , "Security constrained optimal power flow with post contingency corrective rescheduling" , IEEE Transactions on Power Systems :PWRS-2, No. 1, pp.175-182.,1987.

4. Deeb N ,Shahidehpur S.M ,Linear reactive power optimization in a large power network using the decomposition approach. IEEE Transactions on power system 1990: 5(2) : 428-435

5. E. Hobson ,'Network consrained reactive power control using linear programming, ' IEEE Transactions on power systems PAS -99 (4) ,pp 868=877, 1980

6. K.Y Lee ,Y.M Park , and J.L Oritz, "Fuel –cost optimization for both real and reactive power dispatches" , IEE Proc; 131C,(3), pp.85-93.

7. M.K. Mangoli, and K.Y. Lee, "Optimal real and reactive power control using linear programming" , Electr.Power Syst.Res, Vol.26, pp.1-10,1993.

7. C.A. Canizares , A.C.Z.de Souza and V.H. Quintana , " Comparison of performance indices for detection of proximity to voltage collapse ,'' vol. 11. no.3 , pp.1441-1450, Aug 1996 .

8. S.R.Paranjothi ,and K.Anburaja, "Optimal power flow using refined genetic algorithm", Electr.Power Compon.Syst , Vol. 30, 1055-1063,2002.

9. D. Devaraj, and B. Yeganarayana, "Genetic algorithm based optimal power flow for security enhancement", IEE proc-Generation.Transmission and. Distribution; 152, 6 November 2005.

10. A. Berizzi, C. Bovo, M. Merlo, and M. Delfanti, "A ga approach to compare orpf objective functions including secondary voltage regulation," Electric Power Systems Research, vol. 84, no. 1, pp. 187 − 194, 2012.

11. C.-F. Yang, G. G. Lai, C.-H. Lee, C.-T. Su, and G. W. Chang, "Optimal setting of reactive compensation devices with an improved voltage stability index for voltage stability enhancement," International Journal of Electrical Power and Energy Systems, vol. 37, no. 1, pp. 50 − 57, 2012.

12. P. Roy, S. Ghoshal, and S. Thakur, "Optimal var control for improvements in voltage profiles and for real power loss minimization using biogeography based optimization," International Journal of Electrical Power and Energy Systems, vol. 43, no. 1, pp. 830 − 838, 2012.

13. B. Venkatesh, G. Sadasivam, and M. Khan, "A new optimal reactive power scheduling method for loss minimization and voltage stability margin maximization using successive multi-objective fuzzy lp technique," IEEE Transactions on Power Systems, vol. 15, no. 2, pp. 844 − 851, may 2000.

15. W. Yan, S. Lu, and D. Yu, "A novel optimal reactive power dispatch method based on an improved hybrid evolutionary programming technique," IEEE Transactions on Power Systems, vol. 19, no. 2, pp. 913 − 918, may 2004.

16. W. Yan, F. Liu, C. Chung, and K. Wong, "A hybrid genetic algorithminterior point method for optimal reactive power flow," IEEE Transactions on Power Systems, vol. 21, no. 3, pp. 1163 −1169, aug. 2006.

17. J. Yu, W. Yan, W. Li, C. Chung, and K. Wong, "An unfixed piecewiseoptimal reactive power-flow model and its algorithm for ac-dc systems," IEEE Transactions on Power Systems, vol. 23, no. 1, pp. 170 −176, feb. 2008.

18. F. Capitanescu, "Assessing reactive power reserves with respect to operating constraints and voltage stability," IEEE Transactions on Power Systems, vol. 26, no. 4, pp. 2224–2234, nov. 2011.

19. Z. Hu, X. Wang, and G. Taylor, "Stochastic optimal reactive power dispatch: Formulation and solution method," International Journal of Electrical Power and Energy Systems, vol. 32, no. 6, pp. 615 − 621, 2010.

20. A. Kargarian, M. Raoofat, and M. Mohammadi, "Probabilistic reactive power procurement in hybrid electricity markets with uncertain loads," Electric Power Systems Research, vol. 82, no. 1, pp. 68 − 80, 2012.

21. X.-S. Yang, Nature-Inspired Metaheuristic Algorithms, Luniver Press, 2011.

22. A. Salhi and E. S. Fraga, "Nature-inspired optimization approaches and the new plant propagation algorithm," in Proceedings of the The International Conference on Numerical Analysis and Optimization (ICeMATH '11), Yogyakarta, Indonesia,2011.

23. J. Brownlee, Clever Algorithms: Nature-Inspired Programming Recipes, 2011.

24. Muhammad Sulaiman, Abdellah Salhi,Birsen Irem Selamoglu,and Omar Bahaaldin Kirikchi, A Plant Propagation Algorithm for Constrained Engineering Optimisation Problems, Mathematical Problems in Engineering Volume 2014, Article ID 627416, 10 pages http://dx.doi.org/10.1155/2014/627416

25. Chaohua Dai, Weirong Chen, Yunfang Zhu, and Xuexia Zhang, "Seeker optimization algorithm for optimal reactive power dispatch," IEEE Trans. Power Systems, Vol. 24, No. 3, August 2009, pp. 1218-1231.

26. J. R. Gomes and 0. R. Saavedra, "Optimal reactive power dispatch using evolutionary computation: Extended algorithms," IEE Proc.-Gener. Transm. Distrib.. Vol. 146, No. 6. Nov. 1999.

KEEPING UP SECURITY IN ANONYMIZING WIRELESS MESH NETWORKS

K.Venkat Reddy

Student, M.Tech CSE Dept., Institute of Aeronautical Engineering,
Hyderabad-500043, Telangana, India,
venkatreddy90001@gmail.com

Dr. N. Chandra Sekhar Reddy*

Professor, CSE Dept, Institute of Aeronautical Engineering,
Hyderabad -500043, Telangana, *India,*
naguchinnu@gmail.com
*Corresponding Author

ABSTRACT

Remote security has been the interesting issue for different system innovations, for example, cell systems, remote neighborhood (Wlans), remote sensor systems, portable impromptu systems (Manets), and vehicular specially appointed systems (Vanets). Namelessness and protection issues have picked up impressive exploration deliberations in the framework, which have concentrated on exploring secrecy in diverse connection or application situations. One prerequisite for secrecy is to unlink a client's character to his or her particular exercises, for example, the namelessness satisfied in the untraceable e-money frameworks and the P2p installment frameworks, where the installments can't be connected to the personality of a payer by the bank or dealer. Obscurity is additionally needed to shroud the area data of a client to forestall development following, as is critical in portable systems and Vanets. Security in anonymizing systems are executed for fair clients & following of acting up clients for system compelling voices in WMNs. The ensuring essential security necessities including validation, classifiedness, information uprightness, and no disavowal is additionally proposed. Intensive investigation on security and effectiveness is fused, exhibiting the practicality and viability of the proposed framework.

Keywords— *Anonymity, traceability, pseudonym, revocation, wireless network*

1. INTRODUCTION

Remote Mesh Network (WMN) is a guaranteeing engineering and is required to be broad because of its low speculation characteristic and the remote broadband administrations it backs, alluring to both administration suppliers and clients. Be that as it may, security issues characteristic in Wmns or any remote systems need be considered before the organization and multiplication of these systems, since it is unappealing to endorsers of get administrations without security and protection ensures. Remote security has been the hotly debated issue in the writing for different system innovations, for example, cell systems, remote neighborhood (Wlans), remote sensor systems, portable impromptu systems (Manets) and vehicular specially appointed systems (Vanets)[1]. As of late, new suggestions on WMN security have risen. In [7], the creators portray the specifics of Wmns and recognize three key system operations that need to be secured. We propose an assault strong security building design (ARSA) for Wmns, tending to countermeasures to an extensive variety of assaults in Wmns. Because of the way that security in Wmns is still in its early stages as next to no consideration has been dedicated as such, a lion's share of security issues have not been tended to and are studied in. Namelessness and security issues have picked up significant exploration exertions in the writing which have concentrated on exploring obscurity in distinctive setting or application scenarios[4],[5]. One prerequisite for namelessness is to unlink a client's character to his or her particular exercises, for example, the secrecy satisfied in the untraceable e-money frameworks and the P2p installment frameworks where the installments can't be joined to the personality of a payer by the bank or specialist. Namelessness is additionally needed to conceal the area data of a client to avoid development following, as is imperative in versatile systems and Vanets .In remote correspondence frameworks, it is less demanding for a worldwide onlooker to mount movement examination assaults by emulating the bundle sending way than in wired systems. In this way, directing secrecy is key,

which covers the classified correspondence relationship of two gatherings by building an unacknowledged way between them [3]. By and by, genuine secrecy may bring about insider assaults since acting up clients are no more traceable. In this way, traceability is profoundly alluring, for example, in e-money frameworks where it is utilized for distinguishing and following twofold spenders. In this paper, we are inspired by determining the above security clashes, specifically obscurity and traceability, in the developing WMN correspondence frameworks. We have proposed the introductory outline of our security structural engineering in [1], here the possibility and relevance of the building design were not completely caught on. As an issue, we give definite effectiveness investigation regarding stockpiling, correspondence, and processing in this paper to demonstrate that our SAT is an essentially feasible answer for the application situation of premium. Our framework gets the visually impaired mark system from installment frameworks and consequently, can accomplish the namelessness of unlinking client characters from exercises, and additionally the traceability of getting into mischief clients. Moreover, the proposed nom de plume renders client area data unexposed. Our work varies from past work in that Wmns have one of a kind various leveled topologies and depend vigorously on remote connections, which must be considered in the obscurity plan. As an issue, the first namelessness plan for installment frameworks among bank, client, and store can't be specifically connected. Notwithstanding the obscurity plan, other security issues, for example, confirmation, key foundation, and disavowal are basic in Wmns to guarantee the right application of the namelessness plan.
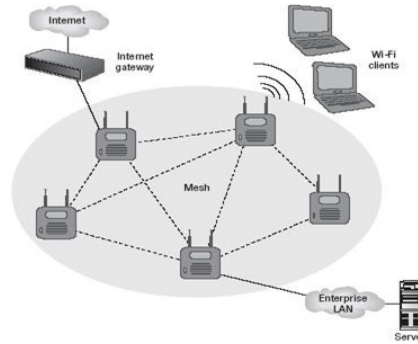
Fig 1: Remote mesh network

2. CONNECTED WORK

IBC FROM BILINEAR PAIRINGS ID-based cryptography (IBC) allows the public key of an entity to be derived from its public identity information such as name and e-mail address, which avoids the use of certificates for public key verification in the conventional public key infrastructure (PKI). Boneh and Franklin introduced the first functional and efficient ID-based encryption scheme based on bilinear pairings on elliptic curves. Specifically, let G_1 and G_2 be an additive group and a multiplicative group, respectively, of the same prime order p. The Discrete Logarithm Problem (DLP) is assumed to be hard in both G_1 and G_2. Let P denote a random generator of G_1 and G2 $e: G_1 \times G_1 \rightarrow G_2$ denote a bilinear map constructed by modified Weil or Tate pairing with the following properties:

- Bilinear: $e(aP, bQ) = e(P, Q)^{ab}$, $\forall P, Q \in G_1$ and $\forall a, b \in Z_P^*$ where Z_P^* denotes the multiplicative group of, Z_P, the integers modulo p. In Particular, $Z_P^* = \{x | 1 \leq x \leq p - 1\}$ since p is prime.
- Non degenerate : $\exists P, Q \in G_1$ such that $e(P, Q) \neq 1$.
- Computable: there exists an efficient algorithm to compute $e(P, Q), \forall P, Q \epsilon G_1$.

BLIND SIGNATURE Blind mark is initially presented by Chaum. When all is said in done, a visually impaired mark plan permits a recipient to acquire a signature on a message such that both the message and the ensuing mark stay obscure to the underwriter. We allude the per users to for a formal meaning of a visually impaired mark plan, which ought to shoulder the properties of certainty, unlink ability, and unforgeability as indicated by. Brands created the first prohibitive visually impaired mark plan, where the limitation property is fused into the visually impaired mark plan such that the message being marked must contain encoded data. As the name recommends, this property confines the client in the visually impaired mark plan to install some record related mystery data into what is generally marked by the bank (overall, the marking will be unsuccessful) such that this mystery can be recuperated by the bank to recognize a client if and on the off chance that he twofold uses. The limitation property is basically the certification for traceability in the prohibitive visually impaired mark frameworks.

VERIFIABLE PLAINTEXT To determine whether or not a given key produces a valid ticket, the client software examines the decrypted ticket fields to see if they make sense. If the wrong key was used, and if the software attempts to find a null terminator for each string, it may find too many or not enough of them for the number of strings in a ticket. It may also discover that some of the other fields, like the timestamp or length fields, are internally inconsistent.

0	1	2	3	4	5	6	7	8	9	10	11	12	13	14	15
X	X	X	X	X	X	X	X	'k'	'r'	'b'	't'	'g'	't'	'\0'	-

X = DES Key byte

It gives the attacker an important piece of information that greatly simplifies this check: The service name" field, which is the second field of the decrypted ticket, is always the string krbtgt for TGT packets. Since those seven bytes (positions 8-14) are always within the second block B1, only the first two blocks of the TGT need to be decrypted before the correctness of the guess can be verified. The probability of this string occurring at random in the right location despite having the wrong key is only 2-56, so finding this string in the second block is a highly reliable indicator of success. For each user, then, only the first two blocks (T0; T1) of his encrypted TGT need to be stored, and each trial password require only one call to STRING-TO-KEY and two DES decryptions.

3. PLANNED WORK

DEFINITIONS First, we give a list of definitions that are frequently used in this paper.

Secrecy (Untraceability): the obscurity of a true blue customer alludes to the untraceability of the customer's system access exercises. The customer is said to be unacknowledged if the TA, the passage, and even the agreement of the two can't connect the customer's system access exercises to his genuine character.. Traceability: a honest to goodness customer is said to be traceable if the TA has the capacity connect the customer's system access exercises to the customer's genuine character if and if the customer gets rowdy, i.e., one or both of the accompanying happens: ticket reuse and different store.

Ticket reuse: one kind of trouble making of an authentic customer that alludes to the customer's utilization of a drained ticket (Val ¼ 0).

Different store: one kind of misconduct of a genuine customer that alludes to the customer's exposure of his legitimate ticket and related insider facts to unapproved elements or customers with rowdiness history, so these blending customers can increase system access from distinctive doors at the same time.

Intrigue: The conniving of malevolent TA and door to follow an authentic customer's system access exercises in the TA's space (i.e., to trade off the customer's namelessness).

Confining: A sort of assault mounted by a malevolent TA keeping in mind the end goal to renounce a honest to goodness customer's system access benefit. In this assault, the TA can create a false record number and partner it with the customer's personality. The TA can then make substantial tickets focused around the false record number and confer misrepresentation (i.e., act up). Thusly, the TA has the capacity dishonestly blame the customer to have acted up, and therefore, to deny his right to gain entrance right
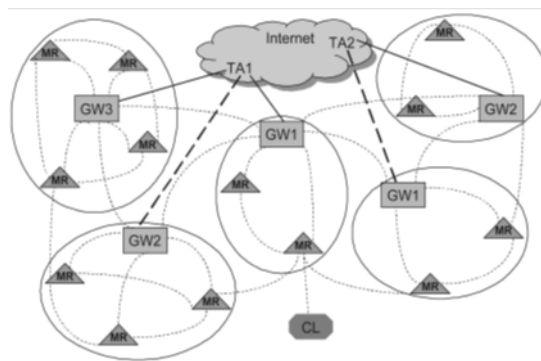
Fig 2: Network topology of a typical WMN.

SYSTEM ARCHITECTURE Consider the system topology of an ordinary WMN portrayed in Fig. 1. The remote cross section spine comprises of lattice switches (Mrs) and passages (Gws) interconnected by customary remote connections (demonstrated as dabbed bends). Network switches and entryways serve as the right to gain entrance purposes of the WMN and the last falls back on the Internet, individually. The healing center, grounds, endeavor, and private structures are occasions of individual WMN areas subscribing to the Internet administrations from upstream administration suppliers, demonstrated as the Internet cloud in Fig. 1. Each wmn domain, or trust area (to be utilized conversely) is overseen by a space manager that serves as an issue power (TA), e.g., the focal server of a facilities WMN. The TA and related passages are joined by high velocity wired or remote connections, showed as strong and striking dashed lines, individually. Tas and entryways are thought to be equipped for taking care of computationally serious assignments. Moreover, they are thought to be ensured in private spots and can't be effortlessly bargained because of their vital parts in the WMN. The WMNs of enthusiasm here are those where the TA gives free Internet get to however require the customers (Cls) to be approved and subsidiary parts by and large for a long haul, as the workers or understudies on account of big business and healing center WMNs or yard WMNs.

TRUST RELATIONSHIP All in all, the TA is trusted inside the WMN area. There is no immediate trust relationship

between the customer and the portal/network switch. We will utilize standard IBC for verification and secure correspondences both at the spine and amid system get to inside a trust space (i.e., intradomain). We further accept the presence of preshared keys and secure correspondence channels between substances (Tas, passages, network switches) at the spine and will singularly consider the validation and key foundation amid the system access of the customers. The customer displays his ID upon enlistment at the TA, which appoints a private key connected with the customer's ID. The customer chooses an one of a kind record number _ processed by a haphazardly picked mystery number u1 (cf., Section 4.1.1). The record number is put away with the customer's ID at the TA. The TA additionally allots an ID/private key pair to every door and cross section switch in its trust area before organization. Favorable circumstances of this general trust association with the TA stem from the immediate confirmation of the customers going among entryways/network switches in the same area, which lessens system access dormancy and correspondence overhead that is relied upon to be overpowering in future WMNs because of the vast client populace and high versatility.
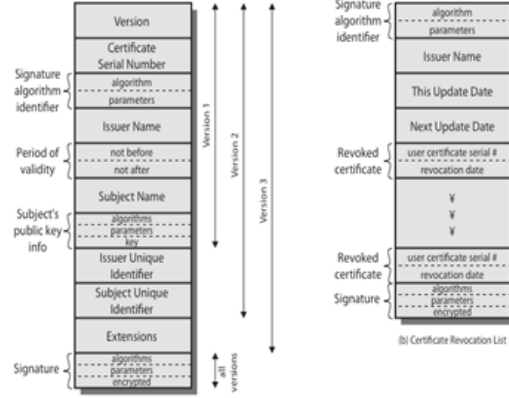
Fig 3

4. SECURITY ARCHITECTURE

TICKET-BASED SECURITY ARCHITECTURE First, we restrict our discussion to within the home domain. The interdomain protocols in our security architecture, which are executed when the client roams outside his home domain, will be presented in Section The ticket-based security architecture consists of ticket issuance, ticket deposit, fraud detection, and ticket revocation protocols. In what follows, we will describe these protocols in detail, together with the fulfillment of authentication, data integrity, and confidential communications that may take place during the execution of these protocols [1].

TICKET DEPOSIT After obtaining a valid ticket, the client may deposit it anytime the network service is desired before the ticket expires, using the ticket deposit protocol shown below. Our scheme restricts the ticket to be deposited only once at the first encountered gateway that provides network access services to the client according to *val* before *exp*. [5]

$$1. \, CL \rightarrow\rightarrow GW : PS_{CL}, m', W, c,$$
$$\sigma = (U', V', X', \rho, \sigma_1', \sigma_2'), t_5,$$
$$SIG_{\Gamma_{CL}} \sim (m' \parallel W \parallel c \parallel \sigma \parallel t_5);$$

$$2. \, GW \rightarrow\rightarrow CL : ID_{GW}, d = H_3(R \parallel W \parallel ID_{GW} \parallel T), t_6, HMAC_k(d \parallel t_6);$$

The ticket is regarded substantial if both the mark confirmation and the above equity check succeed. The store door (DGW), where the ticket is at first kept, will then create a signature on the customer's alias, DGW's ID, and the related misb and exp qualities extricated from c. The mark is obliged to be available in place for different access focuses in the trust area to figure out if and where to forward the customer's right to gain entrance demands, if the stored ticket will be further utilized from different access focuses. This is the motivation behind why the customer is not permitted to change his alias as of now utilizing a saved ticket to which the nom de plume related, since the DGW will decline to offer access administrations to the customer if the present pen name the one recorded with the ticket. As an issue, the ticket worth need to be set to a generally little amount with a specific end goal to permit successive upgrade of the pen name the customer has high prerequisite on his namelessness. It won't put additional flagging overhead into the framework since the TA can give a group of little esteemed tickets amid one single ticket issuance convention. Because of the constrained ticket esteem, the customer is relied upon to have insignificant portability amid the use of the kept ticket. On the other hand, there are likewise situations where the customer moves to different passages after the ticket is stored. To address this issue, conceivable choice making functionalities may be joined into passages. Case in point, if the customer briefly moves to another passage in the DGW's region, the new portal can simply forward all the activity of this customer to the DGW, which then administrations the customer focused around the stored ticket. In the event that the customer forever moves to another door,

the new portal may ask for the DGW to exchange the ticket record so that the new passage can specifically benefit the customer. We don't plan to further address this issue. Rather, a straightforward and productive arrangement can be utilized to desert the utilization of the remaining ticket and stores another one at the new passage since the ticket quality is for the most part not huge. This arrangement is likewise successful when the continuous administration is disturbed because of channel debilitations, course disappointments, or versatility, and in addition when the customer tries to keep away from mixed up numerous store. Embracing this arrangement, Step 4, in the above technique can be excluded. Then again, if secrecy is not entirely needed by the customer, he can demand tickets with higher values that can be utilized for more of an opportunity under a same pen name.

FRAUD DETECTION Misrepresentation is utilized reciprocally with misconduct as a part of this paper, which is basically an insider assault. Ticket reuse by and large comes about because of the customer's failure to get tickets from the TA when system access is coveted, principally because of the customer's past mischief, which causes the TA to oblige his ticket demands. Various -store can likewise be termed customer coalition, which is useful when the combining gatherings are unapproved clients or customers with trouble making history experiencing issues in obtaining tickets from the TA. Note, in any case, that since a customer has the capacity get numerous tickets in one ticket issuance convention and self-create various pen names, can convey these pen name/sets to different customers without being followed the length of each one ticket is kept just once. A conceivable solution for this circumstance is to detail the no covering dynamic time of a ticket rather than only the expiry date/time such that each one time, stand out ticket can be legitimate. This methodology, all in all, obliges synchronization. An alternate arrangement is to receive the carefully designed secure module so that a customer can't reveal his mysteries to different gatherings since the safe module is thought to be costly and illogical to get to or control. This methodology will wipe out the different store misrepresentation yet requires the arrangement of secure modules. In the accompanying exchange, we will at present consider various store as an issue sort of extortion (e.g., in the event that that safe modules are inaccessible). These two sorts of extortion impart a typical peculiarity, that is, a same ticket (exhausted or substantial) is saved more than once such that our one-time store principle is abused. This is the place the limitation of the visually impaired mark calculation takes impact on uncovering the true personality of the making trouble customer. Particularly, when the TA recognizes copy stores utilizing the ticket records reported by passages, the TA will have the perspective of no less than two separate difficulties from entryways and two relating sets of reactions from the same customer. By explaining the comparison sets underneath focused around these difficulties and reactions, the TA has the capacity acquire the character data encoded in the message, and henceforth, the genuine personality of the acting mischievously customer. The extortion recognition convention is appeared

$$GW \rightarrow TA: ID_{GW}, m', W, c,$$

$$\sigma = (U', V', X', \rho, \sigma_1', \sigma_2'), r_1, r_2, T, t_9, H,$$

$$HMAC_k\big((m' \parallel W \parallel c \parallel \sigma \parallel r_1 \parallel r_2 \parallel T \parallel t_9)\big)$$

By a wide margin, we have introduced the procedures to purpose the clashes in the middle of namelessness and traceability. The length of the customer is an overall acted client in this system, his secrecy can be completely ensured. This is accomplished by the blinding methodology of the ticket issuance convention, which breaks the linkage between the ticket and the character, i.e., the TA knows the customer's true ID however does not know which ticket/ pen name fit in with this customer, while the portal knows the linkage between the ticket and the nom de plume adapts no data on the genuine personality of the holder of these sets. Then again, if the customer gets out of hand (i.e., extortion happens), the customer's namelessness can never again be ensured since the TA may have a tendency to distinguish this customer, and thusly, rebuff him conceivably by disavowing the customer's system access benefit, leveraging the traceability property offered by our security construction modeling. What's more, our framework empowers confirmation at the right to gain entrance focuses and meets the right to gain entrance control security necessity that is not fulfilled in, where no validation of the customer is performed at the right to gain entrance point in the controlled.

TICKET REVOCATION Ticket disavowal is fundamental when a customer is traded off, and along these lines, all his mysteries are revealed to the enemy. In our framework, the foe is propelled by picking up system administrations utilizing tickets once the ticket related insider facts are acquired from the bargained customers. In this way, the traded off customer needs to have the capacity to disavow the ticket and keep the enemy from gaining advantages. The bargained customer and the enemy are the main two gatherings that are in ownership of the ticket-related privileged insights, a legitimate disavowal appeal must be sent by the traded off customer for certified denial reason since the foe increases nothing in doing so. The ticket renouncement convention comprises of two cases as takes after:

- Denial of new tickets: the customer may store various unused tickets, as said beforehand. At the point when renouncing these tickets that have not been kept, the customer sends PSCL, TN, t10, Sig_(γ_cl) in the repudiation appeal to any experienced door. This portal confirms the customer utilizing PSCL and records the ticket serial number TN as disavowed.

- Denial of saved tickets: the customer essentially sends PSCL, IDDGW, t11, Sig_(γ_cl) in the renouncement

appeal to the DGW. The DGW confirms the customer and imprints the related ticket repudiated. At the point when doors have records in the renouncement database, they instantly report the denials to the home TA, which will redesign and appropriate the repudiation list for all portals in the trust space to referenced.

PSEUDONYM GENERATION AND REVOCATION The use of pseudonyms has been shown in the ticket-based protocols. This section copes with the pseudonym generation technique and the related revocation issue. The pseudonym is used to replace the real ID in the authentication, which is necessary for both anonymous network access and location privacy. Compared to [6], [8], where a batch of pseudonyms are assigned to each client by the TA, the self-generation method vastly reduces the communication overhead in the system. Moreover, the client is able to frequently update his pseudonyms (with tickets) to enhance anonymity by using this inexpensive method. When accessing the network from a foreign domain, suppose a client CLj residing at level j is requesting Network access from a foreign mesh router MR in a visiting Trust domain. As a final note on the self-generation algorithm, it would render the pseudonym revocation impossible by using the pseudonym alone. The reason is that any adversary who has compromised a client can generate valid pseudonym/ key pairs that are only known to the adversary by running the self-generation algorithm. However, this pseudonym self-generation technique is appropriate in our system because the pseudonym revocation can be realized via revoking the associated ticket since the pseudonym is active only when its associated ticket is actively in use (deposited and not depleted).

5. SECURITY ANALYSIS

In this area, we investigate the security necessities our framework can accomplish as takes after: Again, we utilize hypotheses as a part of for show and the investigation utilizing hypotheses as a part of can be completed in a comparable manner. Major security goals. It is paltry to demonstrate that our security building design fulfills the security prerequisites for confirmation, information respectability, and privacy, which takes after straightforwardly from the job of the standard cryptographic primitives, specifically advanced mark, message validation code, and encryption, in our framework. We are just left with the confirmation of nonrepudiation in this classification. A misrepresentation can be renounced just if the customer can give an alternate representation he knows of m from what is inferred by the TA. In the event that the customer has made trouble, the representation he knows will be the same as the one determined by the TA which guarantees nonrepudiation. Secrecy. Most importantly, it can be effectively demonstrated that a passage can't interface a customer's system access exercises to his true character. Because of the utilization of nom de plumes confirmation which uncovers no data on the genuine ID, the door adapts nothing about the character of the customer asking for system access. Since the alias produced by the customer utilizing his mystery number, unraveling for the true personality from the pen name identical to illuminating the DLP. Besides, the customer's store passage (DGW) can't conclude the customer's ID from the saved ticket, which has been blinded by the customer and does not uncover any recognizable proof data unless misconduct happens. At long last, we demonstrate that even the agreement of the home TA and the DGW can't do the joining. It is clear that by intrigue, the TA can gain no more from the passage than the customer's pen name in relationship with a stored ticket. The hardness of concluding a genuine character from an alias been specified previously. Then again, the portal can take in the accompanying from the TA Traceability (restrictive secrecy). As indicated by its definition, this necessity is twofold: 1) Anonymity for legit customers is unlimited, which can be demonstrated after 2) A getting out of hand customer is traceable where the character can be uncovered. The verification of point 2 takes after from [1, Theorem 2] that the received prohibitive incompletely visually impaired mark conspire in our security building design attains limitation. As such, point 2 expresses that the customer can just acquire marks on messages of which the customer knows a representation for which the structure in the representation (where the character data is encoded) stays, demonstrated by utilizing and two additional necessities on the representations the customer knows ofmandm0 (see [2] for nitty gritty depiction of the two prerequisites). Confining safety. In the event that the customer is fair, with overpowering likelihood, the representation he knows is not quite the same as that the pernicious TA erroneously created. Decent the customer couldn't have thought of this representation independent from anyone else; it demonstrates that the TA endeavors to casing the customer. Thusly, blameless customers can exonerate themselves to keep vindictive Tas from disavowing their system access benefit. Unforgeability. The verification of unforgeability (formally characterized in [2]) is basically the confirmation of [1] that the embraced prohibitive incompletely visually impaired mark plan is existentially unforgeable against adaptively picked message and ID assaults under the suspicion of the obstinacy of CDHP in G1 and the arbitrary prophet. We presume that the proposed security structural planning fulfills the security necessities for namelessness, traceability, confining safety, and unforgeability, notwithstanding the principal destinations including confirmation, information respectability, classifiedness, and nonrepudiation, under the suspicion that CDHP in G1 is hard and the arbitrary prophet.

6. CONCLUSION

We propose a security construction modeling fundamentally comprising of the ticket-based conventions, which determines the clashing security necessities of unqualified secrecy for genuine clients and traceability of acting mischievously clients. By using the tickets, self-created aliases, the various leveled character based cryptography, the proposed structural engineering is showed to accomplish fancied security targets and productivity. The famous issue regular in P2p correspondence frameworks is the free-riding, where a few associates exploit the framework by giving almost no

administration to different companions or by leaving the framework promptly after the administration needs are fulfilled. Peer participation is accordingly the essential necessity for P2p frameworks to work legitimately. Since companions are thought to be self centered, motivator instruments get to be key to advance companion participation as far as both agreeability and accessibility. Commonplace impetus components for advancing agreeability incorporate notoriety and installment based methodologies. In the notoriety based frameworks, companions are rebuffed or remunerated focused around the watched conduct. Nonetheless, low accessibility remains an inconspicuous conduct in such frameworks, which blocks the practicality of the notoriety based component in enhancing companion accessibility. By difference, the installment based methodology gives sufficient motivations to improving both helpfulness and accessibility, and in this manner, is perfect to be utilized in multihop uplink correspondences among associate customers in our WMN framework

REFERENCES

1. IEEE TRANSACTIONS ON DEPENDABLE AND SECURE COMPUTING, VOL. 8, NO. 2, MARCH-APRIL 2011 "SAT: A Security Architecture Achieving Anonymity and Traceability in Wireless Mesh Networks"

2. H. Balakrishnan, C. Barrett, V. Kumar, M. Marathe, and S. Thite. The distance-2 matching problem and its relationship to the maclayer capacity of ad hoc networks. IEEE Journal on Selected Area in Communications, 22, 2004.

3. L. Bui, R. Srikant, and A. L. Stolyar. Novel architectures and algorithms for delay reduction in back-pressure scheduling and routing. INFOCOM Mini-Conference, 2009.

4. P. Chaporkar, K. Kar, and S. Sarkar. Throughput guarantees through maximal scheduling in wireless networks. In 43rd Annual Allerton Conference on Communication, Control, and Computing, 2005.

5. J. G. Dai and W. Lin. Maximum pressure policies in stochastic processing networks. Operations Research, 53:197–218, 2005.

6. H. Dupuis and B. Hajek. A simple formula for mean multiplexing delay for indep endent regenerative sources. Queueing Systems Theory and Applications, 16:195–239, 1994.

7. A. Feldmann, N. Kammenhuber, O. Maennel, B. Maggs, R. D. Prisco, and R. Sundaram. A methodology for estimating interdomain web traffic demand. In IMC, 2004.

8. L. Georgiadis, M. J. Neely, and L. Tassiulas. Resource Allocation and Cross-Layer Control in Wireless Networks, Foundations and Trends in Networking, volume 1. Now Publishers, 2006.

ELECTRIC POWER GENERATION FROM VEGETABLES & FRUITS FOR DOMESTIC POWER APPLICATIONS

Mr. S. Sunisith[*]

Assistant Professor
Dept. of Electrical and Electronics Engg.
GNIT, Hyderabad. JNTUH.
+919502519019
sunisith@gmail.com
*Corresponding Author

Mr. T. Manidhar

Assistant Professor
Dept. of Electrical and Electronics Engg.
GNIT, Hyderabad. JNTUH.
+919440278907
thulamanidhar@gmail.com

Mr. V. DAVID

Assistant Professor
Dept. of Electrical and Electronics Engg.
GNIT, Hyderabad. JNTUH.
+919985796324
david.gnit24@gmail.com

ABSTRACT

DC Electric power production from vegetables and citrus fruits to power a dc lamp or any appliance. We can actually turn fruits and vegetables into electric power sources. Batteries power many things around us; including educational calculators, dc lamps, dc buzzers, digital clocks, cell phones, wireless video game controllers, and smoke detectors. Here, we use potatoes, onions, lemons, oranges, apples and citrus fruits to make a simple battery to power a small light and a buzzer. This paper focuses on all types of vegetables and citrus fruits which will produce electric power for low power applications and these are tested practically in laboratory.

Keywords— Anonymity, traceability, pseudonym, revocation, wireless network

1. INTRODUCTION

Make batteries by pushing zinc and copper electrodes into potatoes. There are many types of batteries, ranging from tiny watch and hearing aid batteries that are just a few millimeters wide, to the normal AA batteries you use in many household electronic devices, to the large batteries you find under the hood of a car. Did you know that you can also use a potato as a battery? That might sound weird, but believe it or not, you can actually use a potato as an electrical battery to power small devices. To understand how, first you will need to learn a little more about batteries.[1]

2. SERIES AND PARALLEL CONNECTIONS OF BATTERIES

Multiple batteries can be connected two different ways: in series or in parallel. When multiple batteries are connected in series, the positive terminal of one battery is connected to the negative terminal of the next battery (and this repeats if there are more than two batteries)[2]. When batteries are connected in parallel, all of the positive battery terminals are connected together, and all of the negative battery terminals are connected together. These two configurations are shown in Figures 2.1 and 2.2.
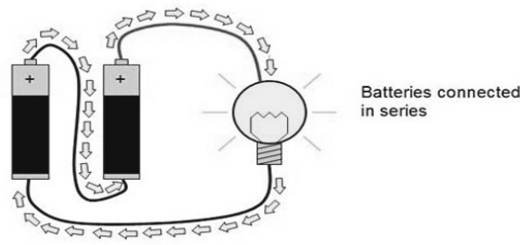
Fig. 2.1 Series Connection of Batteries
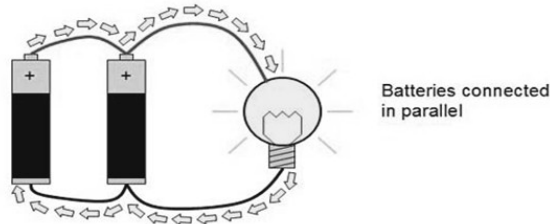
Fig. 2.2 Parallel Connection of Batteries

In figure 2.1, when batteries are connected in series, the positive terminal of one battery is connected to the negative terminal of the next. In figure 2.2, when they are connected in parallel, all the positive terminals are connected to common point, and all the negative terminals are connected to another common point [3].

3. PRACTICAL SETUP

The following points will explain the circuit connection procedure

- Insert the electrodes into the potatoes.

- Note that some juice may leak out of the potatoes during this process, so work on a surface that is easy to clean, or use paper towels.

- Press one copper and one zinc electrode into the middle of a potato, spaced roughly 1 inch apart, as shown in Figure 3.1.

- Press the electrodes in until they almost poke out of the other side of the potato. *Note:* If they do accidentally go through, that's ok. Just pull them back up a little bit.

- Repeat this for another potato.
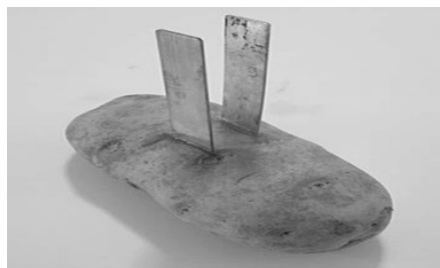
Fig. 3.1 Copper and zinc electrodes inserted into a potato.

- Measure the open-circuit voltage and short-circuit current of a single potato battery. Use alligator clips to connect the multi meter leads to the copper and zinc electrodes of a single potato, as shown in Fig 3.2.
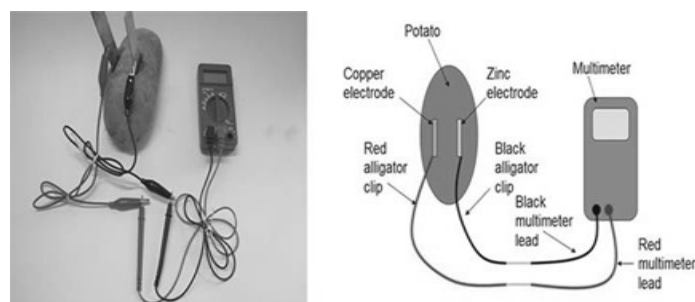
Fig. 3.2 Connection of multimeter leads to the copper and zinc electrodes

- First, plug the red multi meter lead into the multi meter port labelled VΩMA, and the black multi meter lead into the multi meter port labelled COM.

- Now clip one end of the red alligator clip onto the metal part of the red multi meter probe, and the other end onto the copper electrode.

- Finally, clip one end of the black alligator clip onto the metal part of the black multi meter probe, and the other end onto the zinc electrode.
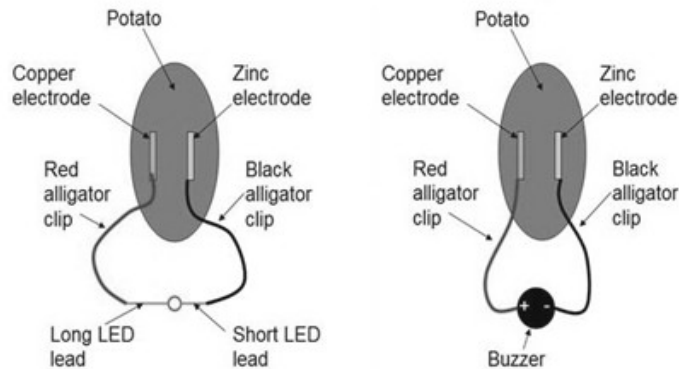
Fig. 3.3 Potato powered LED and Buzzer

CHEMICAL REACTION:

- Actually there is no electricity in any fruits or vegetables. Here is the fact that we can use the chemical properties of certain fruits and vegetables to generate electricity.

- A lemon for example can be made to power a small electrical device because the lemon is quite acidic.

- The way we do this is to stick a piece of zinc metal and a piece of cu metal (electrodes) into lemon.

- Here's the chemistry behind the lemon is that ZINC is an active metal and will reacts with ACID (H+), Acids active ingredient is positively charged hydrogen (H+).

- So, a transfer of electrons takes place between ZINC and ACID.

- The zinc (Zn0) is OXIDIZED to Zn++ and the acid (H+) is REDUCED to (H2) hydrogen gas, which we can see bubbling out around the electrodes.

$$\text{OXIDATION:} \quad Zn à (Zn++) + (2e\text{-})$$

Here Zn loses two electrons

$$\text{REDUCTION:} \quad (2H+) + (2e\text{-}) à H_2$$
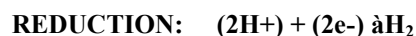
Hydrogen ion gains two electrons

$$\text{NET REDUCTION:} \quad (Zn) + (2H+) à (Zn++) + (H_2)$$
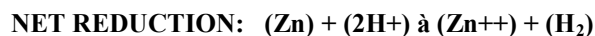
This is the ELECTROLYTE solution which produces electricity.

4. CASE STUDIES AND TEST RESULTS

PRODUCTION OF ELECTRICITY FROM POTATOES Here the Series connected potatoes are producing dc power to power a buzzer.
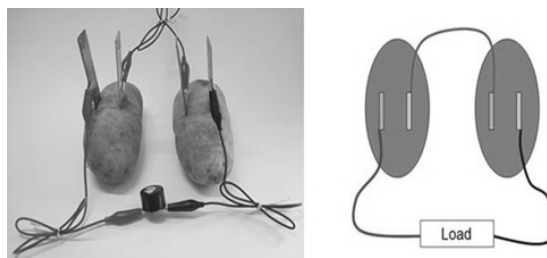
Fig. 4.1 Series connection of Two Potatoes powering a buzzer

Here the Parallel connected potatoes are producing dc power to power a buzzer.
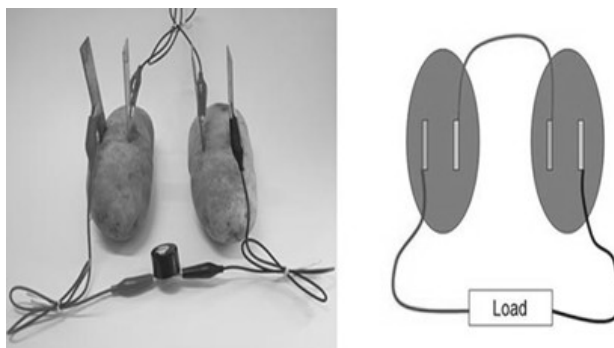
Fig. 4.2 Parallel connection of Three Potatoes powering a buzzer
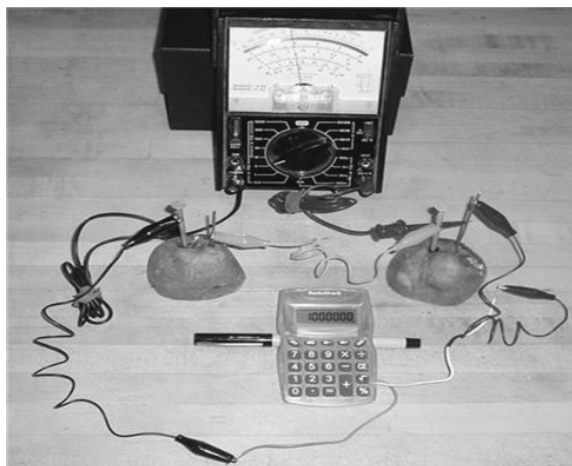
Fig. 4.3 Digital Calculator powered by Potatoes

Fig. 4.4 LED/DC Lamp powered by Potatoes

Test Results are tabulated below:

No. of Potatoes	Type of Connection	No load Output Voltage	Voltage across 1KΩ Load	Light Bulb/Buzzer
1	-	0.95V	0.19V	Lighted Dim
2	Series	1.88V	0.25V	Lighted Bright
3	Series	2.78V	0.31V	Lighted More Bright
2	Parallel	0.95V	0.19V	Lighted Bright
3	Parallel	0.95V	0.19V	Lighted More Bright

PRODUCTION OF ELECTRICITY FROM ONIONS Here the onions are producing dc power to power a buzzer. Test Results are tabulated below:

No. of Onions	Type of Connection	No load Output Voltage	Voltage across 1KΩ Load	Light Bulb/Buzzer
1	-	0.92V	0.13V	Lighted Dim
2	Series	1.89V	0.17V	Lighted Bright
3	Series	2.76V	0.25V	Lighted More Bright
2	Parallel	0.92V	0.13V	Lighted Bright
3	Parallel	0.92V	0.13V	Lighted More Bright

PRODUCTION OF ELECTRICITY FROM LEMONS Here the lemons are producing dc power to power a buzzer.
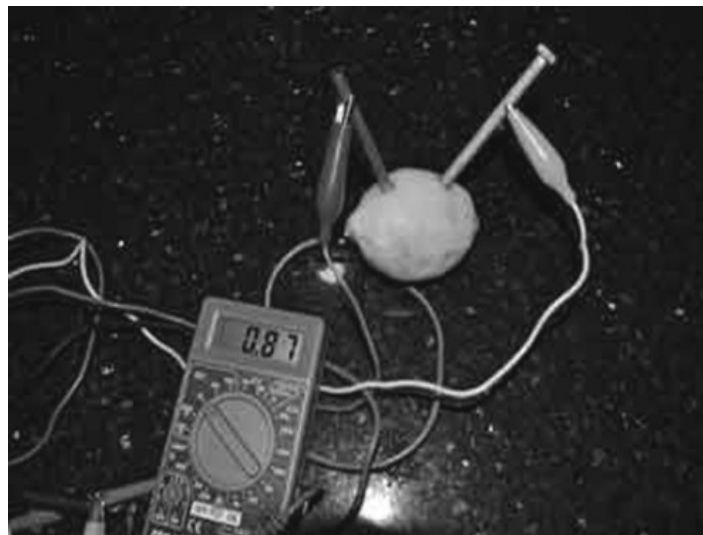
Fig. 4.5 Electric power production from Lemon (More Acidic)
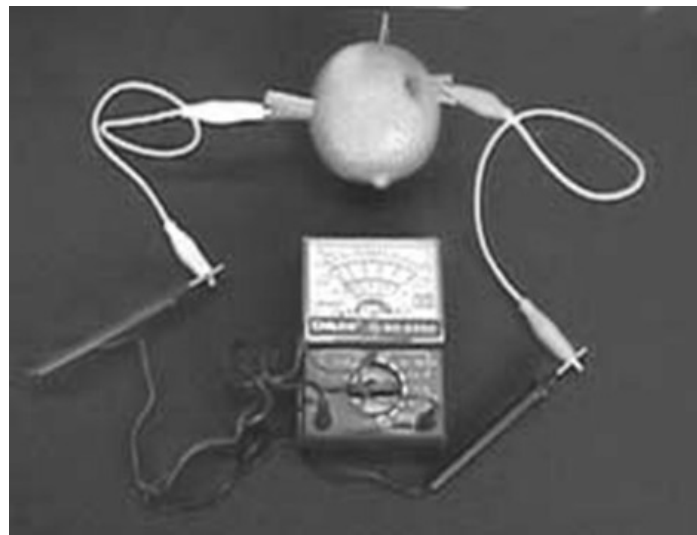
Fig. 4.6 Electric power production from Lemon (Less Acidic)

Fig. 4.7 Lemon powered DC Lamp

Test Results are tabulated below:

No. of Lemons	Type of Connection	No load Output Voltage	Voltage across 1KΩ Load	Light Bulb/Buzzer
1	-	0.87V	0.17V	Lighted Dim
2	Series	1.74V	0.26V	Lighted Bright
3	Series	2.62V	0.34V	Lighted More Bright
2	Parallel	0.87V	0.17V	Lighted Bright
3	Parallel	0.87V	0.17V	Lighted More Bright

PRODUCTION OF ELECTRICITY FROM GREEN APPLES Here the Apples are producing dc power to power a buzzer.
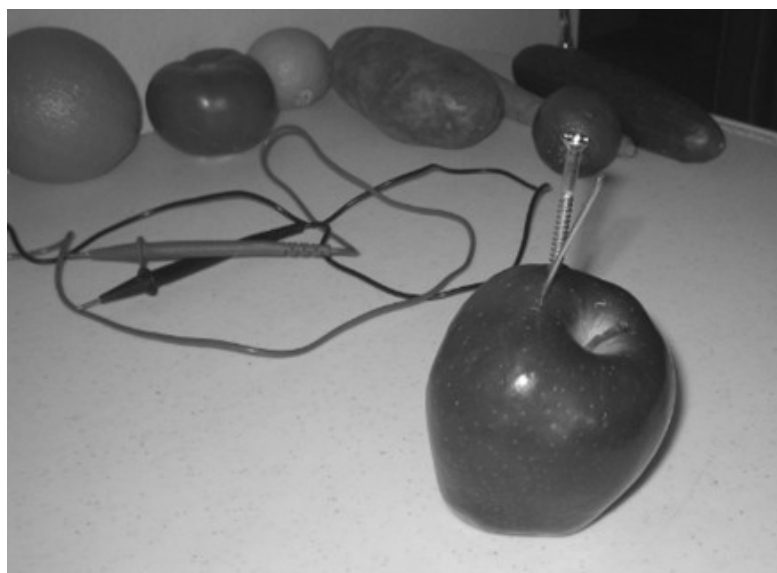
Fig. 4.8 Electric power production from Apple
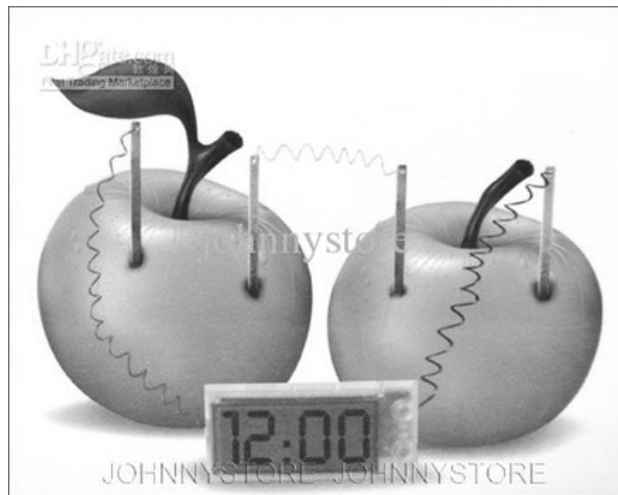
Fig. 4.9 Green Apple powered Digital Clock

PRODUCTION OF ELECTRICITY FROM TOMATOES Here the Tomatoes are producing dc power to power a lamp.
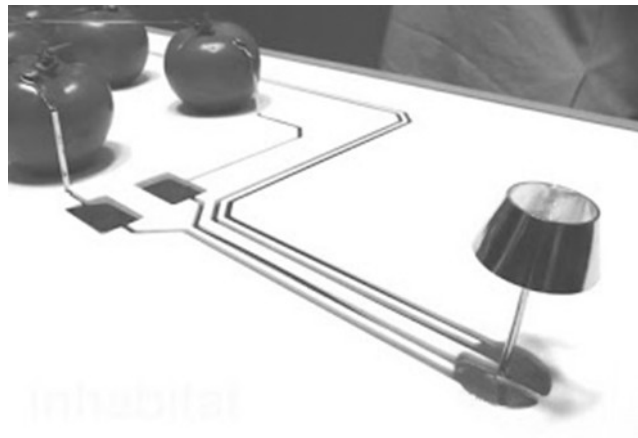
Fig. 4.10 Tomato powered DC Lamp/LED

5. CONCLUSION

This paper presents the production of electric power from different types of vegetables and citrus fruits. This concept of electricity production is very cheap, safer and simple to make. There is no harmful gas production from the fruits when the copper and zinc electrodes are dipped into the fruits. Acidic reaction takes place inside the fruit, so these are safer to use exclusively. We can use these batteries for powering many dc appliances. We can charge a rechargeable 1.5v battery from the power produced by these fruits. Some of the applications of dc power produced by vegetables and fruits are Digital clocks, Digital Calculators, DC Buzzers, DC Lamps, and LED's.

REFERENCES

1.   S. Sunisith, K. S. Mann, K. Janardhan Rao, "Effective algorithm for reducing DC link neutral point voltage and total harmonic distortion" IEEJ, Vol.5 (2014) Issue No.11, ISSN: 2078-2365, pp 1613-1618.

2.   S. Sunisith, K. Meena, "Backward/Forward Sweep Based Distribution Load Flow Method" IEEJ, Vol.5 (2014) Issue No. 9, ISSN: 2078-2365, pp 1539-1544.

3.   S. Sunisith, T. Manidhar, M. Rajendar, "Methodology for alleviation of Voltage Excursions in large power systems" IEEJ, Vol.5 (2014) Issue No. 9, ISSN: 2078-2365, pp 1531-1538.

DUAL AXIS SOLAR TRACKER

Prof Mahesh K*
Research Scholar at Jain University,
Associate Professor & HOD-EEE-NHCE.
Mobile: 09900119252
maheshkgowda@gmail.com ,
*Corresponding Author

Biswadeep Moitra,
New Horizon College of Engineering,
Bangalore-560103
Mobile: 09019943692
biswadeep6170@gmail.com,

Ashish Yadav
New Horizon College of Engineering,
Bangalore-560103
Mobile: 09731066982
ashishyadav542@gmail.com

Bipul Pattnaik
New Horizon College of Engineering,
Bangalore-560103
Mobile: 09538178804.
bipulp123789@gmail.com

ABSTRACT

Solar energy is the most abundant stream of energy. It is available directly as solar insolation and indirectly as wind energy. Solar energy has the sources of renewable energy. Its potential is 178 Billion MW, which is about 20,000 times the world's demand. Sun sends out energy in the form of electromagnetic radiation. In this project we use the solar energy for generation of electrical energy, by using the Solar cells. The solar cells receive the solar energy which is fed to LEDs, maximum intensity of LED indicates maximum solar energy tracked.At present solar electric power generation systems are having fixed solar panels whose efficiency of generation is less. Our aim is to design the system, which will automatically track the sun's position and accordingly change the direction of the solar panel in both east to west (longitudinally) and north to south (latitude) to get the maximum output from the solar cell. For this tracking purpose we use a sensor and the input from the sensor is given to the micro controller and according to the program the panel is fixed to the maximum intensity position. Here we are using PIC micro controller. The 16F877A is a low-power, high-performance CMOS 8-bit microcontroller with 4K bytes of Flash Programmable and Erasable Read Only Memory (PEROM).

Keywords—Azimuth angle, Altitude dual axis trackers, DC Gear Motor, Photovoltaic, PV modules, PICMicrocontroller.

1. INTRODUCTION

The world population is increasing day by day and the demand for energy is increasing accordingly. Oil and coal as the main source of energy nowadays, is expected to end up from the world during the recent century which explores a serious problem in providing the humanity with an affordable and reliable source of energy. The need of the hour is renewable energy resources with cheap running costs. Solar energy is considered as one of the main energy resources in warm countries. In general, India has a relatively long sunny day for more than ten months and partly cloudy sky for most of the days of the rest two months. This makes our country, especially the desert sides in the west, which include Rajasthan, Gujarat, Madhya Pradesh etc. very rich is solar energy. Many projects have been done on using photovoltaic cells in collecting solar radiation and converting it into electrical energy but most of these projects did not take into account the difference of the sun angle of incidence by installing the panels in a fixed orientation which influences very highly the solar energy collected by the panel. As we know that the angle of inclination ranges between -90° after sun rise and +90° before

sun set passing with 0° at noon. This makes the collected solar radiation to be 0% at sun rise and sun set and 100% at noon. This variation of solar radiations collection leads the photovoltaic panel to lose more than 40% of the collected energy [1]. So in our paper we are focusing to utilize this 40% energy.

2. NEED FOR SOLAR TRACKER

From the figure 1.1, one can estimate the exact position of sun in every Solar angle of incidence.
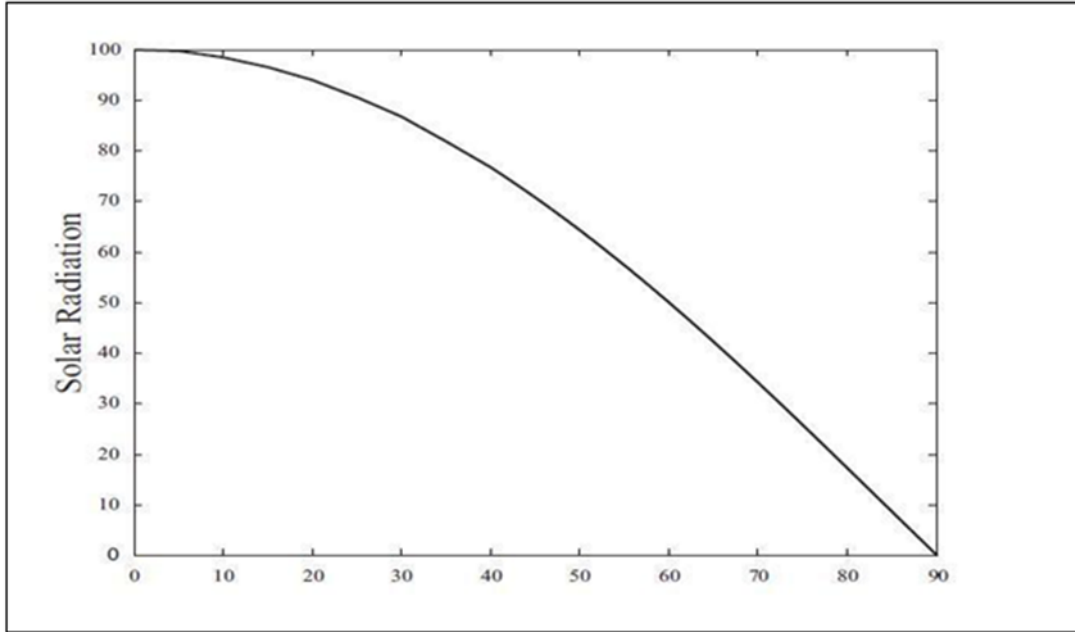
Fig-1.1 Curve for the relationship between the solar radiation and the solar angle of incidence

Each day, the sun rises in the east, moves across the sky, and sets in the west. Whenever the sun is shining on us, it is sending energy in our direction. We can feel the heat from the sun, and we can see objects that are illuminated by the light from the sun as it moves across the sky. However, if we could get a solar cell to turn and look at the sun all day, then it would be receiving the maximum amount of sunlight possible and converting it into the more useful energy form electricity. If we are located in the tropics, we see that the sun appears to follow a path that is nearly directly overhead. However, for locations north or south of the tropics (e.g., latitudes greater than 23.5 degrees), the sun never reaches a position that is directly overhead. Instead, it follows a path across the southern or the northern part of the sky.

OBJECTIVE OF WORK The aim of our projects is to utilize the solar energy through solar panel. For this a automatic solar tracking system is proposed [3]. This project helps the solar power generating equipment to track the maximum sunlight automatically and thereby increase the output efficiency of the system. The most energy is absorbed when a surface's face is perpendicular to the sun; stationary mounted PV panels are only perpendicular to the sun once a day. Thus tracking sun from east to west with respect to season will improve performance from each panel means fewer panels are needed.

SOLAR TRACKER
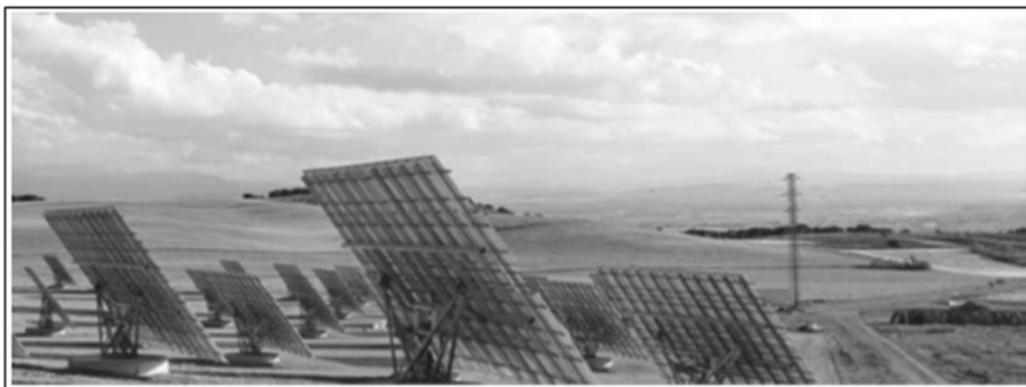
Figure 2.1: Solar Panel

A Solar tracker is a device for orienting a solar photovoltaic panel or concentrating solar reflector or lens toward the sun. The sun's position in the sky varies both with the seasons (elevation) and time of day as the sun moves across the sky [5, 12]. Solar powered equipment works best when pointed at or near the sun, so a solar tracker can increase the effectiveness of such equipment over any fixed position, at the cost of additional system complexity. There are many types of solar trackers, of varying costs, sophistication, and performance. One well-known type of solar tracker is the heliostat, a movable mirror that reflects the moving sun to a fixed location, but many other approaches are used as well.The required accuracy of the solar tracker depends on the application. Concentrators, especially in solar cell applications, require a high degree of accuracy to ensure that the concentrated sunlight is directed precisely to the powered device, which is at (or near) the focal point of the reflector or lens. Typically concentrator systems will not work at all without tracking, so at least single-axis tracking is mandatory.Non-concentrating applications require less accuracy, and many work without any tracking at all. However tracking can substantially improve the amount of power produced by a system. The use of trackers in non-concentrating applications is usually an engineering decision based on economics. Compared to photovoltaic, trackers can be relatively inexpensive. This makes them especially effective for photovoltaic systems using high-efficiency panels.For low-temperature solar thermal applications, trackers are not usually used, owing to the relatively high expense of trackers compared to adding more collector area and the more restricted solar angles required for winter performance, which influence the average year-round system capacity. Some solar trackers may operate most effectively with seasonal position adjustment and most will need inspection and lubrication on an annual basis [4,11].

3. TRACKING TECHNIQUES

There are several forms of tracking currently available; these vary mainly in the method of implementing the designs. The two general forms of tracking used are fixed control algorithms and dynamic tracking. The inherent difference between the two methods is the manner in which the path of the sun is determined. In the fixed control algorithm systems, the path of the sun is determined by referencing an algorithm that calculates the position of the sun for each time period. That is, the control system does not actively find the sun's position but works it out given the current time, day, month, and year. The dynamic tracking system, on the other hand, actively searches for the sun's position at any time of day (or night).Common to both forms of tracking is the control system. This system consists of some method of direction control, such as DC motors, gear motors, and servo motors, which are directed by a control circuit, either digital or analog [6].

SOLAR TRACKER FUNDAMENTALS A solar tracker is a device that is used to align a single P.V module or an array of modules with the sun. Although trackers are not a necessary part of a P.V system, their implementation can dramatically improve a systems power output by keeping the sun in focus throughout the day. Efficiency is particularly improved in the morning and afternoon hours where a fixed panel will be facing well away from the sun's rays. P.V modules are expensive and in most cases the cost of the modules themselves will outweigh the cost of the tracker system. Additionally a well designed system which utilizes a tracker will need fewer panels due to increased efficiency, resulting in a reduction of initial implementation costs.

4. OVERVIEW OF CURRENT TRACKER DRIVE TYPES

Solar trackers can be divided into three main types depending on the type of drive and sensing or positioning system that they incorporate. Passive trackers use the sun's radiation to heat gases that move the tracker across the sky. Active trackers use electric or hydraulic drives and some type of gearing or actuator to move the tracker. Open loop trackers use no sensing but instead determine the position of the sun through pre-recorded data for a particular site.

GAS TRACKERS (PASSIVE TRACKERS) Passive trackers use a compressed gas fluid as a means of tilting the panel. A canister on the sun side of the tracker is heated causing gas pressure to increase and liquid to be pushed from one side of the tracker to the other. This affects the balance of the tracker and caused it to tilt. This system is very reliable and needs little maintenance. Although reliable and almost maintenance free, the passive gas tracker will very rarely point the solar modules directly towards the sun. This is due to the fact that temperature varies from day to day and the system cannot take into account this variable. Overcast days are also a problem when the sun appears and disappears behind clouds causing the gas in the liquid in the holding cylinders to expand and contract resulting in erratic movement of the device. Passive trackers are however an effective and relatively low cost way of increasing the power output of a solar array.The tracker begins the day facing west. As the sun rises in the east, it heats the unshaded west-side canister, forcing liquid into the shaded east-side canister. The liquid that is forced into the east side canister changes the balance of the tracker and it swings to the east. It can take over an hour to accomplish the move from west to east. The heating of the liquid is controlled by the aluminium shadow plates. When one canister is exposed to the sun more than the other, its vapour pressure increases, tracker and caused it to tilt. This system is very reliable and needs little maintenance. Although reliable and almost maintenance free, the passive gas tracker will very rarely point the solar modules directly towards the sun. This is due to the fact that temperature varies from day to day and the system cannot take into account this variable. Overcast days are also a problem when the sun appears and disappears behind clouds causing the gas in the liquid in the holding cylinders to expand

and contract resulting in erratic movement of the device. Passive trackers are however an effective and relatively low cost way of increasing the power output of a solar array [8].

ACTIVE TRACKERS Active trackers measure the light intensity from the sun to determine where the solar modules should be pointing. Light sensors are positioned on the tracker at various locations or in specially shaped holders. If the sun is not facing the tracker directly there will be a difference in light intensity on one light sensor compared to another and this difference can be used to determine in which direction the tracker has to tilt in order to be facing the sun.

OPEN LOOP TRACKERS Open loop trackers determine the position of the sun using computer controlled algorithms or simple timing systems.Timed Trackers – These use a timer to move the tracker across the sky. Incremental movement throughout the day keeps the solar modules facing the general direction of the sun. Trackers of this type can utilize one or two axes depending on their application. The main disadvantage of timed systems is that their movement does not take into account the seasonal variation in sun position. Unless measures are taken to adjust the tracker position seasonally, there will be a noticeable difference in efficiency depending on the season. Altitude / Azimuth Trackers use astronomical data or sun position algorithms to determine the position of the sun for any given time and location. Tracker location, date and time are used by a micro controller to fix the position of the sun. Once the position has been calculated, the modules are moved using servo motors and their position measured by encoders built into the tracker frame.

5. TYPES OF SOLAR TRACKERS

There are many different types of solar tracker which can be grouped into single axis and double axis models[2,7].
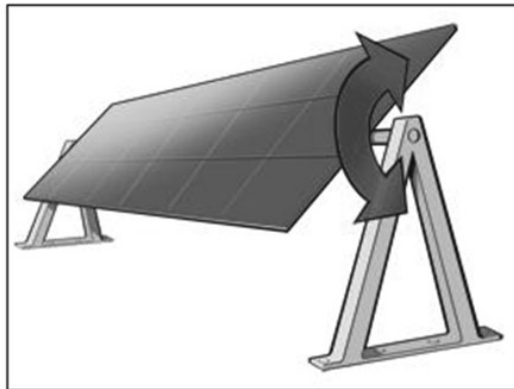
SINGLE AXIS TRACKERS:

Figure 5.1: Single Axis Solar Tracker

Single axis solar trackers can either have a horizontal or a vertical axle. The horizontal type is used in tropical regions where the sun gets very high at noon, but the days are short. The vertical type is used in high latitudes (such as in UK) where the sun does not get very high, but summer days can be very long.These have a manually adjustable tilt angle of 0 - 45 °and automatic-tracking of the sun from East to West. They use the PV modules themselves as light sensor to avoid unnecessary tracking movement and for reliability. At night the trackers take up a horizontal position.

DUAL AXIS TRACKERS

Figure 5.2: Double Axis Tracker

Double axis solar trackers have both a horizontal and a vertical axle and so can track the Sun's apparent motion exactly anywhere in the world. This type of system is used to control astronomical telescopes, and so there is plenty of software available to automatically predict and track the motion of the sun across the sky.Dual axis trackers track the sun both East to West and North to South for added power output (approx 40% gain) and convenience.

6. BLOCK DIAGRAM & WORKING
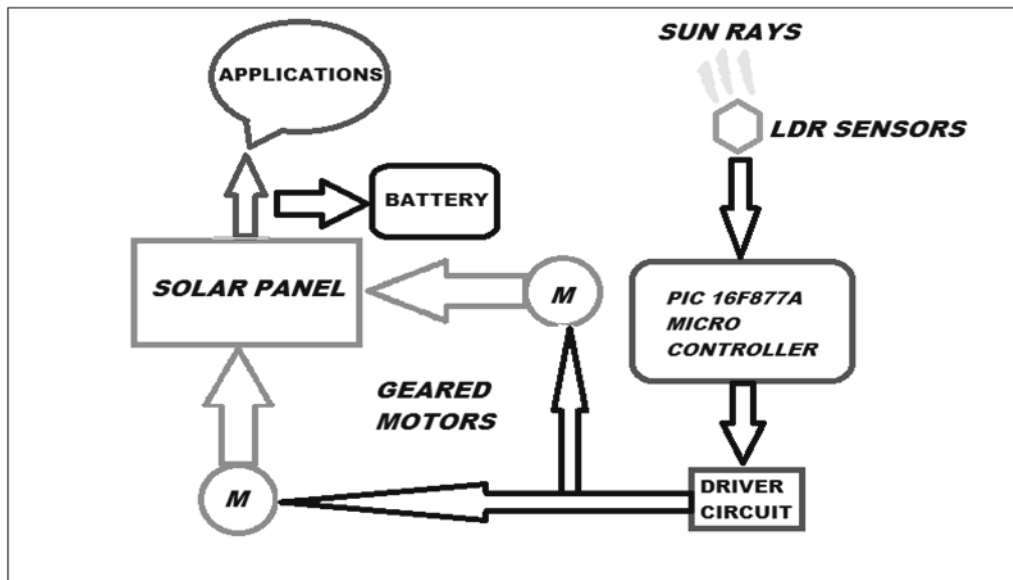
Figure 6.1

Working

SOLAR TRACKING SYSTEM:

- The PIC controller receives analog input from panel.

- The maximum voltage which can be obtained from solar cell is set as reference voltage in microcontroller [9,10].

- The Panel output voltage and current is compared with the reference voltage and current accordingly controller gives signal to the gear motor.

- If the output of ADC is equal to the reference voltage then gear motor keeps the solar panel in same direction.

- And if output is less than reference voltage then gear motor keeps rotating the solar panel till we get the voltage equal to the reference voltage.

7. CONCLUSION

SOLAR ENERGY HAS MANY ADVANTAGES:

- Need no fuel

- Has no moving parts to wear out

- Non-polluting & quick responding

- Adaptable for on-site installation

- Easy maintenance

- Can be integrated with other renewable energy sources

- Simple & efficient

This project which was enhanced with the scope of conserving the conventional fuels is successfully completed. The main objective, to increase the usage of renewableenergy source for power generation is perfectly implemented. Taking

into consideration the future energy scenario in the world, solar energy would be a major energy source. We wish that our project would be a mini encyclopedia for those who want to implement the above system.

REFERENCES

1. [Aliman et al., 2007] Omar Aliman, Ismail Daut, Muzamir Isa and Mohd Rafi Adzman, "Simplification of Sun Tracking Mode to Gain High Concentration Solar Energy" American Journal of Applied Sciences, 2007, Page (s):171-175.

2. [Aliman and Daut , 2007] Omar Aliman, Ismail Daut, "Rotation-Elevation of Sun Tracking Mode to Gain High Concentration Solar Energy", IEEE Conference, 12-14 April 2007, Page(s):551 – 555

3. [Armstrong and Hurley, 2005] S. Armstrong and W.G Hurley "Investigating the Effectiveness of Maximum Power Point Tracking for a Solar System", IEEE Conference on Power Electronics, 2005 Page(s):204 – 209.

4. [Chong et al., 2000], Chee-Yee Chong, Mori, S. Barker, W.H and Kuo-Chu Chang, "Architectures and Algorithms for Track Association and Fusion", IEEE Transaction, Volume15, Issue 1, Jan.2000, Page(s):5-13.

5. [Chung et al., 2003] Henry Shu-Hung Chung, K.K Tse, S.Y. Ron Hui, C.M. Mok, M.T. Ho, "A novel maximum power point tracking technique for solar panels using a SEPIC or Cuk converter", IEEE Transactions on Power Electronics, Volume 18, Issue 3, May 2003 Page(s):717 – 724.

6. [Hua and Shen, 1998] ChihchiangHua and ChihmingShen, "Comparative study of peak power tracking techniques for solar storage system", APEC proceedings on Applied Power Electronics, Volume2, 15-19Feb.1998, Page (s):679-685.

7. [Huang.F. et al.,1998] F. Huang, D.Tien and James Or, "A microcontroller based automatic sun tracker combined with a new solar energy conversion unit" IEEE Proceedings on Power Electronic Drives and Energy Systems for Industrial Growth, Volume 1, 1-3 Dec. 1998, Page(s):488 - 492 .

8. [Kobayashi Kimiyashi et al., 2004] Kimiyoshi Kobayashi, Hirofumi Matsuo and Yutaka Sekine, "A novel optimum operating point tracker of the solar cell power supply system" ,IEEE Conference on Power Electronics, Volume 3, 20-25 June 2004 ,Page(s):2147 - 2151 Vol.3.

9. [Konar and Mandal, 1991] A.Konar and A.K Mandal, "Microprocessor based Sun Tracker", IEEE Proceedings-A, Vol. 138, No.4, July 1991, Page(s):237-241.

10. [Koutroulis et al., 2001] Koutroulis, E.Kalaitzakis, K. Voulgaris and N.C., "Development of a microcontroller-based, photovoltaic maximum power point tracking control system" IEEE Transactions on Power Electronics, Volume 16, Issue 1, Jan. 2001 Page(s):46 – 54

11. [Kuo et al., 2001] Yeong-ChauKuo, Tsorng-Juu Liang and Jiann-Fuh Chen, "Novel Maximum-Power-Point-Tracking Controller for Photovoltaic Energy Conversion System" IEEE Transactions on Industrial Electronics, Volume 48, Issue 3, June 2001 Page(s):594 – 601.

12. Pritchard, 1983] Daniel A. Pritchard, "Sun Tracking by Peak Power Positioning for Photovoltaic Concentrator Arrays" IEEE Transactions on Control System, Volume 3, Issue3, Aug1983, Page(s):2-8.

EFFECTS OF LAND USE CHANGE ON HYDROLOGIC MODELS: A CASE STUDY OF URBAN BASIN ACCRA

Prince Appiah Owusu*

Department of Civil Engineering,
P. O. Box 854, Kumasi Polytechnic, Kumasi, Ashanti, Ghana
Tel:00233244543323
Email: princeappiahus@gmail.com
*Corresponding Author

Emmanuel Kwesi Nyantakyi

Department of Civil Engineering,
P. O. Box 854, Kumasi Polytechnic, Kumasi, Ashanti, Ghana
Tel: 00233268289250
Email: emmanuelkwesinyantakyi@yahoo.com

Julius Kwame Borkloe

Department of Civil Engineering,
P. O. Box 854, Kumasi Polytechnic, Kumasi, Ashanti, Ghana
Tel: 0208163906/0276377093
Email: juliusborkloe1@yahoo.com

ABSTRACT

The study assesses the effects of land use and land cover changes on the hydrology of Odaw basin in Accra, Ghana. Digitized and LandSat TM image of 1964 and 2007 were analyzed using Erdas Imagine and ArcGIS tools. The Soil Conservation Service Curve number (SCS-CN) model was used to simulate runoff for the basin. A total of six broad land use and land cover classes were identified and mapped for both years. These were settlement, closed forest, thickets, grasslands, open forest and water bodies. The analysis showed that between 1964 and 2007, settlement and open forest increased by about 306% and 118% respectively. The study identified population growth, as a major cause of increasing curve number (CN) levels in the catchment area leading to the continuous reduction of the storage capacity of the basin by about 55% consequently creating higher overland water flows a trigger of flush floods. The coefficient of initial abstraction of the model as applied to the basin was found out as 0.09 with Nash-Sutcliffe efficiency (E), coefficient of determination (R^2), and index of agreement (D) as 94.5%, 0.73 and 0.83.The method in this research are replicable in other basins in Ghana and the sub-region.

Keywords: ArcGIS; Erdas Imagine; land use change; rainfall run-off model; SCS-CN runoff model; urban area;

1. INTRODUCTION

Land use changes in a watershed can impact water supply by altering hydrological processes such as infiltration, groundwater recharge, base flow and runoff. For instance, covering large watershed areas with impervious surfaces frequently results in increased surface runoff and reduced local surface erosion rates. Moreover, watershed development changes land use patterns and reduces base flow by changing groundwater flow pathways to surface water bodies. An integrated landscape model can potentially extrapolate from management practices and land use pattern to determine potential environmental impacts [1]. Thus, the development of an integrated approach that can simulate and assess land use changes, land use patterns and their effects on hydrological processes at the watershed level is crucial to land use and water resource planning and management. Numerous studies have developed modeling approaches to simulate the pattern and consequences of land use changes. Different types of models are used to explore land use changes, such as stochastic

models, optimization models, dynamic process based simulation models and empirical models. Recent studies include those conducted by [2-11]. Empirical analysis is applied to determine the relationships between land use spatial distribution and a number of factors that are the drivers and constraints of land use. Based on the competitive advantage of each land use at a location the competition among land uses for a particular location is simulated [12]. Often, the assessment of land use change results in changes in landscape pattern. Landscape composition, configuration, and connectivity are primary descriptors of the landscape patterns [1]. Landscape patterns can be quantified using spatial landscape indices or metrics to characterize and quantify landscape composition and configuration. The composition of a landscape denotes the features associated with the variety and abundance of patch types within a landscape. The spatial configuration of a landscape denotes the spatial character and arrangement, position, or orientation of patches within class or landscape [13]. These metrics may include the number of patches, area, patch shape, total edge of patches, nearest neighbor distance, landscape diversity, interspersion and contagion metrics to represent landscape patterns, including compositions and configurations. Recent studies have applied landscape metrics to quantify landscape patterns [14-17]. Hydrological models provide a framework to conceptualize and investigate the relationships between climate, human activities (e.g., land use change) and water resources [19]. Distributed hydrological models on a watershed scale are frequently used for quantifying the impact of land use change on hydrologic components [20]. The generalized watershed loading functions model developed by [21] is a combined distributed/lumped parameter watershed model that can simulate runoff, sediment, and nutrient loadings in watersheds given source areas of variable sizes (e.g., agricultural, forested, and developed land). Surface loading is distributed in the sense that it allows multiple land use and land cover scenarios in which each area is assumed to have homogeneous attributes when addressed by the model [22]. In this study, an integrated approach that combines land use, landscape metrics and hydrological models is used. Land use scenarios that differ with respect to planning policies and land use requirements are analyzed for their effects on landscape pattern, surface runoff, groundwater discharge and stream flow of the watershed. The Soil Conservation Service (SCS, 1972) model estimates precipitation excess as a function of cumulative precipitation, soil cover, land use, and antecedent moisture. The keystone of the SCS equation is the soil curve number (CN), function of soil classification and land use or cover.[23] assessed the impacts of land use change scenarios on hydrology and land use patterns in the Wu-Tu watershed in Northern Taiwan using the SCS-CN model. Analysis results revealed that future land use patterns differed between spatial policies. Scenarios with low land use demand for land use conversion policies did not lead to significantly different land use patterns. Moreover, patterns of future agricultural land patches obviously differed among agricultural land conversion policies. The stream flow, runoff and groundwater discharge were successfully simulated using a lumped hydrological model that can assess the impact of land use change in the watershed. [24] worked on the hydrological modeling of ungauged Wadis in arid environments a case study of Wadis Madoneh in Jordan using the SCS-CN model. The model was used to simulate streamflow of the Wadis Madoneh catchment. It was realized that the combination of these techniques with the SCS model makes the runoff estimate more reliable. There are several advantages of the SCS-CN over other models. It is a simple conceptual method for estimation of direct runoff amount. However there are limitations in that it does not contain any expression for time and ignores the impact of rainfall intensity and its temporal distribution. Again there is a lack of clear guidance on how to vary the antecedent moisture condition, especially for lower curve numbers and or rainfall amounts and its application to large catchments. The Odaw catchment is part of the coastal basins in Accra, Ghana. There are recent reports of serious flood cases within the basin, a situation attributed to rapid urbanization. This is explained in the fact that as urban areas increase, vegetated land is converted to impervious surfaces, consequently increasing runoff velocity and runoff volume leading to peak runoff also increasing and the time to peak decreasing [25]. Thus, the increase in the urban areas, contributes to increase in flooding because it reduces the natural storage capacity of the soil, removal of floodplain storage for settlement and consequently contributes to increased runoff. Modern technologies such as remote sensing and Geographic information systems (GIS) provide some of the most accurate means of measuring the extent and pattern of changes in landscape conditions over time [26, 27]. The main aim of this study was to assess the impact of land use and land cover changes on the hydrology of the Odaw catchment. The specific objectives were; quantify the changes in land use and land cover, to accurately quantify the ratio of initial abstraction to maximum water potential (I_a/ S) value in order to increase the precision of estimation and to establish its effect on rainfall runoff processes. This river basin is located in one of the fast developing regions of Ghana and unfortunately limited studies are available to provide information of the dangers of surface imperviousness. This information is particularly important to water resource managers, town and country planners and environmental and sanitation policy developers.

STUDY AREA The Odaw River is the major stream draining central Accra, Ghana with its outlet into the Korle Lagoon, while smaller streams lead into lagoons to the east and west of central Accra. Much of the Odaw catchment area is built up and many of the streams are channelized. Rainfall in Accra occurs in the form of intensive storm events, which cause local flooding. The total population of Enumeration Areas that border the Odaw and its tributary streams is roughly 172,000

people based on the 2000 census (Ghana Statistical Services, 2000). The Odaw basin lies in the coastal area of Accra, Ghana. The geographical coordinate of the basin are latitude [0.00, 5.88N] and longitude [0.15W, 0.00]. The Odaw basin is approximately 39.7km long and covers an area of 365.3km^2. The widest part is just about 12.5km. The study area lies in the Coastal Savannah zone within tropical climate [28]. Rainfall depends on the north-south migration of Inter Tropical Convergence Zone. Average annual rainfall is about 730mm. The mean annual temperature is 26.8°C. Elevation varies between 8m and 414m above sea level. The soil type of the Odaw basin originates from the Dahomeyan system (metamorphic) basement rocks of middle-late Precambrian age and consists of quartz schist. The land use is of varying functions. "Fig. 1" shows the Odaw basin

Hydrological soil groups of the basin are determined on the basis of information from statistics of the processed shapefiles of soil map in ArcGIS, "Fig. 2". It is evident from the figure that the region comprises of Hydrologic Soil Group Acrisols (HSGA), Hydrologic Soil Group Leptosols (HSGC) and Hydrologic Soil Group Luvisols (HSGD) respectively. The basin is predominantly sandy loamy and sandy clay loamy type soils with relatively low drainage properties. "Table 1" gives the hydrological distribution of the basin.
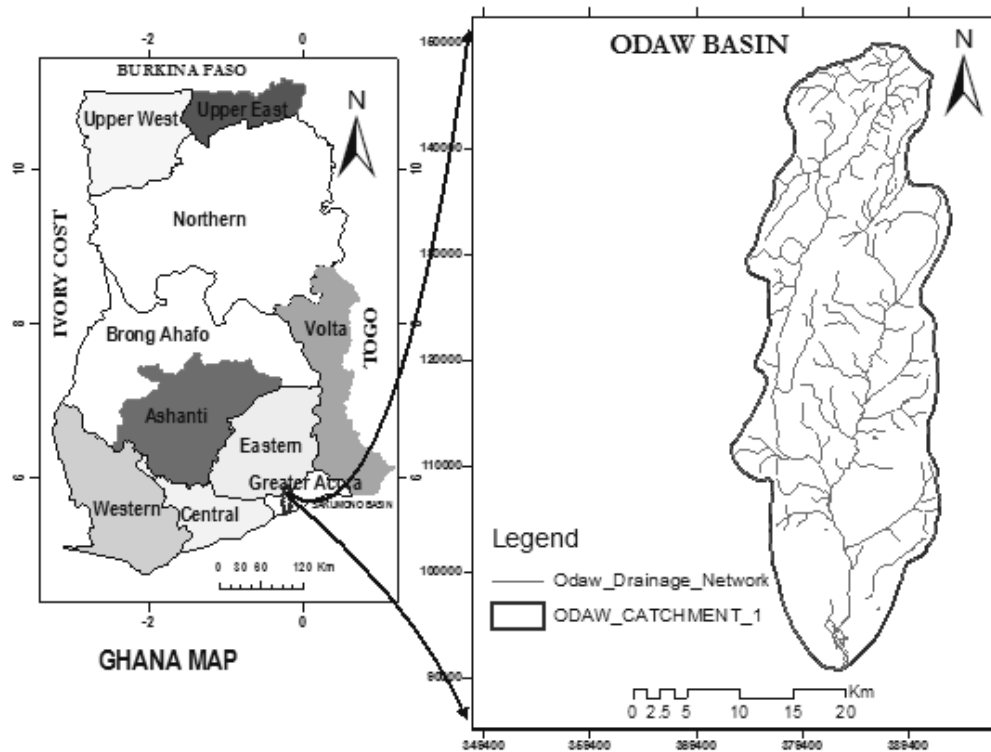
Fig. 1. Map of study Area

Table 1. Hydrological soil group and major soil types of the Odaw Basin

HSG	Description	Taxonomy		Distribution (%)
A	Very shallow, somewhat excessively drained, sandy soils on valleys and gently sloping quartzite hills; moderate stoniness.	Sandy, hyperthermic Ustocherpts	mixed, Lithic	53.3
C	Shallow, well drained, clayee soils on very gently sloping basaltic plateau (with narrow valleys) with moderate stoniness; associated with shallow loamy soils with severe erosion and moderate stoniness.	Loam, hyperthermic Ustrothents	mixed, Lithic	40.3
D	Moderately deep, well drained fine soils on very gently sloping basaltic plateau (with narrow valleys) with moderate erosion; associated with moderately shallow, well drained calcareous fine soils with slight erosion	Fine, hyperthemic Ustocherpts	mixed, Lithic	6.4
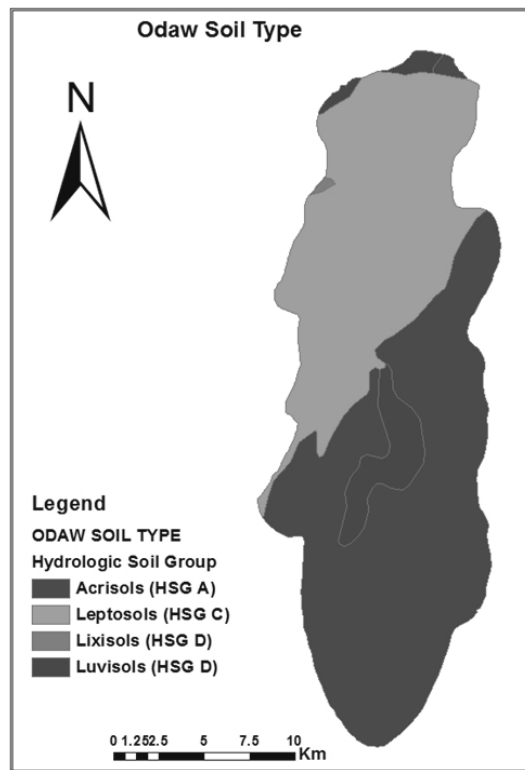
Fig. 2. Soil characteristics of the Odaw basin

MATERIALS AND METHODS In this study, a variety of data concerned with runoff estimation such as satellite images, digitized image, metrological data, soil type data and stream flow data were obtained. Erdas Imagine together with ESRI ArcGIS were used in the processing and analysis of the images. SCS-CN rainfall runoff model was used to generate the runoff and subsequently calibration and validation of the run off model. The summary of the methodology and the phases used in the study is described below.

DATA COLLECTION The data for the study was acquired from various state agencies. It includes soil characteristics of the basin "Fig 2", meteorological data covering the rainfall time series "Fig 3" and fifty three months of stream flow data "Table 2". Digitized land use map of 1964 at a scale of 1:250,000 and satellite image for 2007 at a resolution of 30m were downloaded from the European Digital Archive of Soil Maps (EuDASM) and Global Land Cover Facility (GCLF) at the University of Maryland, USA websites respectively. The images were used for land cover classification through the ERDAS imagine.
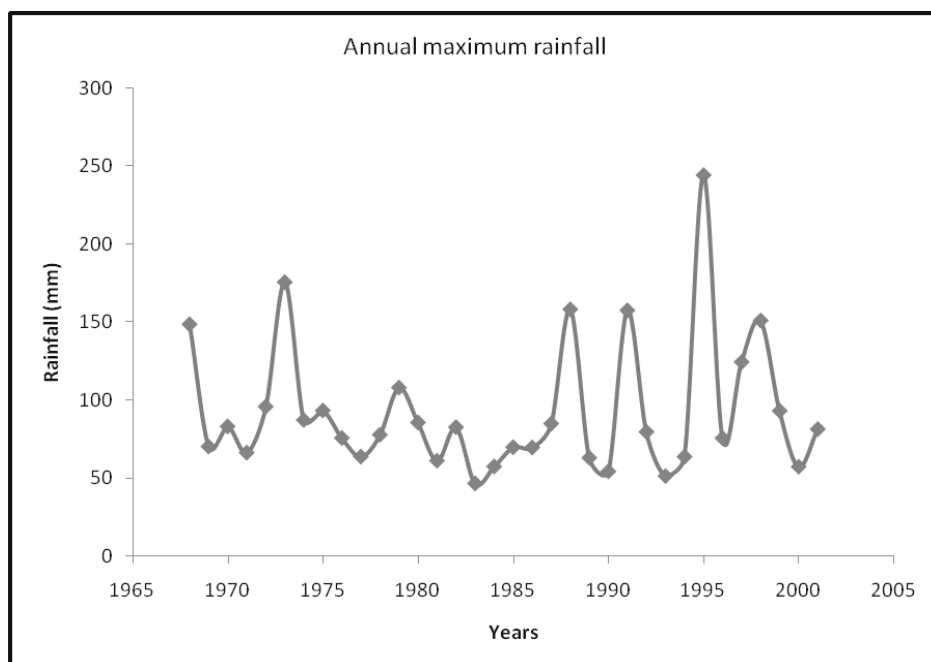
Fig. 3. Annual maximum rainfall

Table 2. Monthly stream flow records for Odaw River Basin

| Year | Observed stream flow (m^3. S^{-1}) | | | | | | | | | | | |
	Mar	Apr	May	Jun	Jul	Aug	Sept	Oct	Nov	Dec	Jan	Feb
1987-1988	0.50	0.22	0.22	0.36	0.26	0.17	4.80	3.00	0.23	0.87	0.72	0.72
1988-1989	4.69	0.71	8.51	5.63	3.97	2.66	0.48	1.28	1.10	0.37	0.42	0.24
1989-1990	0.99	0.97	1.69	1.92	2.95	1.24	1.46	1.73	1.10	1.10	1.17	1.50
1990-1991	1.56	2.02	0.64	0.80	0.44	1.09	0.63	0.30	0.81	1.58	0.25	1.17
1991-1992	0.85	6.52	4.26	1.11	1.10							

IMAGE PROCESSING LandSat Thematic Mapper (TM) image of scene (path: 193, row: 056) of year 2007 was used for the study. Remote sensing tools: Erdas Imagine and ArcGIS were used for the processing of the images. The raw satellite image was converted from Tag Image file format (Tiff) to Imagine (img) format using Erdas in order to be compatible with other Erdas Imagine files. The layers were stacked and sub-set to delineate the catchment area for classification. The UTM Zone 30N Coordinate on the WGS 84 was used to geocode the imported image. The EuDASM image for 1964 for Accra Plains was digitized in ArcGIS to obtain the 1964 land use data for the basin. This was followed by georeferencing using the Transverse Mercator projection with reference units in meters to allow compatibility with other digitized images for further processing. Band combination of red, blue and green was used to display the raw images in standard colour composites. The spectral band combination for displaying images often varies with different applications [29]. This was necessary for the visual interpretation of the images. A band combination of red, blue and green (RGB) is often used to display images in standard colour composites for land use and vegetation mapping [29].

LAND COVER CLASSIFICATION The unsupervised classification method was used to classify the images into the various land cover categories. The unsupervised classification is a method of clustering. It is self-organizing in that the image data are first classified by being aggregated into natural spectral groupings or clusters present in the scene. It enables the specification of parameters that the computer uses to determine statistical patterns in the data [30]. The procedure begins with a specified number of cluster means, and then it processes the image data repetitively, assigning each of the pixels to one of the class means. After each iteration, the initial cluster means shift to represent the new statistical means of the clusters in the data. This continues until there is no significant change of cluster means. Then the land cover identities of these spectral groupings were determined by comparing the classified image to the ground reference data. The statistics of the various classes were generated using the Erdas Imagine tool. Finally maps were composed, using ArcGIS tool and the maps were validated in the field to assess its accuracy. This was conducted through GPS known identified places in the study area as training sites. The procedure used was consistent with method which has been used in several studies, e.g. the [31].

CHANGE DETECTION The most commonly used land change detection methods includes i) image overlay ii) classification comparisons of land cover statistics iii) change vector analysis iv) principal component analysis and v) image rationing and vi) the differencing of normalized difference vegetation index (NDVI) [32]. The method used in this study was that of classification comparison of land cover statistics. This method was adopted because the study sought to find out the quantitative effect of changes in the areas of the various land cover categories on surface runoff. Using the post-classification procedure, the area statistics for each of the land cover classes was derived from the classifications of the images for each date (1964 and 2007) separately, using functions in the Erdas Imagine and ArcGIS tools. The areas covered by each land cover type for the various periods were compared. Then the directions of the changes (positive or negative) in each land cover type 1964 and 2007 were determined.

CURVE NUMBER COMPUTATION The curve number is a function of land use, soil type, and hydrologic condition. A combination of a hydrologic soil group and land use and treatment class (cover) is a hydrologic soil-cover complex. Curve numbers are assigned to such complexes to indicate their specific runoff potential. The greater the CN value the greater the surface runoff volume. Antecedent soil moisture conditions (AMC) are considered in the runoff model. The initial abstraction (I_a) consists mainly of interception, infiltration, antecedent soil moisture and depression storage, all of which occur before surface runoff begins. Curve number *(CN)* values of the catchment area were estimated using ArcGIS. This was accomplished by integrating the shapefiles of delineated catchment area, processed land use and digitized soil type maps produced into ArcGIS. The shapefiles were merged in ArcGIS using the arc toolbox, analysis, overlay and union tools and the resultant shapefile was added to the ArcMap project. The attribute table of the resultant shapefile was processed incorporating the three major Hydrologic Soil Group (HSG) of the basin: Acrisols (A), Leptosols (C) and Luvisols (D) as shown in "Fig. 2" together with *CN* values based on the land use. Subsequently the weighted curve numbers *(CN)* were determined for the time series. Since only two satellite images were available for this study, land use change was assumed to be linear. Land use was thus linearly interpolated and used for the estimation of weighted *CN* value for the unknown periods.

RAINFALL-RUNOFF MODEL: SCS-CN The curve number (CN) method [33] is widely used for estimating storm runoff

from rainfall. It is an infiltration loss model, which does not account for long term losses such as evaporation and evapotranspiration. Interception, surface storage, infiltration, evaporation and evapotranspiration are the hydrologic abstractions that occur during the conversion of rainfall to runoff. Among these various hydrologic abstractions, infiltration is the most important for storm and rainfall analysis. Evaporation and evapotranspiration are important for long-term and short-term seasonal or annual yield evaluations. Interception and surface storage are usually of secondary importance. Since the CN method is an infiltration loss model that does not account for evaporation and evapotranspiration, its use was shown to be restricted to modeling storm losses and surface runoff [34]. However, the method has been used in several long-term hydrologic simulation models with an appropriate soil moisture accounting procedure. The SCS-CN model used in the study is a function of rainfall data, hydrologic soil group and land use characteristics. These variables were used as input for the (SCS-CN) model to derive the runoff for the basin.

The excess rainfall according to (SCS-CN) in "Eq. (1)" uses the CN as its indicator

$$Q = \frac{(P - \alpha S)^2}{(P + S - \alpha S)} \tag{1}$$

$$S(mm) = \frac{25400}{CN} - 254 \tag{2}$$

$$I_a = \alpha S \tag{3}$$

Which is valid for P>αS otherwise, Q = 0, where Q is excess rainfall (mm) resulting from precipitation expressed as depth, P is rainfall (mm). S is the maximum potential abstraction the upper limit of water retention of the basin calculated by "Eq. (2)" and I_a initial abstraction is calculate by "Eq. (3)". The retention parameter is related to the CN as shown in "Eq. (2)".

The value of S in the CN method is related to watershed characteristics and antecedent moisture conditions. The SCS-CN model sets the coefficient α at 0.2 a traditional value for the existing model. The runoff procedure used for this study is summarized in the flow chart in "Fig. 4". The above equations can be summarized as shown in "Eq. (4)".

$$Q = \frac{\left(P - \alpha\left(\frac{25400}{CN} - 254\right)\right)^2}{\left(P + \left(\frac{25400}{CN} - 254\right)(1 - \alpha)\right)} \tag{4}$$

The model shows that runoff (Q) is a function of CN and that it increases with increasing CN. Hence the CN for the time series were used as a major factor to see its corresponding effects on the rainfall model.
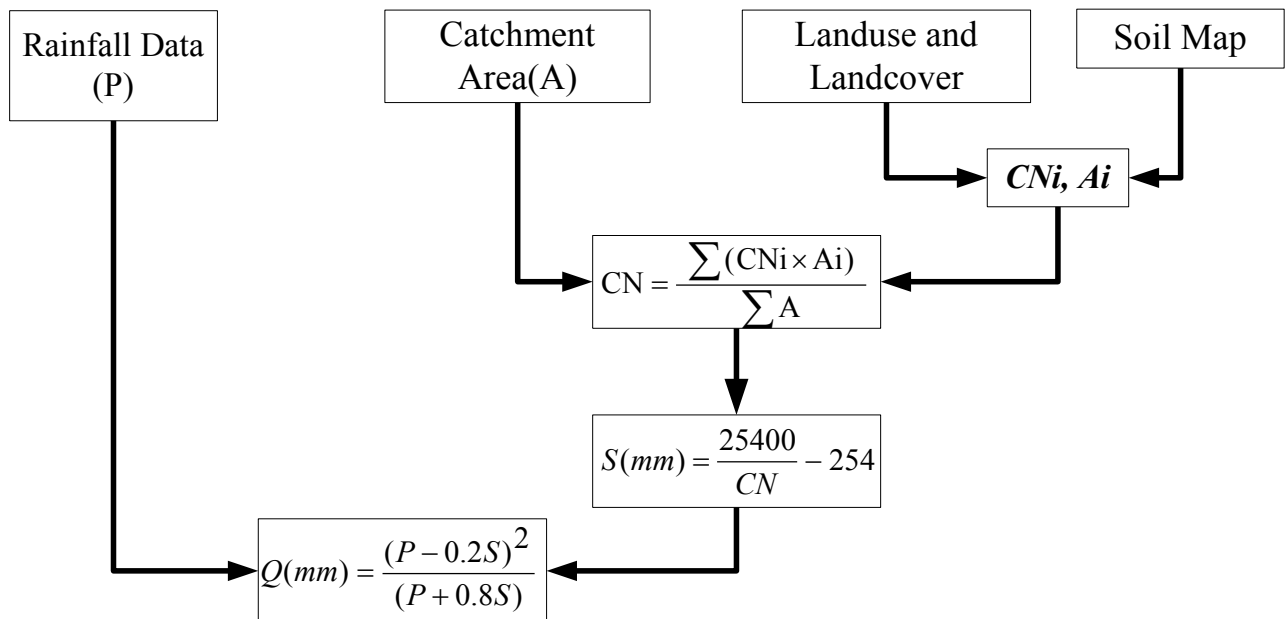
Fig. 4. Flow chart of methodology

MODEL CALIBRATION AND VALIDATION Calibration is the process of estimating values for model parameters that achieve simulation results that best reproduce observed data. Calibration of the watershed model requires gauged rainfall and stream flow observed data. For a given rainfall input, the model parameters are adjusted until computed stream flows are as close as possible to the actual observed stream flow. Klemes split-sample test method (1986) was applied in the process. In this method, the whole observed dataset is split into two independent datasets; the first set of data was used in calibration, whiles the other was used in validation of the calibrated dataset. Thus one set of the data was used in calibrating the model by soundly fine-tuning its physical and numerical parameters by trial-and-error to minimize difference between model results and field observations. Afterwards, the second independent data set is used to validate the model. The objective of the calibration procedure was to optimize the initial abstraction of the SCS-CN model in such a manner that the calculated efficiency (E) would be highest. The model has two basic variables, rainfall which is natural event and maximum storage potential (S), which is a derived parameter from land use and land cover integration. Hence all input parameters are kept constant except (α) in "Eq. 4". Afterwards, the optimised equation was used for the validation.

MODEL EVALUATION The model was evaluated by two indices of agreement coefficient of determination (R^2) and index of agreement (D) as described by [35]. R^2 is given by "Eq. 5", where Xi and $\overline{X}$ denotes the observed and mean of the observed data values; Yi and $\overline{y}$ denotes the simulated and the mean of the simulated values. The value of R^2 can be interpreted, after [35], as given by "Eq. 5".

$$R^2 = \frac{\sum_{i=1}^{r} \left(X_i - \overline{X} \right)\left(Y_i - \overline{Y} \right)}{\left[\sum_{i=1}^{1} \left(X - \overline{X} \right) \right]^{0.5} \left[\sum_{i=1}^{r} \left(Y - \overline{Y} \right) \right]^{0.5}} \tag{5}$$

The index of agreement, D, measures agreement between the observed and simulated data sets and D is given by "Eq. 6". D varies between 0 and 1 with near 1 being perfect agreement.

$$D = 1.0 - \frac{\sum_{i=1}^{r} \left(X_i - Y_i \right)^2}{\sum_{i=1}^{r} \left(\left| Y_i - \overline{X} \right| + \left| X_i - \overline{X} \right| \right)^2} \tag{6}$$

The Nash-Sutcliffe efficiency [36], E, provides a method of determining how the lower dynamics of a model compares with the higher dynamics of observed values. E also shows how well a model can predict observed values. E is given in the "Eq. 7".

$$E = 1.0 - \frac{\sum_{i=1}^{r} \left(X_i - Y_i \right)^2}{\sum_{i=1}^{r} \left(X_i - \overline{Y} \right)^2} ;$$

where

$$\left\{ \begin{array}{l} -1 \leq E \leq 0 \rightarrow Poor \text{ model} \\ 0 < E < 1 \rightarrow Good \text{ model} \\ E = 1 \rightarrow Perfect \text{ model} \end{array} \right\} \tag{7}$$

2. RESULTS AND DISCUSSIONS

EFFECT OF LAND USE CHANGE A total of six land cover categories were identified and classified in the study. These were settlement area, closed forest, thickets, grassland, open forest and water body as shown in "Fig. 5".

The comparison between the two different years of land use in "Table 3" and "Fig. 5" shows significant change detection in almost all the six land use categories and their extent during the period. The most extensive land cover change over the period was found to be settlement followed by open forest representing 306% and 118% respectively. The trend of land cover changes in the study shows general conversion to built up areas. The average annual growth rate of land use change was established approximately as 0.52%. This has potential on the catchment characteristics and hydrology. Since land cover is a function of rainfall regime, soil conditions and geomorphology, the conversion of the land cover to built up

areas would definitely lead to changes in these variables of the catchment disrupting the hydrological cycle by altering the balance between rainfall and evaporation and consequently, the runoff response of the area from sub-surface flow to overland storm flows.

"Table 4" shows the weighted curve numbers over the hydrological soil groups between 1964 and 2007. The change in the land use between 1964 and 2007, "Table 5", shows appreciable reduction of the water holding capacity of the basin (maximum potential abstraction) about 55%, which accounts for corresponding higher levels of surface runoff.

Table 3. Landuse and landcover change detection

Land Cover Class	Year 1964 Area (km^2)	%	Year 2007 Area (km^2)	%	Change (%)
Settlement	62.2	17.0	252.5	69.1	+305.8
Closed Forest	66.0	18.1	52.2	14.3	-20.9
Thicket	108.0	29.6	25.7	7.0	-76.2
Grassland/Shrub	123.9	33.9	24.1	6.6	-80.5
Open Forest	4.5	1.2	9.8	2.7	+118.5
Water Body	0.7	0.2	1.0	0.3	+42.6
Total	365.29	100	365.29	100	

(+) indicates increase   (-) indicates decrease
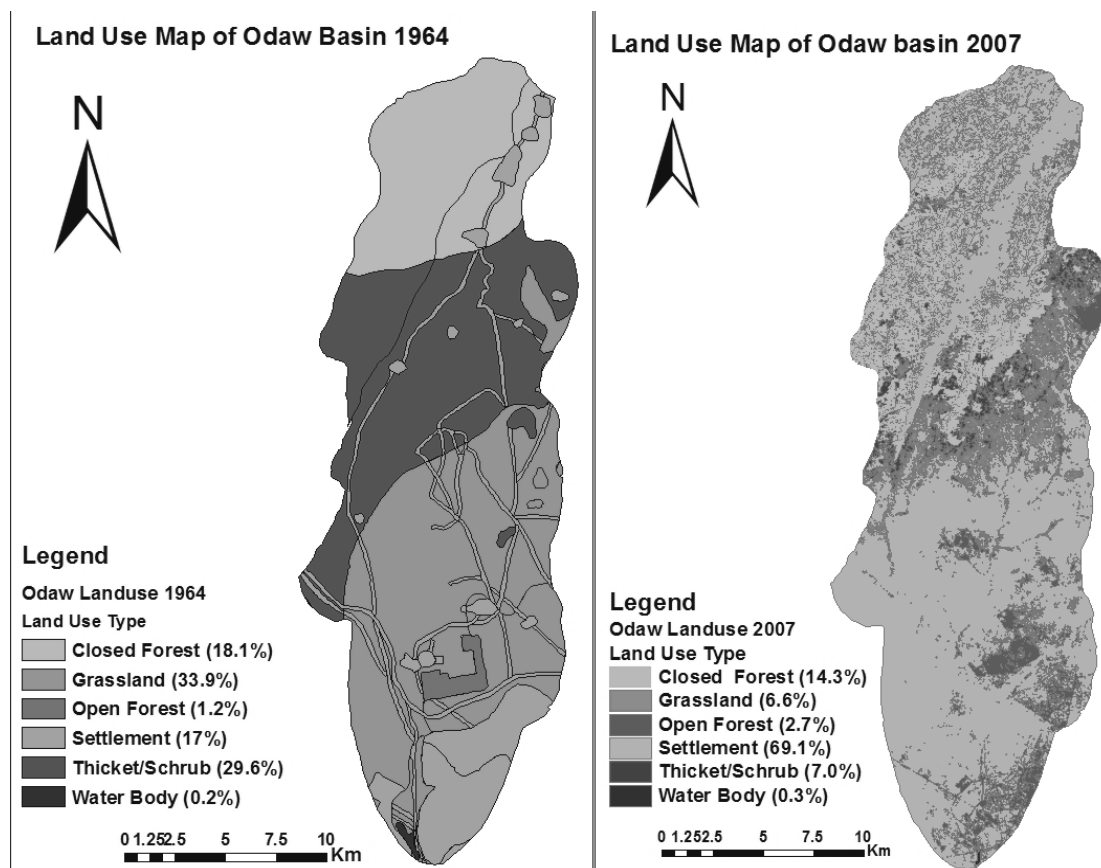
Fig. 5. Digitized landuse map 1964 and unsupervised classification of Landsat image 12th August, 2007 (p193r056)

Table 4. Weighted CN over the Hydrological soil groups

Hydrologic Soil Group	Land Cover Type	Weighted CN (1964)	Weighted CN (2007)
Acrisols	Settlement Closed Forest Grass/herb Grassland/ Shrub Open Forest Water Body	44.21	70.04
Leptosols		73.30	80.33
Luvisols		74.04	88.86

Table 5. Land cover classification and water holding potential of the Odaw Basin

Hydrologic Soil Group	Land Cover Type	Weighted CN (1964)	Weighted CN (2007)	1964 S^* (mm)	1964 I_a^* (mm)	2007 S^* (mm)	2007 I_a^* (mm)
Acrisols Leptosols Luvisols	Settlement Closed Forest Grass/herb Grassland/Shrub Open Forest Water Body	63.86	79.74	143.75	28.75	64.53	12.91

S^* is maximum potential abstraction and I_a^* is initial abstraction

MODEL EVALUATION Due to the fact that surface runoff using the uncalibrated curve number method was not predicted well, a calibration was carried out. The basin has 53 months of observed steam flow data spanning between 1988 and 1992. From the total number of events, a range of representative rainfall-runoff events in terms of discharge amount and seasonal occurrence were taken for calibration and validation (23 for calibration and 30 for validation events). The objective of the calibration procedure was to optimize (α) in the equation $I_a = \alpha S$ (Eq. (3) in such a manner that the calculated efficiency (E) for all calibration event would be highest. During the calibration procedure, all input parameters were kept constant except (α), which was varied between 0.01 and 0.3. Afterwards, the optimized equation was used for validation. The highest E was found when α is 0.09.

The validation and calibration results are shown in "Fig. 6" and "Fig. 7". The runoff model after calibration and validation was evaluated using the Nash–Sutchliffe efficiency (E), coefficient of determination (R^2), and index of agreement (D). The model efficiency was found to be 94.5%, with the coefficient of determination R^2 being 0.73, and the index of agreement D of 0.83. Results of the model show that there is strong agreement between the simulated and observed data. The resulting surface runoff, "Fig. 8" over the time series considered indicates steady increase of surface runoff. There is a sharp shift of the hydrology of the basin from normal sub surface flow to rapid overland flow due to urbanization which is a trigger for flush flood in the basin in recent history.
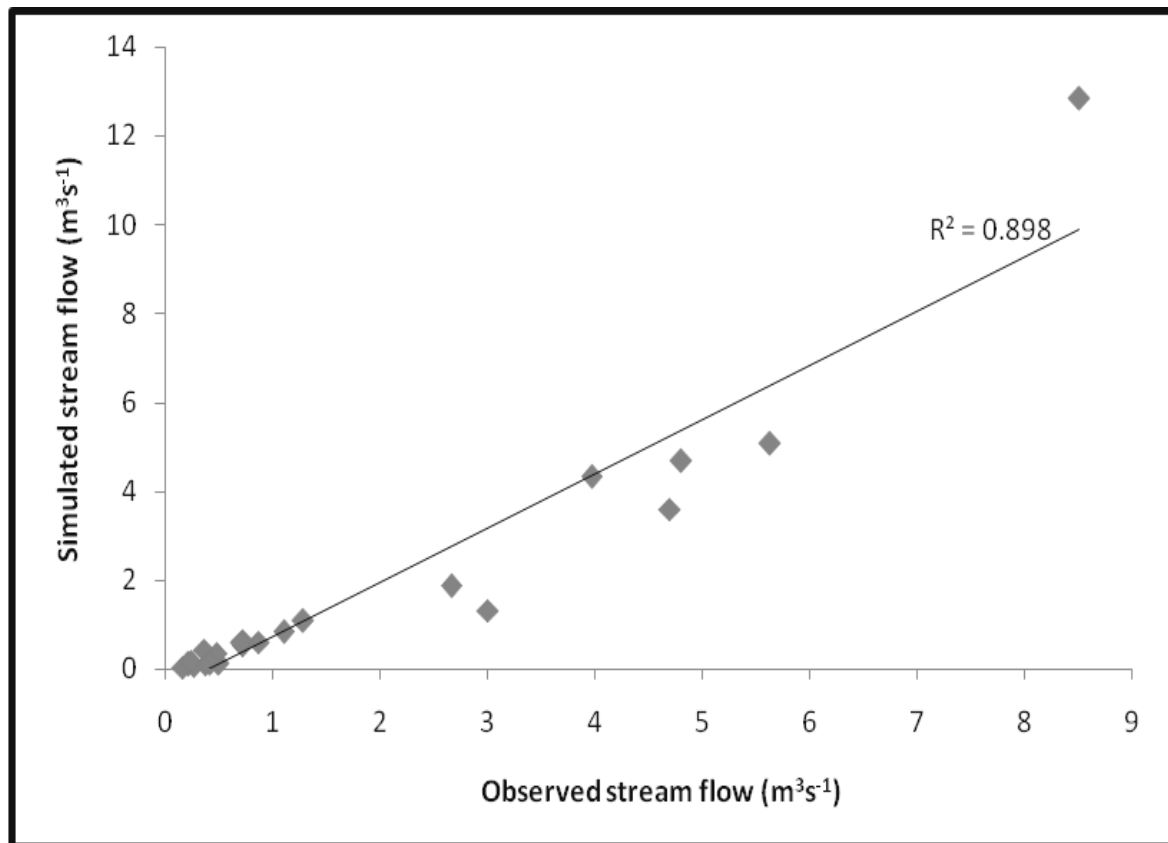
Fig. 6. Calibration of runoff model
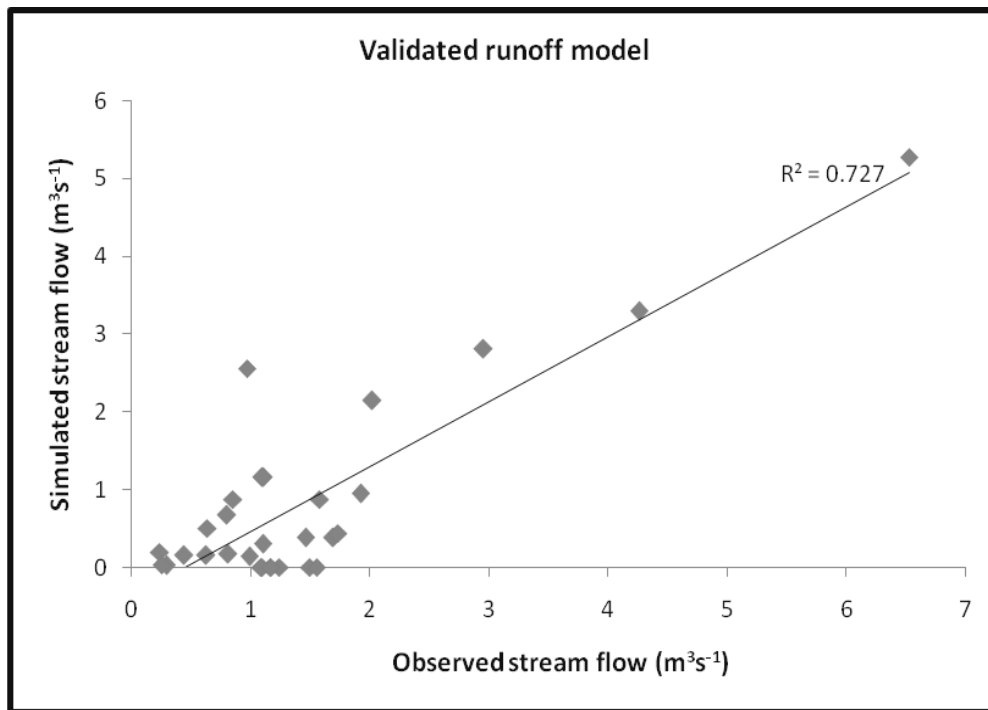
Fig. 7. Validation of runoff model
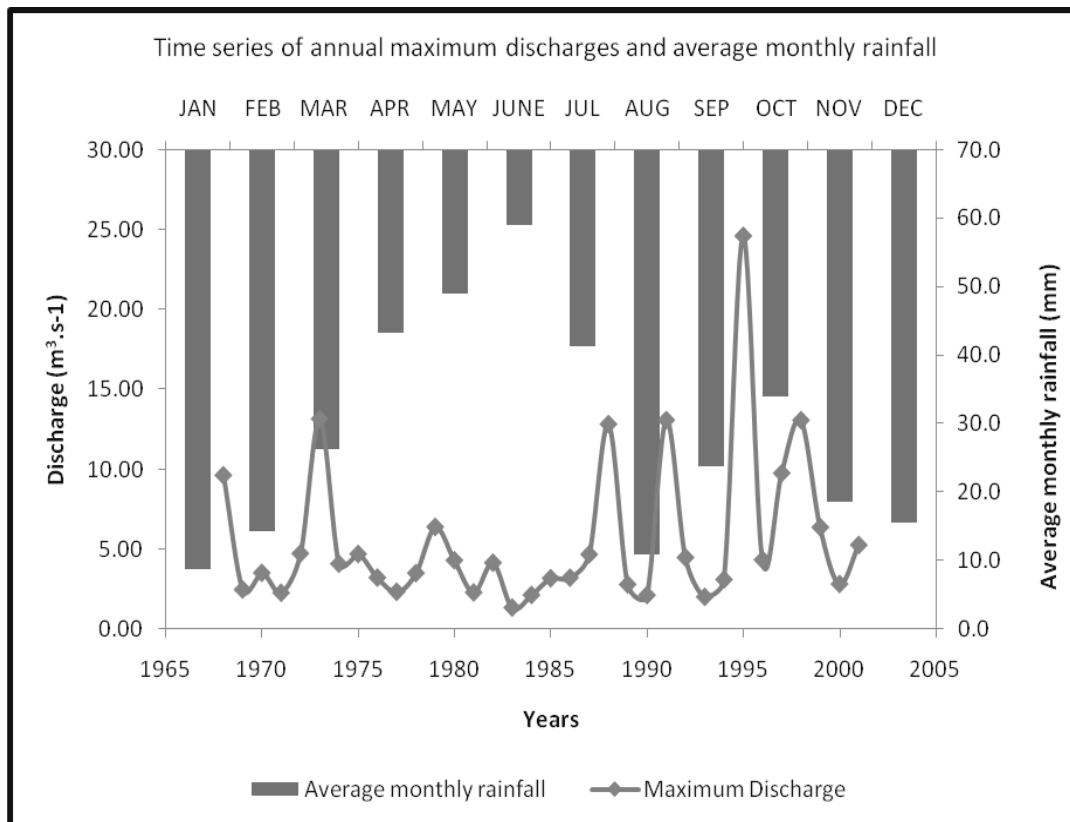
Fig. 8. Surface water flows from 1968 to 2001

3. CONCLUSION

The analysis of the EuDASM image and LandSat TM images of 1964 and 2007 respectively, revealed that land use and land cover of the Odaw catchment has changed significantly over the years. Over the 43 years, changes in land use and land cover of the Odaw catchment were found to be related to population growth and urbanization with a higher rate of surface imperviousness. In the context of hydrologic analysis runoff magnitudes are estimated as a result of precipitation. These estimates consider processes in a watershed such as land use functions that transform precipitation to runoff and further transport water through the drainage basin. Based on the trend of land use changes detected in this study, there is increased in overland surface water flows due to the increasing curve number CN. Hence runoff was found to be strongly

related to the land use and land cover change. The SCS-CN model revealed that the runoff is more sensitive to the changes in the trend of land use than the ratio of initial abstraction to the maximum water potential of the basin. The ratio of the initial abstraction to maximum water potential was optimized as 0.09. It is therefore needful to improve on the basin storage holding capacity as a means to offset the occurrence of increasing overland surface water flows. These results constitute a helpful document for hydrologic modeling that allows the calculation of flow profiles and estimation of runoff functions that affects the hydrology of related urban basins.

4. ACKNOWLEDGEMENTS

REFERENCES

1. Turner, M. G.; & Valone T. J. *Ecological principles and guildelines for managing the use of land: a report from the Ecological Society of America*. Ecol. Appl. (2001), 10, 639–670.

2. Agarwal, C.; Green, G. M.; Grove, J. M.; Evans, T. P.; & Schweik, C. M. (2002) *Areview and assessment of land use change models: dynamics of space time and human choice, CIPEC Collaborative Report*   Series No. 1, USDA Forest Service Indiana, pp. 84.

3. Luijten, J. C., *A systematic method for generating land use patterns using stochastic rules and basic landscape characteristics: results for a Colombia hillside watershed*, Agricult. Ecosyst. Environ (2003), 95, 427–441.

4. Cao, W.; Bowden, W.B.; Davie, T.; & Fenemor, A., *Modelling Impacts of Land Cover Change on Critical Water Resources in the Motueka River Catchment, New Zealand*, Water Resour Manage (2009), 23:137-151.

5. Caruso, G.; Rounsevell, M. D. A.; & Cojacarus, G.; *Exploring a spatiodynamic neighborhood-based model of residential behaviour in the Brussels peri-urban area*. Int. J. Geograph. Inform. Sci. (2005), 19, 103–123.

6. Zhou, F.; Xu, Y. P.; Chen, Y.; Xu, C. Y.; Gao, Y. Q.; & Du, J. K.; *Hydrological Response to Urbanization at Different Spatio-temporal Scales simulated by coupling of CLUE-S and the SWAT model in the Yangtze River Delta region*. Journal of Hydrology, (2013), 485, 113-125.

7. Parker, D.; & Meretsky, V.; *Measuring pattern outcomes in an agent-based model of edge-effect externalities using spatial metrics*. Agricult. Ecosyst. Environ, (2004), 101, 233–250.

8. Cheng, S. J.; & Wang, R. Y.; *An approach for evaluating the hydrological effects of urbanization and its application*. Hydrol. Process, (2002), 16, 1403–1418.

9. Brown, D. G.; Page, S.; Riolo, R.; Zellener, M.; & Rand, W.; *Patch dependence and the validation of agent based spatial models of land use*. Int. J. Geograph. Inform. Sci. (2005), 19, 153–174.

10. Jantz, C. A.; & Goetz, S. J.; Analysis *of scale dependencies in an urban land use change model*. Int. J. Geograph. Inform. Sci. (2005), 19, 217–241.

11. Manson, S. M.; (2005) *Agent-based modeling and genetic programming for modeling land change in the Southern Yucatan Peninsula Region of Mexico*

12. Yu-Pin, L.; Nien-Ming, H.; Pei-Jung, W.; Chen-Fa, W. C.; & Peter, H. V.; (2006) *Impacts of land use change scenarios on hydrology and land use patterns in the Wu-Tu watershed in Northern Taiwan,* Landscape and Urban Planning (2007), 80 111–126

13. McGarigal, K.; & Marks, B. J.; *FRAGSTATS: spatial pattern analysis program for quantifying landscape structure*. USDA Forest Service General Technical Report. (1995), PNW-351.

14. Cushman, S. A.; & Wallin, D. O.; *Rate and patterns of landscape change in the Central Sikhote-alin Mountains, Russian Far East*. Landscape Ecol. (2000), 15, 643–659.

15. Lin, Y. P.; Teng, T. P.; & Chang, T. K.; *Multivariate analysis of soil heavy metal pollution and landscape patterns analysis in Changhua County in Taiwan*. Landscape Urban Plan. (2002), 62, 19–35.

16. Fortin, M. J.; Boots, B.; Csillag, F.; & Remmel, T. K.; *On the role of spatial stochastic models in understanding landscape indices in ecology*. Oikos (2003), 102, 203–212.

17. Berling-Wolff, S.; & Wu, J.; *Modeling urban landscape dynamics: a case study in Phoenix, USA*. Urban Ecosyst. (2004), 7, 215–240.

18. Kearns, F. R.; Kelly, N. M.; Carter, J. L.; & Resh, V. H.; *A method for the use of landscape metrics in freshwater research and management*. Landscape Ecol. (2005), 20, 113–125.

19. Legesse, D.; Vallet-Coulomb, C.; & Gasse, F.; *Hydrological response of a catchment to climate and land use*

changes in Tropical Africa: case study South Central Ethiopia. J. Hydrol. (2003), 275, 67–85.

20. Haverkamp, S.; Fohrer, N.; & Frede, H. G.; *Assessment of the effect of land use patterns on hydrologic landscape functions: a comprehensive GIS based tool to minimize model uncertainty resulting from spatial aggregation*. Hydrol. Process, (2005), 19, 715–727.

21. Grunwald, S.; & Norton, L. D.; *Calibration and validation of a non-point source pollution model,* Agricultural Water Management, (2000), 45 (2000) 17±39

22. Haith, D. A.; & Shoemaker, I. L.; *Generalized watershed loading functions for stream flow nutrients*. Water Resour. Bull. (1987), 107, 121–137.

23. Yu-Pin, L.; Nien-Ming, H.; Pei-Jung, W.; Chen-Fa, W.; & Peter, H. V.; *Impacts of land use change scenarios on hydrology and land use patterns in the Wu-Tu watershed in* Northern Taiwan, Landscape and Urban Planning (2007), 80 111–126

24. Hammouri, N.; & El-Naqa, A.; *Hydrological modeling of ungauged Wadis in arid environments using GIS: a case study of Wadi Madoneh in Jordan*, Revista Mexicana de Ciencias Geológicas, (2007), v. 24, núm. 2, p. 185-196.

25. Campana, A. N.; *Predicting floods from urban Development scenarios: Case study of the Dilúvio Basin, Porto Alegre,* Brazil. Urban Water, (200), 1, **3**, 113-124. 12.

26. Mille, A. B.; Bryant, E. S.; & Birnie, R. W.; *An analysis of land cover changes in the Northern Forest of New England using multi temporal LANDSAT MSS data*. int. j. remote sensing, (1998), Vol. 19, no. 2, 215-265

27. DeFries, R.; & Belward, A. S.; *Global and regional land cover characterization from satellite data; an introduction to the Special Issu"e .int. j. remote sensing,* (2000), vol.21, no. 6&7, 1083-1092.

28. Erdelyi, M.; *The Hydrogeology of Ghana*, Research Institute for Water Resources, Budapest, Hungary, (1964).

29. Trotter, C. M.; *Characterising the topographic effect at red wavelengths using juvenile conifer canopies*. int. j. remote sensing, (1998), vol.19, no.11, 2215-2221

30. ERDAS, *Field guide. Fifth edition ERDAS Inc.* Buford Highwas, NE, Atlanta, Georgia. USA, (1999), 75 (8), 2430-2437.

31. NPS/NBS Vegetation Mapping (2002) USGS-Vegetation Mapping Program. http://biology.usgs.gov/nps/aa/sect1.html

32. Duadze, S. E. K.; *Land-use and land-cover study of the Savannah ecosystem in the Upper West Region (Ghana) using remote sensing*. Cuvillier Verlag, (2004), No**. 16**.

33. SCS, *Hydrology. National Engineering Handbook*, Supplement A, Section 4. Soil Conservation Service, (1956), US Department of Agriculture: Washington, DC; Chapter 10.

34. Boughton, W. C.; *A review of the USDA-SCS curve number method*. Australian Journal of Soil Research, (1989), **27**: 511–523.

35. Coulibaly, P.; & Baldwin, C. K.; *Nonstationary hydrological time series forecasting using nonlinear dynamic methods*, Journal of Hydrology Volume (2005), 307, Issues 1-4, Pages 164-174 J. Appl.

36. Nash, J. E.; & Sutcliffe, J. V.; *River flow forecasting through conceptual models: Part I – A discussion of principles*. Journal of Hydrology, (1970), 282-290.

DATA MINING FOR THE DETECTION OF MICROSATELLITES IN THE CHLOROPLAST GENOME OF SYNTRICHIA RURALIS

Asheesh Shanker

Department of Bioscience and Biotechnology
Banasthali University, Banasthali-304022
Rajasthan, India
+91-9414478655
Email: ashomics@gmail.com

ABSTRACT

Microsatellites are found in DNA sequences and consist of short motifs of 1-6 bp. These repeats are also known as simple sequence repeats (SSRs) and play important role in phylogenetics, population genetics, and also in the development of molecular markers. In present analysis chloroplastic microsatellites in the chloroplast genome sequence of *Syntrichia ruralis* were mined with the help of a Perl script. A total of 69 perfect microsatellites were detected in 122.630 kb sequence mined showing density of 1 SSR/1.75 kb. Depending on the repeat units, the maximum length of microsatellites found to be 19 bp for mono, 30 bp for di, 15 bp for tri, 12 bp for tetra and 15 bp for pentanucleotide repeats. Hexanucleotide repeats were completely absent in chloroplast genome of *Syntrichia ruralis*. Mononucleotide repeats (37.68%) were the most frequent repeat type followed by tri (21.74%) and tetra tetranucleotide (21.74%) repeats.

Keywords— Bryophytes, Chloroplast, Microsatellites, Moss, Simple Sequence Repeats.

1. INTRODUCTION

Bryophytes are the earliest land plants and are broadly classified into liverworts, mosses and hornworts. A small number of available organelle genome sequences of bryophytes helps to know the evolutionary relationship among these plants[1,2]. In bioinformatics analysis based on organelle genome sequences of bryophytes the hornworts appeared as sister group to vascular plants and liverworts as the earliest diverging lineage[3,4,5]. Repeats are ubiquitously present in the organism's genomes. Microsatellites are one of such repeats. These repeats are also known as simple sequence repeats (SSRs) and are found in DNA sequences. Microsatellites consist of short repeat motifs of 1-6 bp and are present in both coding and non-coding regions of DNA sequences[6]. These repeats have been widely used as molecular markers[7]. In the recent past several studies have been conducted to detect microsatellites in chloroplast genomes of bryophytes[8,9]. Additionally, a database named MitoSatPlant has been developed which provides detail information of mitochondrial microsatellites of green plants[10]. Despite these efforts the detailed information of chloroplastic microsatellites in *Syntrichia ruralis* is not available. Computational approaches offer quick and cost-effective microsatellites extraction. These methods use sequences available in public databases[11]. Therefore, the present analysis was conducted to identify chloroplastic microsatellites in *Syntrichiaruralis*. Furthermore, the distribution of microsatellites in coding and non-coding regions of chloroplast genome was analyzed.

2. MATERIALS AND METHODS

SEQUENCE RETRIEVAL OF CHLOROPLAST GENOME SEQUENCE OF SYNTRICHIA RURALIS National Center for Biotechnology Information (NCBI; www.ncbi.nlm.nih.gov) is a public repository for biological data. The complete chloroplast genome sequenceof *Syntrichia ruralis*[12] (NC_012052, 122630 bp) was downloaded from NCBI in FASTA and GenBank format.

DATA MINING TO IDENTIFY CHLOROPLASTICMICROSATELLITES The microsatellites in the chloroplast genome sequence of *Syntrichiaruralis* were mined using a Perl script (MISA; http://pgrc.ipkgatersleben.de/misa/misa). MISA takes FASTA formatted DNA sequence file as an input and generates information of perfect and compound microsatellites, if detected. A minimum length of ≥12 for mono, di, tri and tetranucleotide, ≥15 for pentanucleotide and ≥18 for hexanucleotide repeats was used for the detection of microsatellites. Maximum difference between two compound microsatellites was taken as 0. The GenBank file contains additional information about sequence including the coding and non-coding regions of chloroplast genome. Mined microsatellites were classified in the coding, non-coding and coding-non-coding (few bases occur in coding as well as in non-coding regions or vice-versa) regions based on the presence of these repeats in respective regions of chloroplast genome.

3. RESULTS AND DISCUSSION

In the present analysis microsatellites were mined in the chloroplast genome sequence of *Syntrichiaruralis*. A minimum length of 12 bp was considering for the identification of microsatellites. A total of 69 perfect microsatellites were detected with length variation from 12 to 30 bp. The frequency of various repeat motifs identified (mono-penta) is presented in Fig. 1. Additional information of mined microsatellites motif, their length, start-end position and the region in which they lie is presented in Table 1. Among all microsatellites identified 22 (31.89%) found in coding, 46 (66.67%) in non-coding and only 1 (1.45%) in coding-non-coding regions. Earlier reports suggested that microsatellites are abundant in non-coding regions of the genome[8,13]and the results of the present study showed consistency with it. Mononucleotides were the most frequent repeat (26, 37.68%) followed by tri and tetra, both present with equal frequency (15, 21.74%) and di (9, 13.04%) nucleotide repeats. Pentanucleotide repeats were detected with least frequency (4, 5.8%). Moreover, hexanucleotide repeats were completely absent in chloroplast genome of *Syntrichiaruralis*. The mined microsatellites showed a density of 1 SSR/1.75 kb in 122.630 kb sequence mined. The density of microsatellites in *Syntrichiaruralis* found to be higher than the microsatellites density in *Anthoceros formosae*[8](1 SSR/2.4 kb), *Aneura mirabilis*[9] (1 SSR/5.68 kb) and *Pellia endiviifolia*[14] (1 SSR/7.09 kb), rice[15] (1 SSR/6.5 kb),
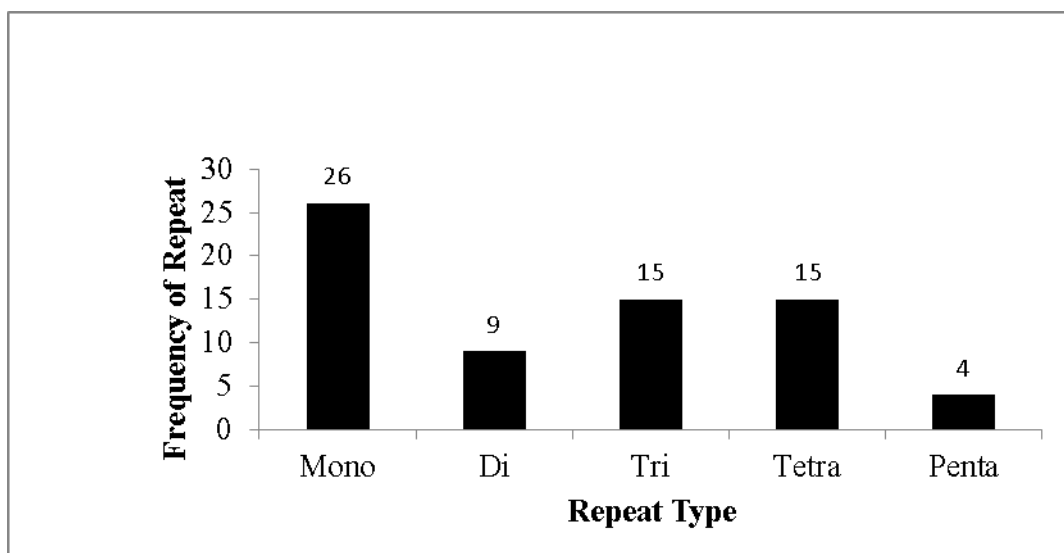
Fig. 1. Frequency distribution of mono-penta repeats identified.

EST-SSRs in barley, maize, wheat, rye, sorghum and rice[16] (1 SSR/6.0 kb), cotton and poplar[17] (1 SSR/20 kb and 1 SSR/14 kb respectively), Unigenes sequences of *Citrus*[6] (1 SSR/12.9 kb; Shanker*et al.,* 2007). However, the densityof microsatellites in *Syntrichia ruralis* found to be lower than the density of microsatellites in, family Solanaceae[18] (1 SSR/1.26kb). The selection of microsatellites detection tools, parameters taken (e.g. minimum length of microsatellites) and amount of data analyzed might be the cause of variations in the density of microsatellites. The absence of hexanucleotide repeats in *Syntrichia ruralis* shows consistency with chloroplast microsatellites based studies on *Aneura mirabilis*[9] and *Pellia endiviifolia*[14]. Previously, it was suggested that the abundance of different type of repeats attributed to the evolutionary processes which is responsible to fine tune distribution of microsatellites in the genome[19].In the recent past mononucleotides were found to be abundant in the chloroplast genome of *Anthoceros formosae*[8], *Aneura mirabilis*[9] and *Pellia endiviifolia*[14]and the results of present analysis are consistent with these findings.

4. CONCLUSION

Computational mining of complete chloroplast genome sequence of *Syntrichia ruralis*, downloaded from National Center for Biotechnology Information, saves time and cost associated with the experiment. The perl script, MISA, provides

sufficient number of mined microsatellites for this moss. These microsatellites are useful to design PCR primers which will be helpful in the development of microsatellite markers. The mined data along with PCR primers are available in a database named ChloroSSRdb[20] and can be freely accessed at www.compubio.in/chlorossrdb/. Flanking sequences of SSRs which include 200 nucleotides are also provided along with primers. The mined SSRs can be used for population genetics and evolutionary studies of *Syntrichia* species.

5. ACKNOWLEDGEMENTS

Table 1: Mined microsatellites motif in chloroplast genome of *Syntrichia ruralis*, along with their length, start-end position and region in which microsatellites lie.

S. No.	Motif	Length	Start	End	Region
1	(A)14	14	529	542	Coding
2	(TTA)4	12	4196	4207	Non coding
3	(TA)8	16	7052	7067	Non coding
4	(AT)6	12	9290	9301	Non coding
5	(AATAA)3	15	9681	9695	Non coding
6	(TA)6	12	10656	10667	Non coding
7	(A)13	13	12985	12997	Non coding
8	(T)12	12	14274	14285	Non coding
9	(AATA)3	12	14604	14615	Non coding
10	(AT)15	30	15231	15260	Non coding
11	(ATA)4	12	16355	16366	Non coding
12	(AT)7	14	16741	16754	Non coding
13	(ATAA)3	12	17094	17105	Non coding
14	(AATA)3	12	17942	17953	Non coding
15	(CAAA)3	12	18624	18635	Coding
16	(TTAA)3	12	18717	18728	Coding-Non coding
17	(T)12	12	19437	19448	Non coding
18	(T)12	12	19520	19531	Non coding
19	(T)12	12	22006	22017	Coding
20	(A)12	12	23844	23855	Non coding
21	(A)12	12	27114	27125	Non coding
22	(TA)6	12	32766	32777	Non coding
23	(T)14	14	32783	32796	Non coding
24	(TTA)4	12	33050	33061	Non coding
25	(TTA)5	15	33278	33292	Non coding
26	(G)14	14	41448	41461	Non coding
27	(TTAA)3	12	41490	41501	Non coding
28	(AT)7	14	41884	41897	Non coding
29	(ATA)4	12	44894	44905	Coding
30	(CTTTT)3	15	45372	45386	Non coding
31	(ATA)4	12	45452	45463	Non coding
32	(AT)7	14	45587	45600	Non coding
33	(A)12	12	46073	46084	Non coding
34	(T)13	13	48277	48289	Coding
35	(TAAA)3	12	49197	49208	Coding
36	(TTA)5	15	49829	49843	Coding
37	(T)13	13	51714	51726	Coding

S. No.	Motif	Length	Start	End	Region
38	(T)12	12	51996	52007	Coding
39	(T)12	12	52111	52122	Coding
40	(T)12	12	52255	52266	Coding
41	(T)13	13	52309	52321	Coding
42	(AAT)4	12	54302	54313	Non coding
43	(A)12	12	55314	55325	Coding
44	(T)19	19	56186	56204	Coding
45	(A)14	14	57185	57198	Non coding
46	(TTTA)3	12	59168	59179	Non coding
47	(AT)8	16	59781	59796	Non coding
48	(T)13	13	62108	62120	Non coding
49	(TAT)4	12	69344	69355	Coding
50	(TATT)3	12	70075	70086	Coding
51	(T)12	12	74052	74063	Non coding
52	(TCTTT)3	15	77176	77190	Non coding
53	(T)18	18	77540	77557	Non coding
54	(AAAT)3	12	78376	78387	Non coding
55	(T)13	13	78612	78624	Coding
56	(T)15	15	78643	78657	Coding
57	(ATA)5	15	79505	79519	Non coding
58	(AAT)4	12	83068	83079	Non coding
59	(AATAA)3	15	84020	84034	Non coding
60	(AATA)3	12	84716	84727	Non coding
61	(AGGT)3	12	90921	90932	Coding
62	(ATA)4	12	101589	101600	Non coding
63	(A)15	15	103733	103747	Non coding
64	(ATT)5	15	104282	104296	Non coding
65	(TATT)3	12	108482	108493	Coding
66	(TAA)4	12	110305	110316	Non coding
67	(TTA)5	15	112600	112614	Coding
68	(CTAC)3	12	115775	115786	Coding
69	(TTTA)3	12	121980	121991	Non coding

REFERENCES

1. Shanker, A. Chloroplast genomes of bryophytes: a review. Archive for Bryology **143,** 2012, p. 1-5.

2. Shanker, A. Sequenced mitochondrial genomes of bryophytes. Archive for Bryology **146,** 2012a, p. 1-6.

3. Shanker, A. Paraphyly of bryophytes inferred using chloroplast sequences. Archive for Bryology **163,** 2013, p. 1-5.

4. Shanker, A. Inference of bryophytes paraphyly using mitochondrial genomes. Archive for Bryology **165,** 2013a, p. 1-5.

5. Shanker, A. Combined data from chloroplast and mitochondrial genome sequences showed paraphyly of bryophytes. Archive for Bryology **171,** 2013b, p. 1-9.

6. Shanker, A., Bhargava, A., Bajpai, R., Singh, S., Srivastava, S. & Sharma, V. Bioinformatically mined simple sequence repeats in UniGene of *Citrus sinensis*. Sci. Hort. **113,** 2007, p. 353-361.

7. Blair, M.W. &Hurtado, N. EST-SSR markers from five sequenced cDNA libraries of common bean (*Phaseolus vulgaris* L.) comparing three bioinformatic algorithms. Mol. Ecol. Resour. **13,** 2013, p. 688-695.

8. Shanker, A. Identification of microsatellites in chloroplast genome of *Anthocerosformosae*. Archive for Bryology **191,** 2013c, p. 1-6.

9.   Shanker, A. Mining of simple sequence repeats in chloroplast genome of a parasitic liverwort: *Aneura mirabilis*. Archive for Bryology **196,** 2013d,p**.**1-4.

10.   Kumar, M., Kapil, A. &Shanker, A. MitoSatPlant: Mitochondrial microsatellites database of Viridiplantae. Mitochondrion, 2014, http: // dx.doi.org/10.1016/j.mito.2014.02.002.

11.   Shanker, A., Singh, A. & Sharma, V. *In silico* mining in expressed sequences of *Neurosporacrassa* for identification and abundance of microsatellites. Microbiol. Res. **162,** 2007a, p. 250-256.

12.   Oliver, M.J., Murdock, A.G., Mishler, B.D., Kuehl, J.V., Boore, J.L., Mandoli, D.F., Everett, K.D., Wolf, P.G., Duffy, A.M. & Karol, K.G. Chloroplast genome sequence of the moss *Tortularuralis*: gene content, polymorphism, and structural arrangement relative to other green plant chloroplast genomes. BMC Genomics **11**, 2010: p. 143.

13.   Hancock, J.M. The contribution of slippage-like processes to genome evolution. J. Mol. Evol. **41,** 1995, p. 1038-1047.

14.   Shanker, A. Computationally mined microsatellites in chloroplast genome of *Pelliaendiviifolia*. Archive for Bryology **199,** 2014,p.1-5.

15.   Rajendrakumar, P., Biswal, A.K., Balachandran, S.M., Srinivasarao, K. &Sundaram, R.M. Simple sequence repeats in organellar genomes of rice: frequency and distribution in genic and intergenic regions. Bioinformatics **23,** 2007, p. 1-4.

16.   Varshney, R.K., Thiel, T., Stein, N., Langridge, P. &Graner, A. *In silico* analysis on frequency and distribution of microsatellites in ESTs of some cereal species. Cell & Mol. Biol. Lett. **7,** 2002, p. 537-546.

17.   Cardle, L., Ramsay, L., Milbourne, D., Macaulay, M., Marshall, D. & Waugh, R. Computational and experimental characterization of physically clustered simple sequence repeats in plants. Genetics **156,** 2000, p. 847-854.

18.   Tambarussi, E.V., Melotto-Passarin, D.M., Gonzalez, S.G., Brigati, J.B., de Jesus, F.A., Barbosa, A.L., Dressano, K. & Carrer, H. *In silico* analysis of simple sequence repeats from chloroplast genomes of Solanaceae species. Crop Breed. Appl. Biotech. **9,** 2009, p. 344-352.

19.   Lin, W.H. &Kussell, E. Evolutionary pressures on simple sequence repeats in prokaryotic coding regions. Nucleic Acids Res. **40,** 2012, p. 2399-2413.

20.   Kapil, A., Rai, P.K. & Shanker, A. ChloroSSRdb: a repository of perfect and imperfect chloroplastic simple sequence repeats (cpSSRs) of green plants. Database **2014**, 2014: article ID bau107; doi:10.1093/database/bau107.

A REVIEW OF RIVER CONSERVATION THROUGH PARTICIPATORY APPROACH WITH SPECIAL FOCUS ON BAGMATI RIVER, NEPAL

Khet Raj Dahal

Head of Department (Civil), Kantipur Engineering College,
P.O. Box: 8849, Kathmandu, Nepal
Corresponding E-mail: krdahal@kec.edu.np

ABSTRACT

This study aims to find the most suitable conservation and protection strategies for the conservation of Bagmati River through mobilization of NGOs, CBOs and people living along the bank of the river. The combined approach (government plus local effort) has been found to be the most effective at maintaining watershed and river integrity as well in the periphery of the Bagmati area. Legal formation of local water conservation groups with a network of upstream and downstream groups are essential for the conservation of the Bagmati River. As the Bagmati River is one of the most religious rivers for Hindus and Buddhists in Nepal, it is necessary to revive the river on its original condition i. e. before degradation of water quality and pollution of the river. There are many methods of river conservation but the most effective and sustainable one is considered the participatory approach of river conservation in the context of Bagmati River.

Keywords— Participatory approach, Bagmati River, Pashupatinath, pollution, Nepal.

1. INTRODUCTION

BACKGROUND OF THE STUDY Rivers are our life lines, which have been used for various purposes. Rivers and river banks reflect the cultural heritage and economic prosperity of the people living there. They also reflect people's respect for nature, environment, and their understanding of the ecological processes [1]. There are thousands of such rivers throughout the world. Among them, the top ten large rivers are the Sepik, the Mississippi, the Volga, the Zambezi, the Mekong, the Ganges, the Danube, the Yangtze, the Nile and the Amazon [2]. These rivers are not only the genesis of human civilizations but also the means of transportation, resource generation and promotion of tourism development. Such rivers maintain the ecological balance as well [1]. But such rivers are being disturbed by several factors. One of them is unregulated extraction of riverbed materials from the beds, banks and floodplains, which invites numerous effects on aquatic environment. Rivers provide physical and biological resources to sustain life [4, 5], but they are being impulsively used by humans to meet their needs. Besides many such anthropogenic activities, urbanization is considered as the pivotal one [6]. Urbanization decreases the mean catchment area of perennial rivers [7]. It results into diversion of rivers for various purposes like irrigation, water supply, and generation of hydro-electricity. The diversion of river water for such purposes breaks the river continuum, which ultimately disturbs the ecology of the river downstream [8, 9]. Since past decades stream ecologists have been paying their attention to the issues of population community and ecosystem dynamics and they have recommended incorporation of all ecological principles in management and river restoration activities from the beginning of development [10]. But ecological principles are not being applied to all spheres of development especially in developing and under developed countries of the world. There is a reciprocal relationship between people and nature and it forms a complex web of interaction to each other [11]. The population pressure is a responsible factor for river disturbance. Due to growing population pressure natural resources have to be used in a sustainable way. As such, many resource managers have been practising it. But natural resource managers are charged of the misuse of resources. They have to decide in a rational way and make a standard to allow public use of resources without damaging the existing environmental value [12, 13]. But in many cases, such standards are not available and natural resources are being used haphazardly.

The effect of urbanization on fresh water bodies is similar both in developing and developed countries in many respects. But some parameters like dissolved materials, fecal and organic pollution are comparatively higher in developing countries than in developed countries [14]. There is now a trend of river protection and restoration; however, it is difficult to bring back the original river environment [11]. Therefore, it is important to protect a river environment before it is

degraded. Industrialization is a common practice throughout the world. But this practice is more in developing countries than in developed ones. Although industrialization creates job opportunities and increases the living standards of the people, it affects the surrounding environment including human health [15]. Many developed and developing countries have no proper treatment plants to discharge the industrial effluents. Therefore, they discharge the untreated waste water into the fresh water bodies [16, 17]. As a result, it not only pollutes surface water but also the ground water of shallow aquifers [18]. Industrialization not only has effects on fresh water bodies but also on forest and biodiversity [19]. Both urbanization and industrialization invite excavation and extraction of riverbed materials to develop required infrastructures. Thus, there is a trend of extraction of riverbed materials without any guidelines in many countries of the world. Both unregulated excavation and extraction of riverbed materials have adverse effects on aquatic environment. Such effects have been studied by many researchers and organizations [20, 21, 22, 23, 24] in Nepal. Aquatic ecology of Bagmati River has been altered due to human activities for the last decade. Bagmati River has been facing both external and internal degradation for years. External degradation is increasing with the pace of increasing population of this region, whereas the internal devastation is caused by geo-environmental degradation of Bagmati River basin. The external degradation includes impacts on water quality, non-treated and non-regulated foul water discharge into the river, dumping of garbage in the river floodplain areas, encroachment of floodplain areas as well as uncontrolled extraction of riverbed materials. Substantially over the last two decades, the vital degradation of river environment attributes mainly disposal of household sewerage, effluent discharge from industries, solid waste disposal on river banks, etc. "The Friends of the Bagmati" is an organization set up in November 2000. According to its website, its aim is "to reverse the degradation of the Bagmati River." In 2014, Bagmati River is claimed to be almost pure after a long effort of 14 years. Every Saturday, Gurkha Army, Nepal Police and General Public gather to clean the waste and sewage from the river. There are over 6000 river and rivulets in Nepal. Bagmati River is one of them. Rivers in Nepal are treated as living Goddesses. Many rivers in Nepal are the ever flowing and inspiring source of beauty, abundance and infinite adventure in the world. The rugged topography, extreme variations and excessive snow melting in Nepal has made the country an attractive place for all tourists from different corner of the world. Many rivers and streams in Nepal have great perspectives for riverbed materials. These natural   resources are the sources of income generation for the local administrative bodies such as District Development Committees (DDCs), Municipalities and Village Development Committees (VDCs). Government of Nepal (GON) enforced the Local Self Governance Act 1999 and Regulation 2000. These acts and regulations provided the rights to the local administrative bodies to use the local natural resources for their income generation. Since then, many rivers and streams are being excavated and extracted without considering adverse environmental consequences [25]. As a result, there are many rivers in Nepal, which have already been over excavated and extracted. Bagmati River is one of them. Bagmati River is one of the most sacred rivers of Nepal. The river has importance of religious and spiritual sentiments among Hindu and Buddhism. It provides platforms to display and bring people close to the river. This river is also the ornament of the capital city Kathmandu, Nepal [26]. The river has the great significance concerned with Hindu religion. There are so many religious temples such as Gokarneshwar, Guheshwari and Pashupatinath temples, which are famous shrines and place of destinations. These are also enlisted in the World Heritage sites. The Many Hindus and Buddhists, for whom the river water has special religious and spiritual values, consider the water of Bagmati River as a holy water 'JAL'. Although being a part of cultural and religious heritage, the activities of dumping of raw solid wastes and discharging of untreated liquid wastes in the Bagmati River have made the river nuisance. In order to stop further environmental degradation of the Bagmati River and adjoining areas as well as to restore the condition of Bagmati River, the Volunteer foundation Nepal is working to public awareness programme and clean Bagmati River since its establishment. All volunteers are fully devoted and committed to keep Bagmati River clean with the support of local peoples, government offices, college, private office, GOs, NGOs, INGO and CBOs. The slogan of clean, cool and pure was the words with which the people used to describe the Bagmati River since past decades. Once upon a time, when the citizens of the Kathmandu Valley used to carry out their early morning activities like taking a holy dip in the Bagmati River, conducting early morning prayers and worships happily. Nepalese Hindus consider this river as goddess, and almost all of them either within or outside the country believe that taking a dip in this water will cleanse them of their sins forever. But this now seems distant history, as today the Bagmati River has turned into a stinking open sewer and unfriendly environment. Rivers are importance for various other aspects such as geologically, biologically, historically and culturally and their civilization for thousand of year. Rivers provide water, energy, habitats, farming, transport and recreation. [27].

PROBLEMS WITH BAGMATI RIVER There are various problems with the Bagmati River. However, water environment problems are rapidly growing, which is becoming serious in human activities. This is because of the rising human population, urbanization and economic activities in these days. The increasing trend of pollution has become vulnerable to Bagmati River. This problem is also in Yamuna and Ganges, which are the major rivers in India. There is negligible flow of water in dry weather in the Yamuna River along Delhi. The Yamuna cannot be controlled fully but by using dilution it may be cleaned to some extent [28]. Similar case is with the Bagmati River. Bagmati River is highly polluted. The major sources of pollution are: disposal of solid and liquid wastes, encroachment of river floodplain areas and settlements, open defecation (although it is declared as open defecation free zone), excavation and extraction of construction materials from the beds, banks and floodplain areas and open markets along the banks of the river, etc. Due to disposal of solid and liquid wastes and no establishment of treatment plant, the river is getting polluted day by day. The holy river Bagmati has the great significance for Hidus. They spread the water from Bagmati River on their heads as the symbol of sacred water of Shiva. But this water is the source of various kinds of diseases for the people. Similarly, in the past there was no participatory approach of river conservation along with the awareness among the people. Thus, it resulted in a devastation of Bagmati River. Bagmati River has been facing both external and internal degradation for years. External

degradation is increasing with the pace of increasing population of this region, whereas the internal devastation is caused by geo-environmental degradation of Bagmati River basin. The external degradation includes degradation of water quality, non-treated and non-regulated foul water discharge into the river, dumping of garbage in the river floodplain areas, encroachment of river floodplain areas as well as uncontrolled extraction of riverbed materials. The erratic distribution of monsoon rainfall combined with geological formations generally results flash floods in Bagmati River basin. Furthermore, human activities such as cultivation of marginal land, mining of riverbed materials, large scale deforestation have increased the incidence of flood in various places of Bagmati watershed. Similarly, unplanned construction of physical infrastructures, such as buildings in hazardous mountain region and cultivation, on steep slopes has increased flood frequency severely in Bagmati River. Sedimentation, bank erosion, inundation on farm land in downstream and wash out of settlements and minor structures are the major types of disasters in the Bagmati basin [5].

BAGMATI RIVER SYSTEM Bagmati River, which comprises 57 rivers and rivulets as its tributaries [31] (Fig. 3.1). The river has a catchment area of 3610 km^2 and total length is 196 km [26].
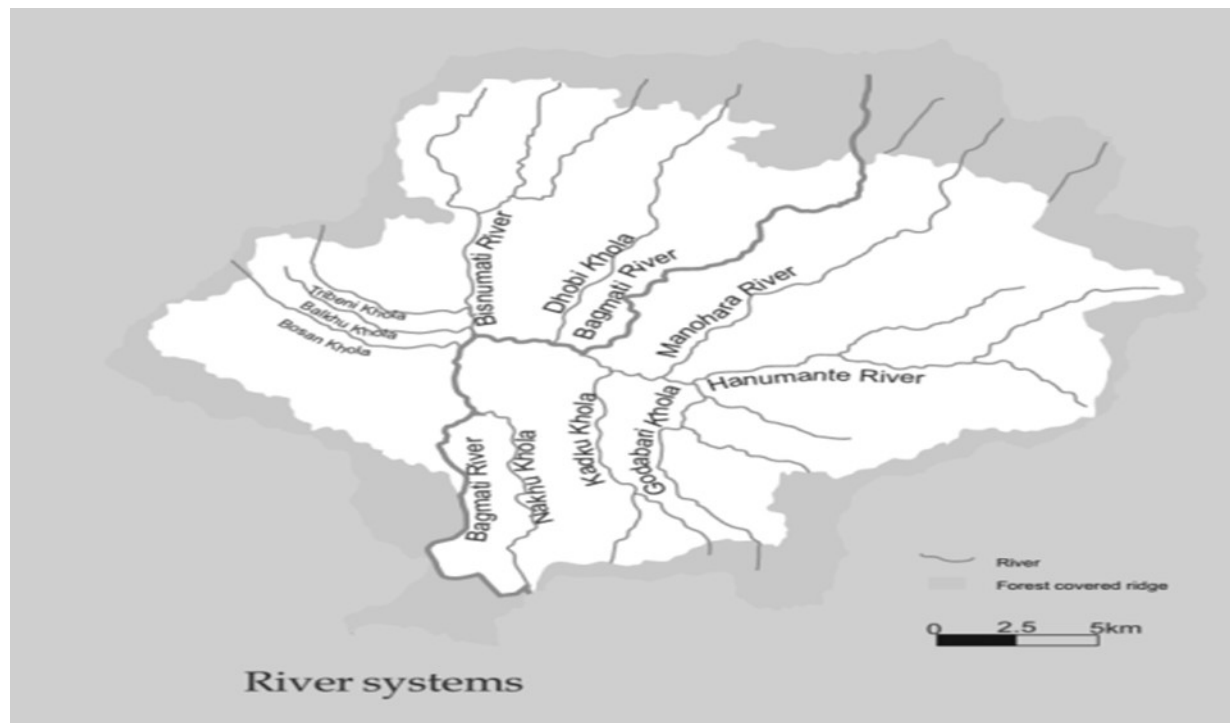

Figure: 3.1 River Systems of the Kathmandu Valley and Bagmati River Network

CONSERVATION PRACTICES IN BAGMATI RIVER Bagmati River is being participated by hundreds of people every Saturday to clean it. The mass participation is the group of volunteers from different sectors. There are various organizations in the country for river conservation. Nepal River Conservation Trust (NRCT) is one of them. NRCT has been involving in Bagmati River conservation since its establishment (1995). This organization hosts for annual river festival. It also helps for awareness programs among the general people. NRCT initiated the river festival with different events and activities [26]. Thus, NRCT has achieved respect from the people, NGOs, INGOs, CBOs and government offices of Nepal [29]. It has taught us that the river can be conserved from the cumulative efforts from various sectors together. Ultimate aim of the NRCT is to restore the previous state of the Bagmati River. However, restoring the water quality of the Bagmati River is now one of the major challenges for technicians, environmentalists, bureaucrats, politicians and non- profit making organizations [30]. Similarly, there is forum for Bagmati River conservation called "Friends of Bagmati". This forum was launched by Prince Philip in 2002 [31]. This forum is also working actively for Bagmati River conservation along the length of the river in the Kathmandu Valley. Government of Nepal (GON) prepared Bagmati Action Plan (BAP) in 2008. This plan includes the four main activities such as protection and enhancement of water quality, protection of terrestrial and aquatic bio-diversity, maintain and renovation of the heritage sites and conservation of aquatic ecosystem. BAP has divided the river in different four zones and made the plan accordingly as per necessity of the zone [32]. Then GON established a Bagmati Civilization Integrated Development Committee (BCIDC). Pashupatinath Temple is located on the bank of Bagmati River in upstream. As Pashupatinath temple is one of the most famous and enlisted heritage sites of Nepal, direct disposal of sewage has discouraged here. Thus, immediately after the enforcement of BAP, GON has constructed a sewage treatment plant in Gaurighat. Likewise, a tunnel was constructed to divert the sewage from Gaurighat to Tilganga. In this way, there is initiation of Bagmati River conservation from the government as well as from private sectors too. The Bagmati Cleaning Mega Campaign was started by the civil societies in collaboration with government and private sectors from the year 2070 B.S. and it was called Bagmati movement. The major task of the campaign was to collect plastics, glasses, and other non-degradable materials from the river. Every Saturday the mass of the people from different sectors gathered in the bank of Bagmati River as earlier identified point and location. They took oath of the Bagmati River cleaning with a national

anthem and worked for three hours. Local people living along the bank of the river also took part in the campaign. They all actively participated in the Bagmati Movement and till now about 8 km stretch of the Bagmati River has been cleaned up [26]. For the first time in the history of Nepal, this is an example of participatory approach of river conservation initiated by the people, GON, NGOs, INGOs and CBOs. As earlier stated, the initiation of river conservation was participatory. Then there was participation of all walks of life. Government also contributed to the cleanup campaigns. People were voluntarily working so as to keep their different identity among others. In Nepal, like the Bagmati Cleanup Campaign, many other projects have also been started in participatory approach. And, this is considered the sustainable approach of development in many sectors not only in river conservation.

2. CONCLUSION

There are over 6000 river and rivulets in Nepal. Bagmati River is one of them. The famous Pashupatinath Temple is located on the bank of the Bagmati River and it is regarded as a holy river for Hindus and Buddhists. There are various organizations in the country for river conservation. Nepal River Conservation Trust (NRCT) is one of them. NRCT is involving in Bagmati River conservation since its establishment (1995). Bagmati River is being participated by hundreds of people every Saturday to clean it. Mainly the mass of participation was the group of volunteers from different sectors (government plus people). Thus, there was a feeling of ownership with the people and the non-profit making organizations. Rivers are our life lines, which provide us physical and biological resources to sustain life. There are thousands of such rivers in the world. However, many rivers have already been polluted due to anthropogenic activities. Bagmati River is also an example of most polluted river due to anthropogenic activities. Thus, the use of appropriate method is necessary to conserve the health of this river. There are various methods of river conservation but the participatory approach is considered the most appropriate one in the context of Bagmati River.

ACKNOWLEDGEMENTS

REFERENCES

1. Baidya, H. (2003) Twelve years struggle for the conservation of Bagmati River. Nepal Water Conservation Foundation, Kathmandu.

2. Touropia (2013) Ten most important rivers in the world. www.touropia.com assessed in June 15, 2013.

3. Lowe, W.H. (2006) The Trouble with Rivers. BioScience 56(3):260-263.

4. Hering, D., Feld, C. K.,Moog, O., Ofenbock,T. (2006) Cook book for the development of a multimetric index for biological condition of aquatic ecosystem: experiences from the European AQEM and STAR projects and related initiatives. Hydrobiologia 566:311-324

5. Dahal, K, 2014. Assessment of riverbed excavation and its effects on aquatic environment of Tinau River, Nepal. A PhD thesis submitted to K athmandu University, Nepal.

6. Roach, W.J., Hofferman, J.B., Grimm, N.B., Arrowsmith, J.R., Eisinger, C., Rychener, T. (2008) Unintended consequences of urbanization for aquatic ecosystems: a case study from the Arizona Desert. Bioscience 58(8):715-727.

7. Roy, A.H., Freeman, M.C., Wenger, B.J., Ensign, W.E., Meyer, J.L. (2005) Investigating hydrologic alteration as a mechanism of fish assemblage shifts in urbanizing streams. Journal of the North American Benthological Society 24(3):656-678.

8. Vorosmarty, C.J., Sahagian, D. (2000) Anthropogenic disturbance of the terrestrial water cycle. BioScience 50 (9):753-765.

9. Allan, J.D., Flecker, A.S., Segnini, S., Taphorn, D.C., Sokol, E., Kling, G.W. (2006) Limnology of Andean piedmont rivers of Venezuela. Journal of the North American Benthological Society 25(1):66-81.

10. Stanley, E.H., Powers, S.M., Lottig, N.R. (2010) The evolving legacy of disturbance in stream ecology: concepts, contributions, and coming challenges. Journal of the North American Benthological Society 29(1):67-83.

11. Liu, J., Dietz, T., Carpenter, S.T., Folke, C., Alberti, M., Redman, C.L., Schneider, S.H., Ostrom, E., Pell, A.N., Lubchenco, J., Taylor, W.W., Ouyang, Z., Deadman, P., Kratz, T., Provencher, W. (2007) Coupled human and natural systems. AMBIO: A Journal of the Human Environment 36(8):639-649.

12. Pease, M.L., Rose, R.K., Butler, M.J. (2005) Effects of human disturbances on the behavior of wintering ducks. Wildlife Society Bulletin 33(1):103-112.

13. UNDP (2011) A review of current practices of revenue generation from natural resources for the local bodies of Nepal. Ministry of Local Development, Local Governance and Community.

14. Sikder, M.T., Kihara, Y., Yasuda, M., Yustiawati, Yoshihiro, M., Tanaka, S., Odgerel, D., Mijiddorj, B., Syawal, S.M., Hosokawa, T., Saito, T., Kurasaki, M. (2013) River water pollution in developed and developing countries: judge and assessment of physicochemical characteristics and selected dissolved metal concentration. Clean: Soil, Air,Water 41(1):60-68.

15. Douglas, I., Hodgson, R., Lawson, N. (2002) Industry, environment and health through 200 years in Manchester. Ecological Economics 41:235-255.

16. Ibe, K.M., Njemanze, G.N. (1998) The impact of urbanization and protection of water resources in Owerri and Environs SE, Nigeria. Environmental Monitoring and Assessment 58:337-348.

17. Banarjee, U.S., Gupta, S. (2013) Impact of industrial waste effluents on river Damodar adjacent to industrial complex, West Bengal, India, Environmental Monitoring and Assessment 185:2083-2094.

18. Latha, P.S., Rao, K.N. (2012) An integrated approach to assess the quality of groundwater in a coastal aquifer of Andhra Pradesh, India. Environmental Earth Sciences 66: 2143-2169.

19. Joshi, P.K., Kumar, M., Paliwal, A., Midha, N., Dash, P.P. (2008) Assessing impact of industrialization in terms of LULC in a dry tropical region (Chattisgarh), India using remote sensing data and GIS over a period of 30 years. Environmental Monitoring and Assessment 149:371-376.

20. WECS (1987) Erosion and sediment in the Nepal Himalaya. Water and Energy Commission Secretariat (WECS), Nepal.

21. Gyawali, D., Dixit, A. (1999) Fractured institutions and physical interdependence, challenges to local water management in Bagmati River Basin. In: Gyawali, D., Dixit, A. (eds). Rethinking the mosaic, investigations into local water management Nepal. Water Nepal, Kathmandu. pp. 58-121.

22. Khanal, S.N. (2001) Effects of Human Disturbances in Nepalese Rivers on the Benthic Invertebrate Fauna. PhD Thesis, the University of Agricultural Sciences (BOKU), Vienna, Austria.

23. BTM (2001) Save the Bagmati. Report prepared by Nepal Engineers' Association, Lumbini Regional Centre, Butwal.

24. JICA (1999) The Study on Flood Mitigation Plan for selected Rivers in the Terai plain in the Kingdom of Nepal, Vol. III. Report prepared by Nikken Consultants Inc., Nippon Koei Co. Ltd, submitted to Japan International Co-operation Agency (JICA).

25. Dahal, K.R., Guragain, H.P. (2013) Local resources to conservation practices in use for the protection of Tinau River, Nepal. Hydro-Nepal 2:32-38.

26. Ale, m., Dahal, A., 2011. Bagmati River Festival: Conservation of Degrading River. Proceeding of the 2011 Georgia Water Resource Conference held on April 11-13, 2011, at the University of Georgia.

27. Barrow, M. 2013, Primary Homework help Rivers.

28. Nallathiga, R., 2008, River Water Conservation through Management interventions: A Case Study of Yamuna Action Plan in India, Water Today journal , pp 68-73

29. www.nrct.org.np- accessed on Jan.3, 2015.

30. Nepal Water Conservation Foundation (NWCF), 2009. The Bagmati: Issues, challenges and prospects

31. www.friendsofthebagmati.org.np- accessed on Jan3. 2015.

32. Shrestha, P. 2014. Bagmati River now and then: Impacts of Bagmati River Action Plan on the river environment. A thesis submitted to Nepal Engineering College, Kathmandu.

A CASE STUDY OF VIRTUAL REALITY APPLICATION IN RELATION TO AUGMENTED REALITY FOR GEOMETRY VERIFICATION

Aydin Tabrizi*
School of Architecture, Design and Planning,
Department of Architecture
University of Kanas, Lawrence, KS
A088a591@ku.edu
*Corresponding Author

Paola Sanguinetti
School of Architecture, Design and Planning,
Department of Architecture
University of Kanas, Lawrence, KS

ABSTRACT

Addition of augmented reality (AR) to virtual reality (VR) is a challenging multidisciplinary field and a particularly promising new user interface paradigm. It integrates computer graphics and electronically generated simulation models with added data to enhance the observer's awareness and perception of the real world by providing the means for intuitive knowledge absorbance. With the rapid development and adoption of AR applications, there are numerous opportunities for integrating VR with AR and improving conventional methods used in the fields of architecture, engineering and construction (AEC). In this paper, current trends in the development of VR+AR applications are identified, and a case study is proposed to investigate the application of VR for measurement and verification of building geometry. VR techniques including photogrammetry and laser scanning are applied to enhance the speed and accuracy of data collection from construction sites. The AR data are overlapped on VR surface to provide further information.

Keywords—Augmented reality, AEC industry, building geometry, laser scanning, photogrammetry, virtual reality.

1. INTRODUCTION

Virtual reality (VR) has defined as a set of interacting policies, processes and technologies that generates a methodology to manage the essential building design and project data in digital format throughout the building's life cycle [1] with incorporation of 2D and parametric 3D dimensions [2]. On the other spectrum, augmented reality (AR) has introduced as a technology which allows the user to see, hear, touch, smell and taste things that others cannot [3]. It is a technology to perceive elements and objects within real world experience in a complete computational environment. It applies creatures and structures that could be used in daily activities unconsciously through interaction with others such as enabling mechanics to see instructions for repairing an unknown piece of equipment, surgeons to see ultrasound scans of organs while performing surgery on them, fire fighters to see building layouts to avoid invisible hazards and people to read reviews for each restaurant on their way [4].

(Wang et al. 2004) describes AR+VR as a tool allowing users to work with real world environment while visually receiving displays of additional computer-generated information about the item by superimposition of additional information onto the real world scene. This approach enhances the user's perception of the real environment by showing information that cannot sensed unaided.

2. AUGMENTED REALITY IN RELATION TO VIRTUAL REALITY

AR (indoor or outdoor, fixed or mobile workplace settings) enhances the observer's awareness and perception of the real world by providing the means for intuitive knowledge absorbance [5]. With the application of Virtual Reality (VR), virtual objects can be registered in relation to real objects and the combination of VR + AR can be seen in the same position and orientation of other available objects of the scene as perceived by the observer (Error! Reference source not found.). The VR + AR approach is achieved by placing virtual objects or information cues into the real world by the application of virtual camera calibration or tracking process to compute the virtual camera parameters in line with the position and orientation of the observer of the real scene. Then, real objects are tracked and their 3D shape are reconstructed from pictures [4].

3. VR+AR IN THE ARCHITECTURE, ENGINEERING & CONSTRUCTION (AEC) INDUSTRY

Estimations show that at least 5% of total building construction costs are due to occurrence of problems in the early design process, causing insufficiency, inconsistency and omission of design-related information towards construction phase [6]. In the architecture, engineering and construction industry (AEC), gaps between planned solutions and practical implementations, poor communications between project participants and inefficient scheduling are the main issues for the lack of sufficient information/communication technology (ICT) support and innovative business procedures [7]. The construction industry heavily relies on 2D paper media and the worksite planners sketch the future layout adjacent to their real environment. However, this traditional approach is ineffective and prone to error due to the reliance on the experience of the planners where only well-trained staff is able to generate the effective layout design with paper sketch [8]. With the progress of ICT use in the AEC industry, higher quality visualization platforms are necessary for the efficient use of shared information among involved teams. Available research studies show the attempts of construction activities simulation with feedback generation through visualizing construction information for easier understanding and data share among project participants [9]. However, this approach only enables the visualization of activities in the virtual environment without enough resemblance to the actual tasks in the real world. VR+AR approach enables the generation of digital project information prior to construction with transfer onto construction site and process in a fully digital and ubiquitous way. This process facilitates the comparison of the actual situation at the construction site with the building's planned appearance at the given moment to identify the concerned component or entity [10]. Significant number of researchers has utilized this approach to address problems in the AEC industry to provide a feasible solution through visualization by superimposing 3D virtual models on real-time videos [11, 12]. Studies by [13, 14] have shown that VR + AR refers to scenarios where the real part is predominant and virtual information about the environment and its objects are overlaid on the real world by the application of VR [15]. This combination can enhance visualization in assisting the presentation of 3D environments and increase of user comprehension.

4. BENEFITS OF AR+VR IN THE AEC

A major opportunity presented by the use of AR+VR technique is the ability to work at real-scale in all phases. Involved people in the building process, such as clients or prospective buyers, often have difficulties understanding and translating 2D CAD architectural representations into real 3D spatial models where they basically need to build up their individual mental models to understand the project [16]. There is also a need for a powerful and proper visualization approach to supply information to the onsite workers. VR can make the interdependencies between work tasks more explicit with making the existing complexity more visible and manageable onsite. It can be a proactive approach where the potential negative impacts of any action can be identified earlier and mitigated avoided easily. Spatial collision analysis between trades by 3D modeling systems such as CATIA or Navisworks is an example of this approach [17]. However, during the actual construction process, there is a possibility of collisions occurrence due to the change of building elements, site facilities and the movement of construction machinery. Therefore, it is challenging to introduce the onsite real-time dynamic collision detection approach to include the variations of construction sequence and schedule. Addition of AR to VR enables real-scale representations of the existing situation to be communicated and augmented by further information where misunderstandings between planner, client and involved parties can be better avoided with savings on additional cost measures and time-delays [16].

5. CASE STUDY FOR GEOMETRY VERIFICATION

The KU Mobile Collaboratory (KU MoCo Lab) is a project sponsored by the University of Kansas center for research, Inc. to promote expanded research opportunities for KU researchers and community partners. This project builds and utilizes a mobile laboratory to foster one-on-one, collaborative, interactive planning and design (Figure 1). The goal is

to imagine publicly shared spaces that promote positive community life, engagement through art and culture, and healthy lifestyles. The project involves adapting an existing recreational vehicle trailer to create a "community room" on wheels – taking scholars to the people to seek specific needs, assess opportunities, make connections, and propose small-scale projects that attempt to transform a community's built environment. Having such a mobile lab would make KU competitive for external grants that require researchers to have a regular presence in a local community. One specific area of AR+VR application (assembly guidance and geometry detailing/verification) in the AEC is investigated in the following section through the case study method.

Figure 1: KU MoCo Lab (a) Inside, (b) Outside

6. MODELING APPROACH

A building model of the MoCo Lab assembly is created based on the measured data inside and outside the vehicle. To quicken the modeling process time, measure the complex geometry of curves/edges and identify the possible geometric discrepancies between the real conditions and the building model, two alternative VR scenarios were evaluated to collect data for accurate dimensions and production of components. In the first scenario, photogrammetry technique was used to create the vehicle geometry and second scenario was the application of laser-scanning technique for the comparison study. After obtaining data by VR, AR approach was used to measure and identify the vehicle dimensions.

PHOTOGRAMMETRY Photogrammetry is useful to extract geometrical properties of objects from photo images. The availability of high quality and precise still image cameras has advanced the 3D modeling from photo images [18]. The process works by strategically placing targets on objects to be photographed and identifying the target coordinates. Then several photos of each object are taken from different positions and angles. The advantage of photo imaging is the capability of extracting information pertinent to object texture and color where this process makes it versatile and complementary to laser scanning measurement approach. However, the use of photo imaging alone, may cause practical limitations and it is clear in extracting geometrical properties of surfaces with little texture or poor definition as in the case of earth moving operations where quantities of material can be easier determined using laser scanners [19] instead of photo imaging.

LASER SCANNING In the construction industry, laser scanning is used for making spatial measurements. Applications include surveying, earth moving operations, progress of concrete casting, highway alignment, paving operations and construction quality control [20]. Laser scanning yields data in the form of 3D points, known as "point clouds" which are later displayed as useful images using specialized software systems. These images can be viewed at different angles [21]. Laser scanners can capture up to 50,000 points per second. The data points are given in x, y, z, coordinates. This technology works by sending illumination pulses to an object (reference sphere set) where the distance between that object and the laser scanner is referred to as the "Range" (Figure 2). The limitations of applying laser scanner are the long time required to do each scan and the high cost associated with the equipment. The best results are obtained when many scans are taken from different locations to increase resolution and avoid physical obstructions that may lie between the scanner and the object.

Figure 2: Reference sphere set to receive pulse from laser scanner

The geometry and dimensions of the vehicle were measured using the two introduced VR approach. The results showed the matching alignment between the actual vehicle measurements and results from laser scanning and photogrammetry.

LASER SCANNING PROCEDURE TX5 3D laser scanner of TRIMBLE[®] [22] was used and the scanned object was the MoCo Lab vehicle placed at an average distance of about 3 m from the scanner (Figure 3). The scanner was placed in different locations and reference spheres (at least 3 or more) were placed in different heights around the vehicle and a total of 9 experiments were conducted inside and outside the vehicle to capture all the details and to generate point cloud data by stitching the scans of various angles. The proposed method utilizes commercially available modeling software (Trimble RealWorks), which models 3D point cloud images to generate 3D "point clouds" from different positions.
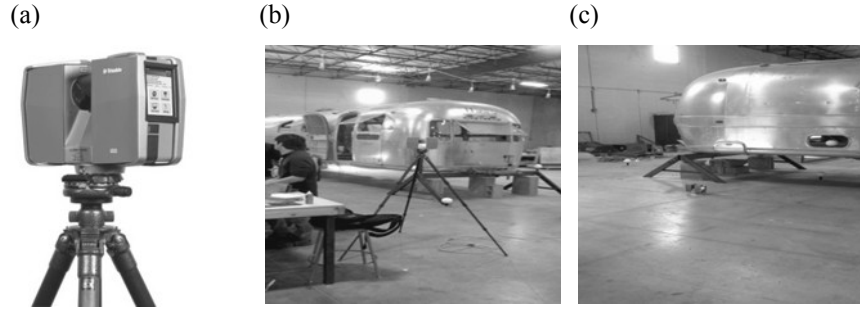
(a) (b) (c)

Figure 3: (a) Trimble TX5, (b,c) laser scanner + ref sphere around vehicle

Error! Reference source not found. presents the obtained results from laser scanner in different angles with the location of reference sphere on different heights. After analysis of results and attaching cloud points, the full geometry of the vehicle can be seen in **Error! Reference source not found.** and the distance between components are measurable using Trimble RealWorks program through AR application process to match the measurements with actual data and provide additional information for the users on real-time.
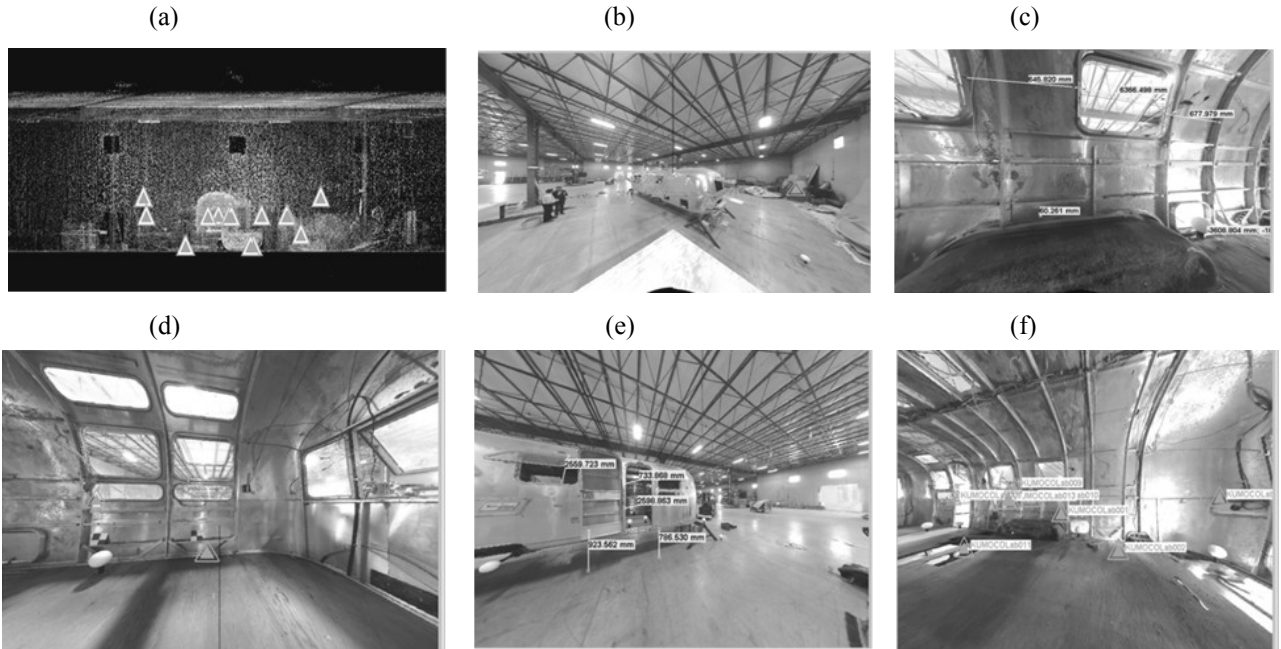
(a) (b) (c)

(d) (e) (f)

Figure 4: (a,b,c,d) Ref sphere locations, (e,f) Distance between components

PHOTOGRAMMETRY PROCEDURE To accurately measure to the vehicle curve and baseline layer, old existing surfaces must be removed to make a physical template. However with photogrammetry technique the smooth contour can be measured and cut to perfection on a CNC router, in minimum time. There is no guesswork with the measurements as would have been with hand measuring the template and transferring those hand measurements to CAD. This method uses algorithms to figure spatial geometries. It triangulates the positions of the markers that are placed in the job, and then when photographs of the markers are taken from various angles, it processes them.

ETemplate™ [23] digital measuring system was used to measure curves of this vehicle. The two types of Intelli-Marks were used for measurement. The Intelli-Marks which are circular targets with a unique segmented ring-like bar code were placed along the wall surfaces. They can be automatically recognized by the ETemplate software process. The Intelli-Mark Edge Markers were placed flat on the ends/faces of the windows and openings of vehicle for all necessary profiles. In addition, Intelli-Mark scales, which provide accurately specified measurements, were used between the markers (Figure 5). The ETemplate photo™ software was used for image processing and Integrator (a program that accesses 3D data points from an active ETemplate project) was used for processing data into another format such as 2D/3D CAD (DXF) drawing for visual reference and inspection.

ETemplate BackPlot ™, which has unique ability to overlay the finished CAD template onto the job site photos was used in order to see the design/fit and to make on-the-spot changes before the components are manufactured. This process means fewer changes and mistakes and increased profits.

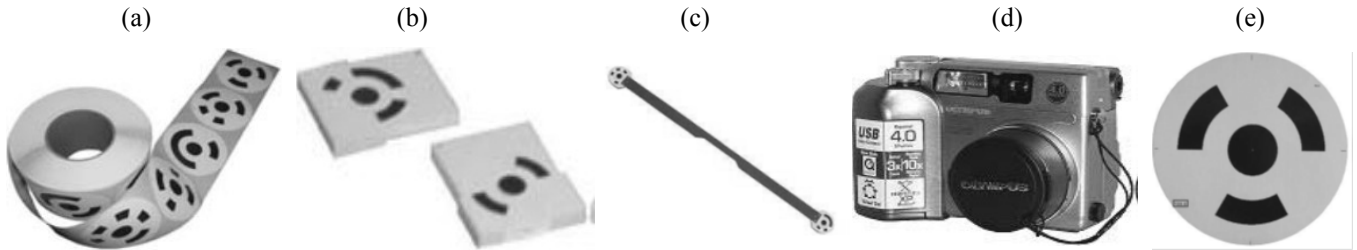| (a)	(b)	(c)	(d)	(e)

Figure 5: (a) Intelli-Mark Wall Markers, (b) Intelli-Mark Edge Markers, (c) Intelli-Mark Scales, (d) ETemplate Digital Measuring Camera (Ricoh Caplio GX100), (e) Barcode

Figure 6 represents the markers placement in various locations inside and around the vehicle. The markers were placed on different locations/components to cover the whole geometry of the vehicle and increase the accuracy of the measurement. Two types of markers were used to coves the surfaces and edges. After finishing photogrammetry process, the obtained images were analyzed in ETemplate photo™ software and the vehicle geometry size and shape were produced accordingly with all the required measurements.
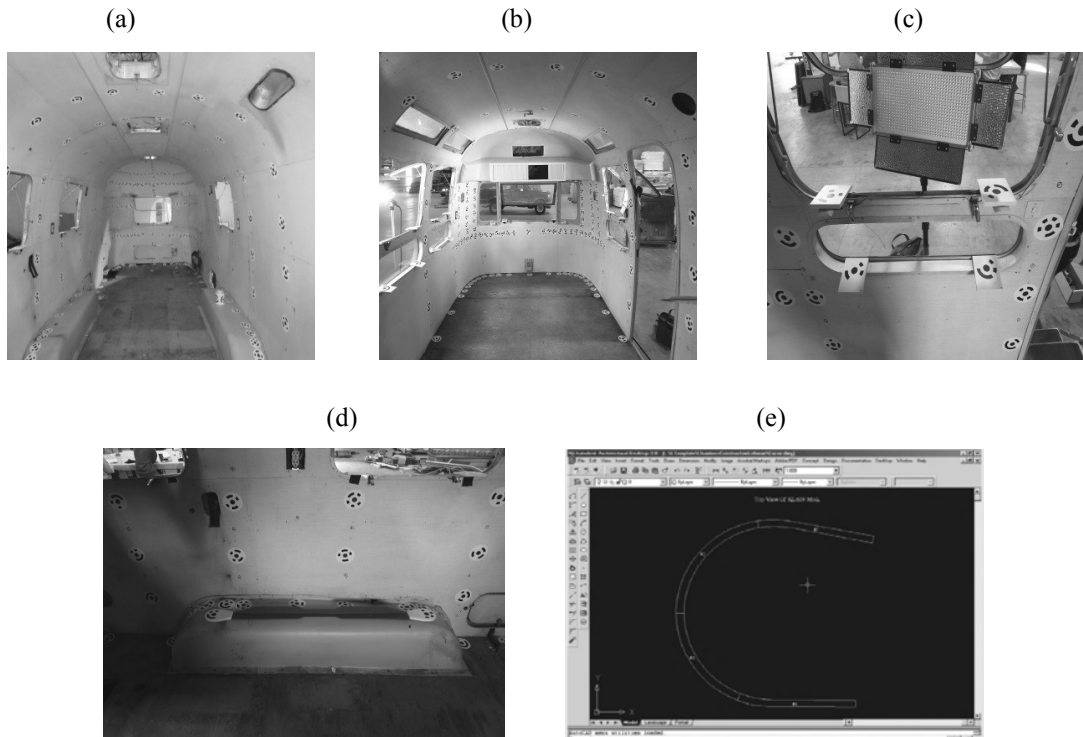
Figure 6: (a,b,c,d) Markers on surface and edge, (e) Measured model of vehicle

8. DISCUSSION

In this paper, the concept of VR+AR was introduced and a case study of a mobile vehicle was presented with the intention of obtaining its geometry through the use of VR in order to produce required components for the interior design of this vehicle. Two methods were introduced in order to reduce the time and resources required to measure the dimensions

manually and avoid possible risks associated with this approach. Photogrammetry is one method for data collection where the geometrical properties of an object on site are generated from its photo image. Another method used to collect actual work data is 3D laser scanning, where the construction site is scanned at different heights to generate data, which can then be used to estimate the dimensions of property accurately and to evaluate the quantity of work required to perform within the time range. The obtained results from each method were presented in the paper and based on the required time to monitor and analyze the data and in order to enhance the speed and accuracy of data collection from construction site and despite the limitations associated with each scenario, the laser scanning method is presented as the most accurate solution for this project. The photogrammetry method is performed from one direction of the project and it does not give a clear picture of user observation for data analysis. However, with the use of reference spheres in laser scanning in various locations around the object, other than providing higher resolution and faster analysis, this method provides clear picture of observation location and latitude. However, based on the project type, site access limitations, required flexibility, availability of resources and budget each method could be selected accordingly. In the meantime, after obtaining the VR data of the vehicle, the geometry dimensions, distance among components and required modification was augmented on the data, and modified VR images with overlaid AR data was used to identify the exact location of proposed changes on the surface/edges of vehicle. This process created clear description of any possible changes in an understandable way to the involved parties in the project. However, the application of AR dimension to the VR data is not just limited to the measurement and geometry verification and the research of AR addition to the model to provide semantics of the components and other related information requires further research in the future.

9. CONCLUSION

With the rapid development and adoption of VR+AR applications, there are numerous opportunities for integrating VR+AR and improving conventional methods used in the fields of architecture, engineering and construction (AEC). In this paper, current trends in the application of VR for geometry verification and measurement purpose for a mobile laboratory (MoCo Lab) case at the University of Kansas were identified. In order to compare the results to the traditional time-consuming manual measurements, photogrammetry and laser-scanning techniques were applied on this project and additional data about the measured components were provided with the use of AR approach. The results showed a promising approach in processing and analyzing data with possible advantages and drawbacks of each technique. It was observed that, the laser-scanning technique can provide significantly accurate results but based on the project assembly, location, size and accessibility of resources, each technique can bring useful results to enhance the speed of construction projects data analysis. According to [24], the limitations associated with 3D scanning and digital photo imaging can be alleviated by integrating both technologies. Integrating 3D scanning and photo imaging can reduce the time required to obtain reliable construction project data. Also, such integration reduces the cost involved as it allows for the use of less expensive, low accuracy scanners and using photographs can eliminate several scans execution from different positions. In conclusion, in order to overcome the limitations associated with VR technologies, the proposal of integrating 3D laser scanning and photogrammetry in modeling 3D images and gathering data from the integrated approach with comparison to the current method, requires further research in the future studies. Also, the application of AR for data analysis and post-processing to calibrate the model and analysis of possible modification with real-time process is in its' infancy in the AEC industry and should be studied in the future.

REFERENCES

1. Penttilä, H., *Describing the changes in architectural information technology to understand design complexity and free-form architectural expression*, 2006, ITcon.

2. Taylor, J.E. and P.G. Bernstein, *Paradigm trajectories of building information modeling practice in project networks.* Journal of Management in Engineering, 2009. **25**(2): p. 69-76.

3. Van Krevelen, D. and R. Poelman, *A survey of augmented reality technologies, applications and limitations.* International Journal of Virtual Reality, 2010. **9**(2): p. 1.

4. Feiner, S.K., *AUGMENTED REALITY: A NEW WAY OF SEEING.* Scientific American, 2002.

5. Klinker, G., D. Stricker, and D. Reiners, *Augmented reality for exterior construction applications.* hand, 2001. **35**: p. 1.

6. Hwang, B.-G., et al., *Measuring the impact of rework on construction cost performance.* Journal of Construction Engineering and Management, 2009. **135**(3): p. 187-198.

7. Chi, H.-L., S.-C. Kang, and X. Wang, *Research trends and opportunities of augmented reality applications in architecture, engineering, and construction.* Automation in Construction, 2013.

8. Wang, X., *Using augmented reality to plan virtual construction worksite.* International Journal of Advanced Robotic Systems, 2007. **4**(4): p. 501-512.

9. Kang, J.H., S.D. Anderson, and M.J. Clayton, *Empirical study on the merit of web-based 4D visualization in collaborative construction planning and scheduling.* Journal of Construction Engineering and Management, 2007. **133**(6): p. 447-461.

10. Froese, T. *Impact of emerging information technology on information management.* in *International Conference on Computing in Civil Engineering, ASCE, Cancun, Mexico, Paper.* 2005.

11. Shin, D.H. and P.S. Dunston, *Identification of application areas for augmented reality in industrial construction based on technology suitability.* Automation in Construction, 2008. **17**(7): p. 882-894.

12. Azuma, R.T., *A survey of augmented reality.* Presence, 1997. **6**(4): p. 355-385.

13. Dunston, P.S. and X. Wang, *Mixed reality-based visualization interfaces for architecture, engineering, and construction industry.* Journal of construction engineering and management, 2005. **131**(12): p. 1301-1309.

14. Wang, X. and P.S. Dunston, *Potential of augmented reality as an assistant viewer for computer-aided drawing.* Journal of computing in civil engineering, 2006. **20**(6): p. 437-441.

15. Saggio, G. and D. Borra, *Augmented Reality for Restoration/Reconstruction of Artefacts with Artistic or Historical Value.* Augmented Reality-Some Emerging Application Areas, 2011: p. 59-86.

16. Donath, D., et al., *Augmented reality techniques for design and revitalisation in existing built environments.* Angenommener Beitrag zur ACADIA, Buffalo, 2001.

17. Wang, X. and P. Love. *BIM+ AR: Onsite information sharing and communication via advanced visualization.* in *Computer Supported Cooperative Work in Design (CSCWD), 2012 IEEE 16th International Conference on.* 2012. IEEE.

18. Styliadis, A.D., *Digital documentation of historical buildings with 3-d modeling functionality.* Automation in Construction, 2007. **16**(4): p. 498-510.

19. Baltsavias, E.P., *A comparison between photogrammetry and laser scanning.* ISPRS Journal of photogrammetry and Remote Sensing, 1999. **54**(2): p. 83-94.

20. Cheok, G.S. and W.C. Stone. *Non-intrusive scanning technology for construction assessment.* in *IAARC/IFAC/ IEEE. International symposium.* 1999.

21. Wu, Q., H. Xu, and X. Zou, *An effective method for 3D geological modeling with multi-source data integration.* Computers & Geosciences, 2005. **31**(1): p. 35-43.

22. ZAZO, A., D. JIMENEZ, and M. FARJAS, *GUIA VISUAL DE TRIMBLE REALWORKS.* SOFTWARE LASER D, 2011. **3**: p. 2011-60.

23. Dueholm, K.S., *Geologic photogrammetry using standard small-frame cameras.* Geological Analysis and Mapping Using Multi-model Photogrammetry, 1992. **156**: p. 7-17.

24. El-Omari, S. and O. Moselhi. *Hybrid methodology for automated collection of data from construction sites.* in *International Symposium on Automation & Robotics in Construction ISARC-2007 Kochi, Kerala, India.* 2007.

AIR POLLUTION TOLERANCE INDEX (A.P.T.I.) OF FEW TREE SPECIES GROWING IN AIR POLLUTION STRESS CAUSED BY AUTOMOBILES

Abhishek Swami

Department of Applied Science
Dronacharya Group of Institutions, Greater Noida-201308
Tel.No.9899932076
abhishek.swami@gnindia.droancharya.info

ABSTRACT

Vegetation naturally cleanses the atmosphere by absorbing gases and some particulate matter through leaves. Plants have a very large surface area and their leaves function as an efficient pollutant-trapping device. Some plants have been classified according to their degree of sensitivity and tolerance towards various air pollutants. Sensitive plant species are suggested to act as bio-indicators. Present study was carried out to determine level of tolerance of air pollution by automobile exhaust of few tree species viz, Mangifera indica Linn.f.,Tectona grandis Linn. f., Shorea robusta Gaertn .f. and Eucalyptus citridora Hook. Syn. around Haridwar. On the basis of total chlorophyll content, ascorbic acid, pH, and relative moisture content, air pollution tolerance index value (APTI) of above tree species was determined. Highest value of air pollution tolerance index for polluted site was recorded for Shorea robusta Gaertn .f., 11.27, and lowest, 7.19 value of air pollution tolerance value was recorded for Eucalyptus citridora Hook. Syn., Thus this study reveals that Shorea robusta Gaertn .f. is more suitable species to work as pollution sink and can be planted in areas which are facing very high vehicular pollution specially near the road side.

Keywords— Air pollution tolerance index (A.P.T.I.), Automobiles, Air pollution, Vegetation.

1. INTRODUCTION

Air pollution was primarily a problem of urban and industrial regions in the developed nations. In the last three decades, however, changes in the pattern of air pollutant emissions, including increases in those from motor vehicles, have led to greater pollutant impacts in more remote rural areas. Furthermore, the rapid pace of industrial development and urbanization in many developing countries means that adverse impacts on agriculture are beginning to be felt in many parts of the world outside the industrialized West. Air pollution poses an acute problem for the world as its control through effective remedial measure is rather difficult to achieve. Vegetation sustain and support the biosphere of which also a part. Any damage to vegetation, therefore, results in damage to the entire natural balance. It is well known that plants have an excellent capacity to withstand the polluted environment. They probably act as a vas sink for the air pollution. At the same time they also filter the particulate matter before it reaches the earth (Tiwari and Rai, 2004)[1]. Different plant species vary considerably in their susceptibility to air pollutants. Screening of plants for their sensitivity to air pollutants is of vital importance. Capacity of plants to reduce air pollution is very well known (Tingey, 1968; Bannett and Hill, 1973)[2-3]. To check the spread of such air pollutants emitted from an industrial complex, many workers recommended the growth of green vegetation around it (Fleming, 1967; Warren, 1973 Agrawal et al., 1988, 1989; Tiwari, 1991)[4-8]. The present study examines the air pollution tolerance index of few selected pants species, plants which have higher tolerance index have higher capacity to withstand polluted environment than plants which have lower air pollution index values.

2. DETAILS OF PAPER

MATERIAL AND METHODS:

SAMPLING SITE Sampling site located in newly formed state of Uttarakhand, is one of the important holy cities of India

and is extended from latitude 29° 58' in the north to longitude 78°13' in the east with a subtropical climate. It receives millions of tourists every month, sometimes just in one day, which increases the number of automobiles of various categories up to 120% per day. Being in the foot hills of newly carved State of Uttarakhand, the State Government has developed the State Industrial Development Corporation Ltd., in the City and some 540 industries are expected to be established in the area. This has further increased the load of vehicular concentration on the roads of Haridwar. These vehicles emit lots of harmful gases in the environment which directly affect to living organisms and plants exposed to it, especially to road side plants which remain in direct contact of this type of pollutants.

TREE SPECIES The tree species of *Mangifera indica* L.*, Tectona grandis* Linn.f.*, Shorea robusta* Gaertn.f., and *Eucalyptus citridora* Hook. Syn. selected in the present study are grown all along the road side. These have air pollution tolerance value less than 10, and are termed as sensitive species, which can be used for bio-monitoring of air pollutants.

SAMPLE COLLECTION Plant leaf samples were collected mainly from Highway no 58 during 2005-06. The vehicular concentration of heavy vehicles, light vehicles, cars and two-wheelers was recorded at different sampling sites on each of the sampling day and an average of 8 hours count was calculated, which comes about 25 vehicles per minute. Six plant leaf samples (5 replicates of each sample) were collected for the purpose of chemical analysis (total chlorophyll, ascorbic acid, pH of leaf extract and relative water content) and all values were mentioned as an average. Samples of tree leaves were collected in polyethylene bags for further analysis in the laboratory.

ANALYTICAL METHODS The chlorophyll 'a', 'b' and total chlorophyll and carotenoids in the leaves of selected plant species were determined as per Arnon (1949)[9]. Ascorbic acid was determined by the method used by Sadasivam and Manikam (1991)[10]. Air quality monitoring of gaseous pollutants viz., SO_2 and NO_x was carried out using the method of West and Gaeke (1956)[11] and Jacob and Hochheiser (1958)[12] respectively. The ascorbic acid content mg g^{-1} dry wt. was estimated by the method of Sadasivam and Manikam, 1991[10]. Total chlorophyll mg g^{-1} dry wt. was estimated by following Arnon, 1949 [9]. Relative water content was determined by method proposed by Weatherly, 1965 [13]. pH of leaf extract was measured with a digital pH meter. To evaluate the tolerance level of plant species to air pollution, Singh and Rao (1983) [14] used four leaf parameters to derive an empirical number indicating the Air Pollution Tolerance Index (APTI). APTI is thus calculated as follows:

APTI = [A (T+P)] +R / 10

Where:
A = ascorbic acid content of leaf mg g^{-1} dry wt.
T = total chlorophyll of leaf in mg g^{-1}
P = pH of the leaf extract
R = per cent relative water content of leaf.

Samples of air pollutants were collected fortnightly with the help of Respiratory Dust Sampler (APM-460) from each site, where plant sampling was done. The apparatus was kept at a height of 2 m from the surface of the ground. For the collection of samples of SPM at each sampling site, GF/A filter paper was used. It was weighed before and after sampling. Air quality monitoring of gaseous pollutants viz., SO_2 and NO_x was carried out using the methods of West and Gaeke (1956)[11] and Jacob and Hochheiser (1958)[12], respectively.

3. RESULTS AND DISCUSSION

Seasonal variation in the concentration of primary air pollutants has been given in Table - 1. The concentration of RSPM was highest, 150.00 µgm[-3] during the summer season, while the SPM was highest, 401.00 µgm[-3] during the winter season. The concentration of sulpher dioxide at polluted site was highest, 10.21 µgm[-3] during summer season, which was 38.12% higher as compared to control site. The highest concentration of NO_x, 20.33 µgm[-3] was also recorded during the summer season at the polluted sites, which was again 29.19% higher as compared to control site. **Table-2** showing status of different plant parameter due to stress of automobile emission. Table also contain air pollution tolerance index which results combinations of all other parameters such as ascorbic acid, pH, relative moisture content and total chlorophyll. Highest value of total chlorophyll content was found in *Mangifera indica*, 10.00 mg.g [-1] whereas lowest value was found in *Tectona grandis* 2.35 mg.g [-1]. It was observed that highest decrease in chlorophyll content was at site affected by heavy traffic, whereas sites with low traffic recorded lower decreases in chlorophyll content. (Garthy et al., 1993; Speadding and Thomas, 1973)[15-16]. Plants appearing green and normal at low concentration of SO_2, show reduced efficiency of photosynthesis (Varshney, 1982)[17]. So if Plants having high chlorophyll content under natural condition are high tolerant to air pollution. In case of ascorbic acid highest value was found in *Shorea robusta,* 2.00 mg.g [-1], whereas lowest value of ascorbic acid was found in *Tectona grandis*, 1.28 mg.g [-1]. Ascorbic acid is powerful reluctant responsible for the photo reduction of photochlorophllide and its reduction power depends on its concentration (Lewis, 1976)[18]. Ascorbic acid is a strong reluctant protects chloroplasts against SO_2 induced H_2O_2 O_2^- and OH^- accumulation and thus protects the enzymes of the CO_2 fixation cycle and chlorophyll from inactivation (Tanaka et al., 1982)[19]. Together with leaf pH, it plays a significant role in

determining the SO_2 sensitivity of plants (Chaudhary and Rao, 1977)[20]. Thus plants maintaining high ascorbic acid concentration under polluted conditions are considered to be tolerant to air pollution stress. pH of plant show deviation towards acidic side, which may be due to the NO_2 and SO_2. It is reported that in presence of an acidic pollutant the leaf pH is lowered and the decline is greater in sensitive species (Scholz and Reck, 1977)[21]. A shift in cell sap pH towards the acid side in presences of and acidic pollutants might decrease the efficiency of conversion of hexose sugar to ascorbic acid. The reducing activity of ascorbic acid is pH controlled being more at higher and less at lower pH. Thus the leaf extract on the higher side give tolerant to plants against pollution (Agrawal, 1988)[6]. Relative moisture content recorded highest in *Shorea robusta* 87.33 % whereas lowest value found in *Eucalyptus citridora* 55.05 %. Large quantities of water maintain the physiological balance under stress conditions especially during the air pollution (Dedio, 1975 [22] and Lewis, 1976 [18]). Amount of moisture loss and moisture retaining capability is related with size and number of the stomata. Smaller size and less number of stomata result into higher moisture retaining capacity and less moisture loss. Larger the size and higher the number of stomata, lower is the moisture retaining capacity. The various factor of air pollution tolerance index such ascorbic acid and all other factors as chlorophyll, leaf pH, and relative water content generally show depletion under stress. Plants, which can resist this depletion, become resistant air pollution. The highest air pollution tolerance index value calculated by using formula of Singh and Rao (1983)[24] was observed in *Shorea robusta*, 11.27, and lowest in *Eucalyptus*, 7.19. Thus the present study reveals that *Shorea robusta* with highest air pollution tolerance value has highest power to combat air pollution. It can thus be use in bio-monitoring. The tolerant species of plant function as pollution sink and therefore planting tolerant species plant in polluted areas can derive a number of environmental benefits. Plantation of suitable tolerant species is this is one of the ways to reduce the pollution load.

4. CONCLUSION

Plant species show striking variation in their sensitivity to air pollution. Air pollution tolerance index value represents the tolerance level of plants to air pollution. Air pollution tolerance index value helps in the selection of the plant species for plantation at the polluted areas where as plant with lower air pollution tolerance index value can be used in bio-monitoring works. In present investigation APTI values (Table -2) were calculated for both plant species. Maximum APTI, value was observed in case of *Shorea robusta*. On the basis of APTI values, species can be categorized from tolerant to sensitive: *Shorea robusta > Magngifera indica > Tectona grandis > Eucalyptus.* The tolerant species of plants function as pollution sink and therefore a number of environmental benefits can be derived by planting tolerant species of plant in polluted areas. Plantation of suitable tolerant species in this area is one of the ways to reduce the pollution load due to automobile emissions. Plant species with lower air pollution tolerance values are sensitive while species with higher air pollution tolerance values can better withstand in the adverse condition and can be used as potential sink for the mitigation of the air pollution and its adverse effects.

REFERENCES

1. Tiwari, S.L and Rai, S. Current environment issues. Mahdu publications, Bikaner 2004.

2. Tingey, D.T. M.Sc. Thesis, Botany Deptt. University of Utakal, Sal lake City, Utkal 1978.

3. Bennet, J.H. and H.C. Hill. Inhibition of apparent photosynthesis by air pollutioion. J. Environ. Qual 1973; 2: 526-530.

4. Fleming,G.When can forest belt reduce the emissions concentration. Luft and Kacltetchni 1967, 22: 255-258.

5. Warren, J.L. Green space for air pollution. Tech. Rep. No.l 50, School of forest resources, North Carolina. State University, Raleigh, North Carolina; 1973.

6. Agrawal, A.L.. Air pollution control studies and impact assessment of stack and fugitive emission from CCI Akaltara cement factory, Project Sponsored by M/s CCI Akaltara cement factory. NEERI, Nagpur 1988.

7. Agrawal, A.L. Air pollution control and impact on air environment for Mandhar cement factory. Project Report; sponsored by CCI, Mandhar cement factory. NEERI, Nagpur 1989.

8. Tiwari, S.L. Studies of air pollution tolerance indices of some planted trees in urban area of Bhopal with reference to Eco-planning of industrial area. Ph.D. Thesis, Barkatullah University, Bhopal 1991.

9. Arnon, D.I. Copper enzyme in isolated chloroplasts. polyphenoloxidase in Beta vulgaris. Plant Phsysiology 1949; 24: 1-15.

10. Sadashivam, S. and Manikam, A. Biochemical methods for agriculture science. Wiley Eastern Ltd., New Delhi, India 1991.

11. West, P.W., and Gaeke, G.C. Fixation of Sulphur Dioxide as Sufitomercurate III and Subsequent Colorimetric Determination Anal. Chem1956; 28, 1816.

12. Jacob, M.B and Hochheiser, S. Continuous sampling and untra-microdetermination of nitrogen dioxide in air

Anal. Chem 1958 30**,** 426.

13. Weatherly, P. E. The state and movement of water in the lea. Symposium of the society of Experimental Biology 1965**;** 19: 157-184.

14. Singh, S.K. and Rao, D.N. Evaluation of plants for their tolerance to air pollution. Proc. of symposium on air pollution control 1983: 218-224.

15. Garty, J., Karary, Y. and Harel, J.The impact of air pollution on the integrity of cell membranes and chlorophyll in the lechen Ramalina duriaei (De Not.) Bagl. Transported to industrial sites in Israel. Arch. Environ. Contam. Toxicol 1993; 24**:** 455-460.

16. Speadding, D.J. and W.J. Thomas. Effect of sulphur oxide on the metabolism of glycolic acid by barley (*Hordeum vugare*) leaves. Australian Jour. of Biol. Sci 1973; 26**:** 281-286.

17. Varshney, S.K. Effect of SO_2 on plants processes. Ph.D Thesis, J.N. University, New Delhi 1982.

18. Lewis, S. Vitamin C: Its molecular biology and medicinal potential, Academic Press London 1976.

19. Tanaka, K., Otsubo, T and Kondo, N. Participation of hydrogen peroxide in the inactivation of Calvin cycle – SH enzyme in SO_2 fumigated spinach leaves. Plant Cell Physiology1982; 28: 1009-1018.

20. Chaudhary, C.S. and Rao, D.N. Study of some factors in plant controlling their susceptibility to SO_2 pollution. Proc. Of the Indian Natle. Sci. Academy1977; 43: 236-241.

21. Scholz, F. and S. Reck. Effects of acids on forests trees as measured by titration *in-vitro* inheritance of buffering capacity in Picea abies. Water, Air and Soil pollution 1977; 8: 41-45.

22. Dedio, W. Water relation in wheat leaves as screening test for drought resistance. Can. J. Plant Science1975; 55: 369-378.

Table- 1: Primary air pollutants recorded from control and polluted sites (average of 24 readings) during the study period

S.No.	SITE	RSPM (μgm^{-3})			SPM (μgm^{-3})			NO_x (μgm^{-3})			SO_x (μgm^{-3})		
		Winter	Monsoon´	Summer	Winter	Monsoon´	Summer	Winter	Monsoon´	Summer	Winter	Monsoon´	Summer
1	Polluted	122.00	128.40	150.00	401.00	350.22	363.12	12.18	10.22	20.33	7.62	6.11	10.21
2	Control	81.00	96.02	97.15	288.48	215.00	297.45	10.16	9.45	14.39	5.20	4.33	6.31
3	% Higher at polluted site	33.60	25.21	32.23	28.05	38.61	18.08	16.58	7.53	29.19	37.69	29.13	38.19

Where:
RSPM = Respirable particulate matter
SPM= Suspended particulate matter

Table 2- Comparative air pollution tolerance index (APTI) of few tree species of Haridwar.

Tree Species	Parameters						
	Chlorophyll 'a' mg.g^{-1}	Chlorophyll 'b' mg.g^{-1}	Total Chlorophyll mg.g^{-1}	Ascorbic Acidic mg.g^{-1}	pH	Relative water content (%)	Air pollution Tolerance index (APTI)
Magngifera indica Linn.	5.50	4.50	10.00	1.88	5.93	63.73	9.58
Tectona grandis Linn.f.	1.72	0.63	2.35	1.28	5.64	62.58	9.29
Eucalyptus citridora Hook. Syn.	1.91	0.58	2.49	1.95	6.27	55.05	7.19
Shorea robusta Gaertn .f.	3.40	1.66	5.06	2.00	6.39	87.33	11.27

BULK VISCOUS BIANCHI TYPE I, BIANCHI TYPE III AND KANTOWSKI- SACHS COSMOLOGICAL MODELS WITH GENERALIZED CHAPLYGIN GAS AND WITH DYNAMICAL COSMOLOGICAL, GRAVITATIONAL CONSTANTS

S. Kotambkar[*]

Department of Applied Mathematics,
Laxminarayan Institute of Technology,
Rashtrasant Tukadoji Maharaj Nagpur University, Nagpur.
*Corresponding author
shubha.kotambkar@rediffmail.com

G. P. Singh

Department of Mathematics,
Visvesvaraya National Institute of Technology, Nagpur.
gpsingh@mth.vnit.ac.in

R. K. Kelkar

Department of Applied Mathematics,
S. B. Jain Institute of Technology, Nagpur.
rupali.kelkar@yahoo.com

ABSTRACT

This paper is devoted to study the Bianchi type I, Bianchi type III and Kantowski – Sachs models filled with bulk viscous cosmic fluid in presence of Generalized Chaplygin gas and variable cosmological and gravitational constants. A new set of exact solutions of Einstein's field equations by considering the power law relations $R_1 = a_0 t^a$ and $R_2 = b_0 t^b$ have been obtained in Eckart, truncated and full causal theories. Physical behavior of the models have also been discussed

Keywords: Bianchi Type I, Bianchi type III, Kantowski- Sachs, Bulk viscosity, cosmological constant, Gravitational constant, Generalized Chaplygin gas.

1. INTRODUCTION

Recent cosmology is based on FRW model which is completely homogeneous and isotropic. In the early stages universe did not have the property of homogeneous – isotropy as we have today. According to the group theoretic criterion the spatially space–time are of two types i) Bianchi type (I to IX) and ii) Kantowski-Sachs. In the early phase, isotropic model play very important role not only to describe evolution of the universe but also help in finding more general cosmological models than FRW models. Homogeneous but anisotropic models explain number of observed phenomena quite satisfactorily. This motivates researchers for obtaining exact anisotropic solutions for Einstein's field equations, as a cosmologically accepted physical models for the universe . Singh and Singh [1] and Singh *et. al.* [2] have studied Bianchi type III cosmological models with varying cosmological and gravitational constants by assuming conservation law for the energy momentum tensor. Chakraborty and Roy [3] have investigated Bianchi type I, Kantowski-Sachs and Bianchi type III

space-time models with bulk viscosity, where the gravitational constant G and cosmological constant Λ vary with time. Singh and Kale [4] have investigated anisotropic bulk viscous cosmological models with variable G and Λ. Recently several authors [5-9] have investigated anisotropic Bianchi type space-time cosmological models in different context. Very recently Pradhan *et. al.* [10] have investigated viscous fluid cosmology with time dependent q and lambda term in Bianchy type I space-time and late time acceleration.

The astronomical observations [11-15] support that the expansion of the universe is presently accelerated. To understand the accelerated behavior of the universe the variation of cosmological constant has played significant role. A wide range of observations strongly favour a small positive value of the effective cosmological constant at the present epoch. Number of researchers have investigated cosmological models with time varying cosmological constant [16-20].

Gravitational theories with G have been discussed in the literature in the context of induced gravity model. Where G is generalized by means of non vanishing vacuum expectation value of scalar field. Canuto and Narlikar [21] have shown that G varying cosmology is consistent with what so ever cosmological observations available at present. Singh and Kotambker [22] have discussed higher dimensional cosmological models with varying G and Λ. Shriram and Verma [23] have presented spatially homogeneous bulk viscous fluid models with time dependent gravitational constant and cosmological constant. Bianchi type I transit cosmological models with time dependent gravitation and cosmological constants have been investigated by Pradhan *et.al.* [24]. A number of researchers have discussed various anisotropic cosmological models with variable G and Λ [25-29].

In the literature it has been discussed that during the early stages of evolution of the universe, bulk viscosity could arise in many circumstances and could lead to an effective mechanism of galaxy formation [30]. To consider more realistic models one must take into account the viscosity mechanism, which have already attracted the attention of many researchers. Bulk viscosity leading to an accelerated phase of the universe today has been studied by Fabris *et.al.* [31]. Singh e*t.al.* [32] have presented a number of classes of solutions of Einstein's field equations with variable G and Λ and bulk viscosity coefficient in the frame work of non causal theory. Singh and Chaubey [33] and Singh and Baghel [34-35] have discussed some Bianchi type models with bulk viscosity. Recently Kotambkar *et.al.* [36] have investigated anisotropic cosmological models with Quintessence considering the effect of bulk viscosity.

According to recent observational evidence the expansion of the universe is accelarating, which is dominated by a smooth component with negative pressure, the so called dark energy. For recent review on candidates of dark energy refer [37-38].

Cosmological constant is the most promising candidate for dark energy, which is entangled with i) fine tuning problem and ii) coincidence problem. To avoid problems associated with Λ and quintessence models, recently it has been shown that Chaplygin gas may be useful. The unification of the dark matter and dark energy component created a considerable theoretical interest. For representation of such a unification, the generalized Chaplygin gas (GCG) with exotic condition of state $p = \dfrac{-B}{\rho^{\alpha}}$ is considered, where constant B and α satisfy B > 0 and $0 < \alpha \leq 1$ respectively. Due to effectiveness of Chaplygin gas explaining the evolution of the universe, several generalization of Chaplygin gas have been proposed in the literature [39-41]. Due to observational evidence cosmological models based on CG-EOS is very encouraging. Kamenshchik *et. al.* [42] have first time proposed Chaplygin gas and generalized Chaplygin gas cosmological models. WMAP constraints on the generalized Chaplygin gas model have been investigated by Bento *et. al.* [43]. Paul *et. al.* [44] have dicussed observational constraints on modified Chaplygin gas in Horava-Litschitz gravity with dark radiation.

FIELD EQUATION: For perfect fluid distribution Einstein's field equations with gravitation and cosmological constant may be written as

$$R_i^{\ j} - \frac{1}{2} R\, g_i^{\ j} = -8\pi\, G T_i^{\ j} - \Lambda\, g_i^{\ j} \ , \tag{1}$$

where $T_i^{\ j}$ is the energy momentum tensor of the cosmic fluid which in the pressure of bulk viscosity takes the form

$$T_i^{\ j} = \left(\rho + p + \Pi\right) u_i\, u^{\ j} - \left(p + \Pi\right) g_i^{\ j} \tag{2}$$

where p is equilibrium pressure, Π is the bulk viscous stress and ρ is the energy density.

During the investigation it can be assume that an observer has a commoving velocity $u_i = \delta_4^{\ i}$ and the space-time metric may be of the form

$$ds^2 = dt^2 - R_1^2(t) dx^2 - R_2^2(t) d\Omega_k^2 \tag{3}$$

$d\Omega_k^2 = dx^2 + dy^2$ for k = 0 (Bianchi type I model),

$d\Omega_k^2 = d\theta^2 + \sinh^2\theta\, d\phi^2$ for k = -1 (Bianchi type III model) ,

$$d\Omega_k^2 = d\theta^2 + \sin^2\theta \, d\phi^2 \quad \text{for k = 1 (Kantowski – Sachs model)}.$$

Einstein's field equation (2) for space time metric (3) yields the following field equations

$$\left[2\frac{\dot{R}_1}{R_1} + \frac{\dot{R}_2}{R_2}\right]\frac{\dot{R}_2}{R_2} + \frac{k}{R_2^2} = 8\pi G\rho + \Lambda, \tag{4}$$

$$\frac{\ddot{R}_1}{R_1} + \frac{\ddot{R}_2}{R_2} + \frac{\dot{R}_1\dot{R}_2}{R_1 R_2} = -8\pi G(p + \Pi) + \Lambda, \tag{5}$$

$$2\frac{\ddot{R}_2}{R_2} + \left(\frac{\dot{R}_2}{R_2}\right)^2 + \frac{k}{R_2^2} = -8\pi G(p + \Pi) + \Lambda. \tag{6}$$

For the full causal non- equilibrium thermodynamics the causal evolution equation for bulk viscosity is given by [45]

$$\Pi + \tau\dot{\Pi} = -\eta\left(\frac{\dot{R}_1}{R_1} + 2\frac{\dot{R}_2}{R_2}\right) - \frac{\varepsilon\tau\Pi}{2}\left(\frac{\dot{R}_1}{R_1} + 2\frac{\dot{R}_2}{R_2} + \frac{\dot{\tau}}{\tau} - \frac{\dot{\eta}}{\eta} - \frac{\dot{T}}{T}\right). \tag{7}$$

$T \geq 0$ absolute temperature, η is bulk viscosity coefficient which cannot become negative, τ denote the relaxation time for transient bulk viscous effects. Causality requires $\tau > 0$. When $\varepsilon = 0$, equation (7) reduces to evolution equation for truncated theory. For $\varepsilon = 1$ equation (7) reduces to evolution equation for full causal theory and for $\tau = 0$ equation (7) reduces to evolution equation for non-causal theory (Eckart's theory).

Non - Causal Cosmological Models: For non causal solution $\tau = 0$, therefore equation (7) reduces in the form of

$$\Pi = -3\eta H \tag{8}$$

The expansion scalar Θ is defined by

$$\Theta = 3H, \quad H = \frac{\dot{R}}{R} \tag{9}$$

$$\text{Therefore } \Pi = -\eta\Theta \tag{10}$$

Case I: Bianchi Type I Cosmological Model Taking, k = 0 equation (3) reduces to Bianchi type I i. e.

$$ds^2 = dt^2 - R_1^2 dx^2 - R_2^2 dy^2 - R_2^2 dz^2, \tag{11}$$

The field equations (4) to (6) may be written as

$$\left[2\frac{\dot{R}_1}{R_1} + \frac{\dot{R}_2}{R_2}\right]\frac{\dot{R}_2}{R_2} = 8\pi G\rho + \Lambda, \tag{12}$$

$$\frac{\ddot{R}_1}{R_1} + \frac{\ddot{R}_2}{R_2} + \frac{\dot{R}_1\dot{R}_2}{R_1 R_2} = -8\pi G(p - \eta\Theta) + \Lambda, \tag{13}$$

$$2\frac{\ddot{R}_2}{R_2} + \left(\frac{\dot{R}_2}{R_2}\right)^2 = -8\pi G(p - \eta\Theta) + \Lambda. \tag{14}$$

Equations (12) to (14) produce continuity equation as

$$\dot{\rho} + (p - \eta\Theta + \rho)\left(\frac{\dot{R}_1}{R_1} + 2\frac{\dot{R}_2}{R_2}\right) = -\frac{\dot{G}}{G}\rho - \frac{\dot{\Lambda}}{8\pi G}. \tag{15}$$

The conservation of energy momentum equation $T^{ij}_{;j} = 0$ splits equation (15) into two equations

$$\dot{\rho} + (p - \eta\Theta + \rho)\left(\frac{\dot{R}_1}{R_1} + 2\frac{\dot{R}_2}{R_2}\right) = 0, \tag{16}$$

and
$$\dot{\Lambda} = -8\pi\,\dot{G}\rho \tag{17}$$

Cosmological Solutions: Since there are three basic equations (12) –(14) and seven unknowns viz. $R_1, R_2, p, \rho,\ G,\ \Lambda$ *and* η therefore four more physically plausible relations among these variables will be considered for solving the set of equations.

In all cases we consider following physically plausible relations.
An exotic background fluid, the Generalized Chaplygin gas described by the equation of state

$$p = \frac{-B}{\rho^{\alpha}}\,, \tag{18}$$

where B and α are constants with the conditions $B > 0$ and $0 < \alpha \le 1$ respectively.

The cosmological constant Λ as

$$\Lambda = \frac{A}{t^2}\,, \tag{19}$$

The power law relations

$$R_1 = a_0\,t^{a}\,, \tag{20}$$

$$R_2 = b_0\,t^{b}\,, \tag{21}$$

where a_0 and b_0 are constants.

From equations (17) and (19), we get

$$\frac{2A}{t^3} = 8\pi\,\dot{G}\rho\,, \tag{22}$$

with the help of equations (19)-(21), equation (12) yields

$$\left[\frac{2a}{t} + \frac{b}{t}\right]\frac{b}{t} = 8\pi\,G\rho + \frac{A}{t^2}\,,$$

Then
$$8\pi\,G\rho = \frac{2ab + b^2 - A}{t^2}\,. \tag{23}$$

From equations (22) and (23), one can easily calculate

$$G = G_0\,t^{\frac{2A}{C}} \tag{24}$$

where $C = 2ab + b^2 - A$.
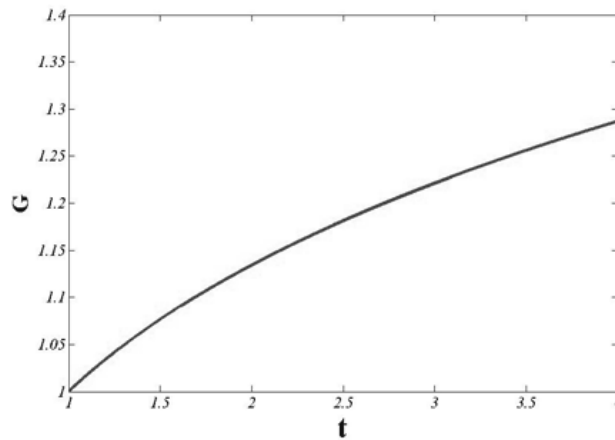
Fig. 1: shows variation of gravitational constant with respect to cosmic time t.
Here we consider A = 1, a = 2, b = 2 . $G_0 = 1$

From equation (24) and fig. 1 one can see that G is increasing with cosmic time t which goes with observation.

From equations (23) and (24), we get

$$\rho = \rho_0 t^{-\frac{2(C+A)}{C}} , \qquad (25)$$

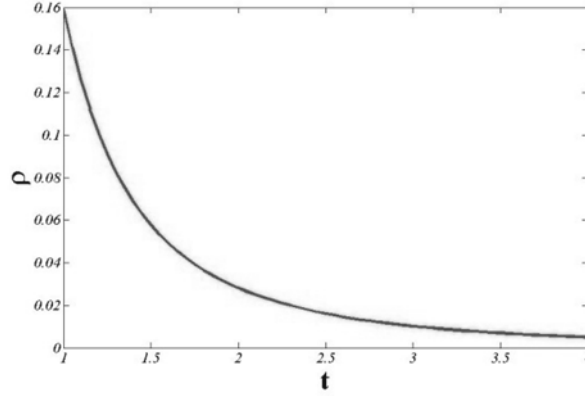where $\rho_0 = \dfrac{C}{8\pi G_0}$.

Fig. 2 shows variation of energy density with respect to cosmic time t. Here we consider A = 1, a = 2, b = 2 $G_0 = 1$

From equation (25) and fig. 2 one can see that energy density is decreasing with cosmic time t. Which is in fair agreement with observations.

Using equations (9) and (20)-(21), we get

$$\Theta = \frac{a + 2b}{t} \qquad (26)$$

By use of equations (10), (18)-(21) and equations (24)-(26), equation (13) becomes

$$\frac{a(a-1)}{t^2} + \frac{b(b-1)}{t^2} + \frac{a}{t}\frac{b}{t} = -8\pi G_0\, t^{\frac{2A}{2ab+b^2-A}}\left(\frac{-B}{\rho^\alpha} - \eta\,\frac{a+2b}{t}\right) ,$$

which on simplification yields expression for bulk viscosity coefficient as

$$\eta = \frac{t}{a+2b}\left[\eta_0 t^{\frac{-2(C+A)}{C}} - \eta_1 t^{\frac{2\alpha(C+A)}{C}}\right] , \qquad (27)$$

where $\eta_0 = \dfrac{(a+b)(a-1) - 2ab + C}{8\pi G_0}$ and $\eta_1 = \dfrac{B(8\pi G_0)^\alpha}{C^\alpha}$.
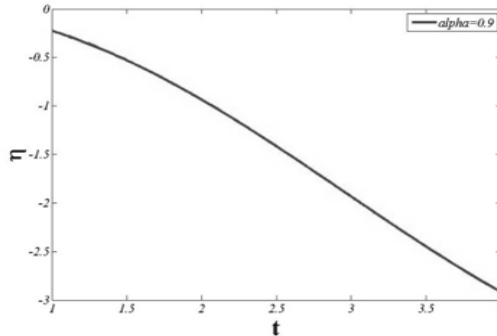
Fig. 3 shows variation of bulk viscosity coefficient with respect to cosmic time t.

Here we consider A = 1, a = 2, b = 2 $G_0 = 1$

The shear scalar may be defined as [46],

$$\sigma^2 = \frac{1}{12}\left[\left(\frac{\dot{g}_{11}}{g_{11}} - \frac{\dot{g}_{22}}{g_{22}}\right)^2 + \left(\frac{\dot{g}_{22}}{g_{22}} - \frac{\dot{g}_{33}}{g_{33}}\right)^2 + \left(\frac{\dot{g}_{33}}{g_{33}} - \frac{\dot{g}_{11}}{g_{11}}\right)^2\right] \tag{28}$$

The shear scalar for our model becomes

$$\sigma^2 = \frac{2(a-b)^2}{3t^2} \tag{29}$$

From equation (29) one can see that when $t \rightarrow \infty$, $\sigma^2 \rightarrow 0$, i. e. shear dies out.

The deceleration parameter is related to the expansion scalar as

$$q = -\frac{3\dot{\Theta} + \Theta^2}{\Theta^2}, \tag{30}$$

Further, with the help of equations(26) and (30), the expression for the deceleration parameter q may be obtained as

$$q = \frac{3}{a+2b} - 1, \tag{31}$$

For a + 2b > 3, q < 0, therefore a > 1 and b >1.

Since $\dfrac{\sigma}{\Theta} = \dfrac{\sqrt{2}\,(a-b)}{\sqrt{3}\,(a+2b)}$ = constant, the model does not approach isotropy.

Relative anisotropy $M = \dfrac{16\pi G_0 (a-b)^2}{3C}$, where $\dfrac{\sigma^2}{\rho} = M\,t^{\frac{4b(1-a)-2A}{C}}$.

Case II:
Bianchi Type-III Cosmological Model

Taking, k = -1 equation (3) reduces to Bianchi type III i. e.

$$ds^2 = dt^2 - R_1^2 dx^2 - R_2^2\left[d\theta^2 + \sinh^2\theta\, d\phi^2\right], \tag{32}$$

The field equations (4) to (6) may be written as

$$\left[2\frac{\dot{R}_1}{R_1} + \frac{\dot{R}_2}{R_2}\right]\frac{\dot{R}_2}{R_2} - \frac{1}{R_2^2} = 8\pi G\rho + \Lambda, \tag{33}$$

$$\frac{\ddot{R}_1}{R_1} + \frac{\ddot{R}_2}{R_2} + \frac{\dot{R}_1\dot{R}_2}{R_1 R_2} = -8\pi G(p - \eta\,\Theta) + \Lambda, \tag{34}$$

$$2\frac{\ddot{R}_2}{R_2} + \left(\frac{\dot{R}_2}{R_2}\right)^2 - \frac{1}{R_2^2} = -8\pi G(p - \eta\,\Theta) + \Lambda. \tag{35}$$

with the help of equations (19)-(21), equation (33) yields

$$\left[\frac{2a}{t} + \frac{b}{t}\right]\frac{b}{t} - \frac{1}{\left(b_0 t^b\right)^2} = 8\pi G\rho + \frac{A}{t^2},$$

$$8\pi G\rho = \frac{\left[2ab + b^2 - A\right]b_0^2 t^{2b} - t^2}{b_0^2 t^{2b+2}}, \tag{36}$$

From equation (22) and (36),

$$\frac{\dot{G}}{G} = \frac{2\,Ab_0^2\,t^{2b-3}}{\left((2a+b)b\,b_0^2 - Ab_0^2\right)t^{2b-2} - 1}\ ,$$

(37)

By solving equation (37), one can easily calculate

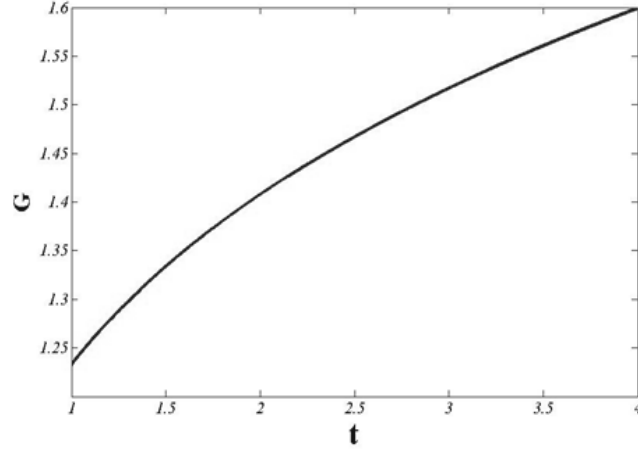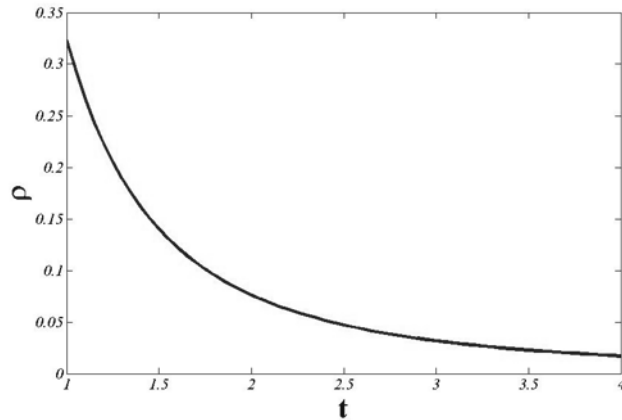$$G = G_0\left[C\,b_0^2\,t^{2b-2} - 1\right]^{\frac{A}{C\,(b-1)}} .$$

(38)

Fig. 4 shows variation of gravitational constant G with respect to cosmic time t.
Here we consider A = 1, a = 2, b = 2 G_0 = 1, b_0 = 1.

From equation (38) and fig. 4 one can see that G is increasing with cosmic time t. Which agree with observation.

Use of equation (36) and equation (38) suggests

$$\rho = \rho_1\,t^{-2b}\left(C\,b_0^2\,t^{2b-2} - 1\right)^{1 - \frac{A}{C\,(b-1)}}\ ,$$

(39)

Where $\rho_1 = \dfrac{1}{8\pi\,G_0\,b_0^2}$.

Fig. 5 shows variation of energy density with respect to cosmic time t.
Here we consider A = 1, a = 2, b = 2 G_0 = 1, b_0 = 1 .

From equation (39) and fig. 5 one can see that energy density is decreasing with cosmic time t. Which is in fair agreement with observations.

By use of equations (15) – (16) , (26) and equations (38)-(39), equation (34) yields

$$\eta = \frac{t}{a+2b}\left[\eta_4 t^{2b\alpha}\left(C b_0^2 t^{2b-1}-1\right)^{\left(\frac{A}{C(b-1)}-1\right)\alpha} - \eta_0 t^{-2}\left(C b_0^2 t^{2b-1}-1\right)^{\frac{-A}{C(b-1)}}\right],$$

(40)

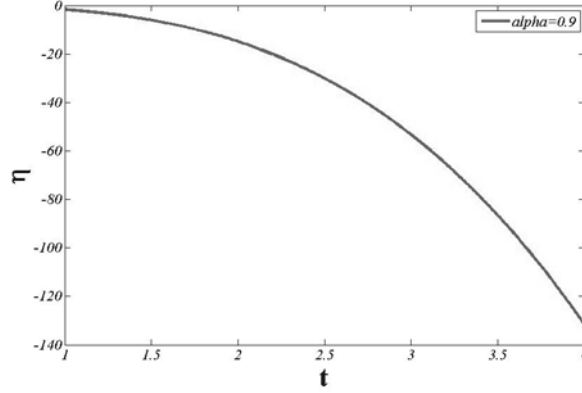where $\eta_4 = B\left(8\pi G_0 b_0^2\right)^\alpha$, $\eta_0 = \dfrac{(a+b)(a-1)-2ab+C}{8\pi G_0}$.

Fig. 6 shows variation of bulk viscosity coefficient with respect to cosmic time t.
Here we consider A = 1, a = 2, b = 2 $G_0 = 1$.

Case III:
Kantowski-Sachs Cosmological Model

Consider, k = 1 the equation (3) reduces to Kantowski-Sachs space-time metric

$$ds^2 = dt^2 - R_1^2 dx^2 - R_2^2\left[d\theta^2 + \sin^2\theta d\phi^2\right],$$

(41)

Therefore the set of field equations (4)- (6) takes the form

$$\left[2\frac{\dot{R}_1}{R_1}+\frac{\dot{R}_2}{R_2}\right]\frac{\dot{R}_2}{R_2}+\frac{1}{R_2^2} = 8\pi G\rho + \Lambda ,$$

(42)

$$\frac{\ddot{R}_1}{R_1}+\frac{\ddot{R}_2}{R_2}+\frac{\dot{R}_1\dot{R}_2}{R_1 R_2} = -8\pi G\left(p-\eta\Theta\right)+\Lambda ,$$

(43)

$$2\frac{\ddot{R}_2}{R_2}+\left(\frac{\dot{R}_2}{R_2}\right)^2+\frac{1}{R_2^2} = -8\pi G\left(p-\eta\Theta\right)+\Lambda ,$$

(44)

For this new set of field equations (42)-(44) and with the help of equations (19)-(21) and (42) , we get

$$8\pi G\rho = \frac{C b_0^2 t^{2b-2}+1}{b_0^2 t^{2b}},$$

(45)

with the equation of (22) and (45), we get

$$\frac{\dot{G}}{G} = \frac{2 A b_0^2 t^{2b-3}}{C b_0^2 t^{2b-2}+1},$$

(46)

95

By solving equation (46), one can easily calculate

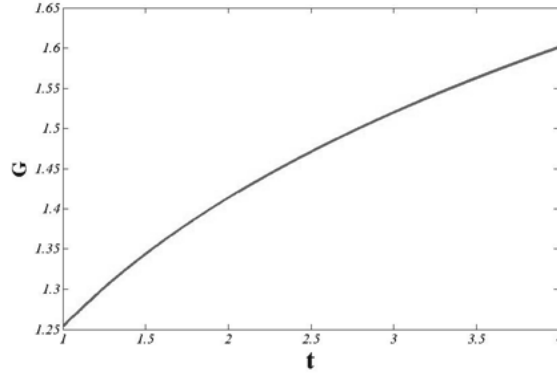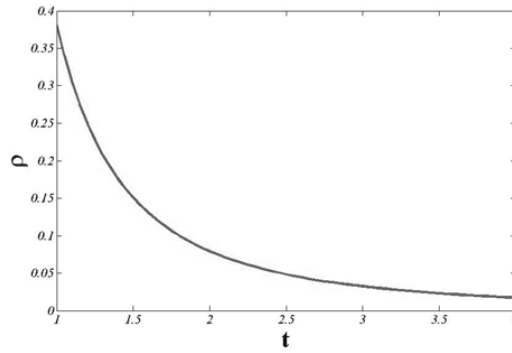$$G = G_0 \left[C\, b_0^2\, t^{2b-2} + 1 \right]^{\frac{A}{C(b-1)}} .$$ (47)

Fig. 7 shows variation of gravitational constant G with respect to cosmic time t.
Here we consider $A = 1$, $a = 2$, $b = 2$, $G_0 = 1$, $b_0 = 1$.

From equation (47) and fig. 7 one can observe that G is increasing with evolution of the universe. Which agree with observation.

From equation (45) and (47), we get

$$\rho = \rho_2\, t^{-2b} \left(C\, b_0^2\, t^{2b-2} + 1 \right)^{1 - \frac{A}{C(b-1)}} ,$$ (48)

where $\rho_2 = \dfrac{1}{8\pi\, G_0\, b_0^2}$

Fig. 8 shows variation of energy density with respect to cosmic time t.
Here we consider $A = 1$, $a = 2$, $b = 2$, $G_0 = 1$, $b_0 = 1$.

Equation (48) and fig. 8 shows that energy density is decreasing with cosmic time t. Which validate observations.

By use of equations (18) –(21), (26) and equations (47)-(48), equation (43) yields

$$\eta = -\eta_6\, t^{2b\alpha+1} \left(C\, b_0^2\, t^{2b-2} + 1 \right)^{\alpha\left(\frac{A}{C(b-1)} - 1 \right)} + \frac{\eta_0}{a+2b}\, t^{-1} \left(C\, b_0^2\, t^{2b-2} + 1 \right)^{\frac{-A}{C(b-1)}} ,$$ (49)

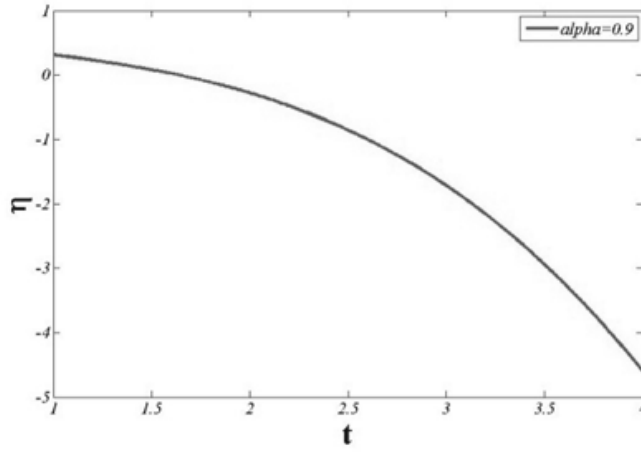where $\eta_6 = \dfrac{B\left(b_0^2\, 8\pi\, G_0 \right)^{\alpha}}{a+2b} .$

Fig. 9 shows variation of bulk viscosity coefficient with respect to cosmic time t.
Here we consider A = 1, a = 2, b = 2 $G_0 = 1$.

Causal - Cosmological Model:

From equations (4) and (6) we have

$$\frac{\ddot{R}_1}{R_1} + \frac{\ddot{R}_2}{R_2} + \frac{\dot{R}_1}{R_1}\frac{\dot{R}_2}{R_2} = 2\frac{\ddot{R}_2}{R_2} + \left(\frac{\dot{R}_2}{R_2}\right)^2 + \frac{k}{R_2^2} \ . \tag{50}$$

Which gives $a = b \ or \ a + 2b = 1 \ for \ k = 0$

case (i):

In this case considering a = b and k = 0, therefore

$$R_1 = a_0 t^a, \qquad\qquad R_2 = b_0 t^a. \tag{51}$$

From equations (19) and (51), equation (4) becomes

$$2\frac{a}{t}\frac{a}{t} + \left(\frac{a}{t}\right)^2 = 8\pi G\rho + \frac{A}{t^2},$$

$$8\pi G\rho = \frac{3a^2 - A}{t^2} \tag{52}$$

From equations (22) and (52), one can easily obtain
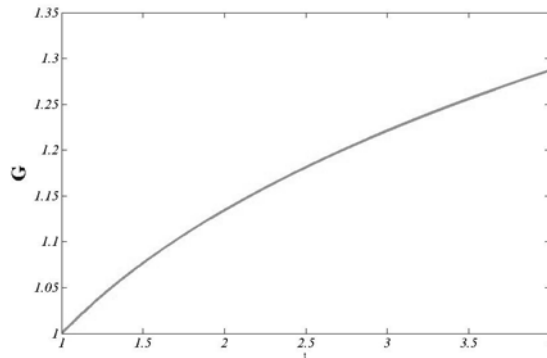
$$G = G_0 \, t^{\frac{2A}{3a^2 - A}} \ . \tag{53}$$

Fig. 10 shows variation of gravitational constant G with respect to cosmic time t.
Here we consider A = 1, a = 2, $G_0 = 1$.

97

From equation (53) and fig. 10 one can observe that G is increasing with evolution of the universe. Which goes with observation.

From equations (52) and (53), we get

$$\rho = \rho_5 \, t^{-\frac{6a^2}{3a^2-A}},$$
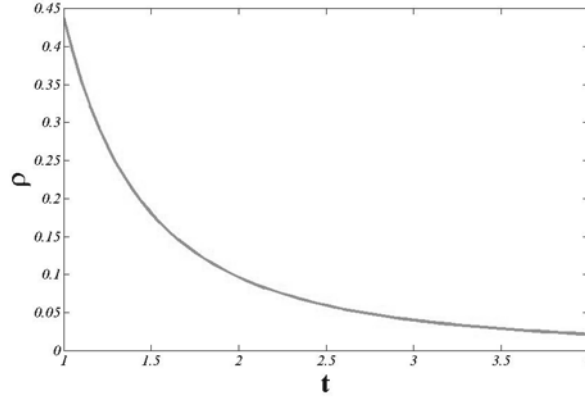
(54)

where $\rho_5 = \dfrac{3a^2-A}{8\pi G_0}$.

Fig. 11 shows variation of energy density with respect to cosmic time t.
Here we consider A = 1, a = 2, $G_0 = 1$.

Equation (54) and fig. 11 shows that energy density is decreasing with cosmic time t. Which validate observations.

Substitute the values of equations (18)-(19) , (51)-(53) in equation (5), we get

$$\Pi = \Pi_0 \, t^{\frac{6a^2\alpha}{3a^2-A}} - \Pi_1 \, t^{\frac{-6a^2}{3a^2-A}},$$

(55)

where $\Pi_0 = \dfrac{B(8\pi G_0)^\alpha}{(3a^2-A)^\alpha}$, $\qquad \Pi_1 = \dfrac{3a^2-2a-A}{8\pi G_0}$.

Evolution of Bulk Viscosity in Truncated Causal Theory. Now, we are interested in study of the variation in bulk viscosity coefficient (η) and relaxation time (τ) with respect to cosmic time. For truncated theory $\varepsilon = 0$ and hence equation (7) reduces to

$$\Pi + \tau \, \dot{\Pi} = -3\eta H$$

(56)

Further, in order to have exact solution of the system of equations one more physical plausible relation is required. Thus we consider

$$\tau = \frac{\eta}{\rho}$$

(57)

With the help of equations (51), (54)-(55) and (57), we get

$$\eta = \frac{\Pi_0 \, t^{\frac{6a^2\alpha}{3a^2-A}} - \Pi_1 \, t^{\frac{-6a^2}{3a^2-A}}}{\eta_8 \, t^{\frac{6a^2(\alpha+1)}{3a^2-1}} + \eta_9 t^{-1} + 3a\,t^{-1}}$$

(58)

Where $\eta_8 = \dfrac{B(8\pi G_0)^{\alpha+1} 6a^2\alpha}{(3a^2-A)^{\alpha+2}}$, $\qquad \eta_9 = \dfrac{(3a^2-2a-A)6a^2}{(3a^2-A)^2}$

Evolution of Bulk Viscosity in full Causal Theory.

$$T \propto \exp \int \frac{dp}{\rho + p} \quad \text{and equation (18) we get}$$

$$T = T_0 \left\{ 1 - B\rho^{-(\alpha+1)} \right\}^{\frac{\alpha}{\alpha+1}} \tag{59}$$

With equations (57) and (59), equation (7) becomes

$$\Pi + \frac{\eta}{\rho}\dot{\Pi} = -\eta\left(\frac{\dot{R}_1}{R_1} + 2\frac{\dot{R}_2}{R_2}\right) - \frac{\eta\Pi}{2\rho}\left[\left(\frac{\dot{R}_1}{R_1} + 2\frac{\dot{R}_2}{R_2}\right) + \frac{\dot{\tau}}{\tau} - \frac{\dot{\eta}}{\eta} - \frac{\dot{T}}{T}\right]$$

Which on simplification gives

$$\eta = \frac{-\Pi_0 t^{D\alpha} - \Pi_1 t^{-D}}{C_1 t^{D(\alpha+1)} - C_2 t^{-1} + 3at^{-1} + \left(C_3 t^D + C_4\right)\left[3at^{-1} + C_5 t^{D-1}\left(1 - \frac{B}{\rho_5^{\alpha+1}} t^D\right)^{-1} + Dt^{-1}\right]} \tag{60}$$

Where $D = \dfrac{6a^2}{3a^2 - A}$, $\quad C_1 = \dfrac{6a^2 \alpha B(8\pi G_0)^{\alpha+1}}{(3a^2 - A)^{\alpha+2}}$, $\quad C_2 = \dfrac{3a^2 - 2a - A}{(3a^2 - A)^2}$

$$C_3 = \frac{16\pi G_0 \Pi_0}{(3a^2 - A)}, \quad C_4 = \frac{16\pi G_0 \Pi_1}{3a^2 - A}, \quad C_5 = \frac{-48B\alpha a^2 \pi G_0}{(3a^2 - A)^{\alpha+1}}$$

case (ii):

In this case we consider a + 2b = 1 and k = 0, then

$$R_1 = a_0 t^a, \; R_2 = b_0 t^{\frac{1-a}{2}} \tag{61}$$

Using equations (18)- (19) and (61) in equation (4), we get

$$8\pi G\rho = \frac{4\left[2a(1-a) - A\right] + (1-a)^2}{4t^2} \tag{62}$$

From equations (22) and (62), one can easily calculate

$$G = G_0 t^S, \tag{63}$$

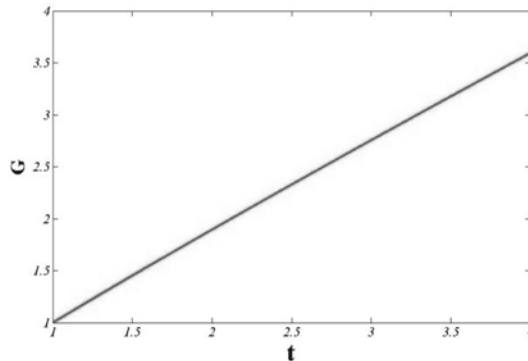Where $S = \dfrac{8A}{4\left[2a(1-a) - A\right] + (1-a)^2}$.

Fig. 12 shows variation of gravitational constant G with respect to cosmic time t.
Here we consider A = 0.15, a = 0.5, $G_0 = 1$.

From equation (63) and fig. 12 one can observe that G is increasing with evolution of the universe. Which is in fair agreement with observation.

From equations (62) and (63), we get

$$\rho = \rho_6 \, t^{-(S+2)} \ , \tag{64}$$

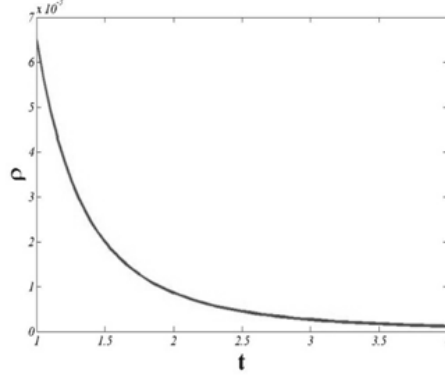where $\rho_6 = \dfrac{4\left[2a(1-a) - A\right] + (1-a)^2}{32 \, \pi \, G_0}$

Fig. 13 shows variation of energy density with respect to cosmic time t.
Here we consider A = 0.15, a = 0.5, $G_0 = 1$.

Equation (64) and fig. 13 shows that energy density is decreasing with cosmic time t. Which goes with observation.

Using equations (18)-(19) , (61)-(64) in equation (5), we get

$$\Pi = \frac{B \, t^{(S+2)\alpha}}{\rho_6^{\alpha}} - \Pi_2 t^{-(S+2)} \ . \tag{65}$$

Where $\Pi_2 = \dfrac{(a-1)(7a+1) - 4A}{32 \, \pi \, G_0}$.

Evolution of Bulk Viscosity in Truncated Causal Theory.

With the help of equations (56)- (57), (61) and (65), we have

$$\eta = \frac{\dfrac{-B \, t^{(S+2)\alpha}}{\rho_0^{\alpha}} + \Pi_2 \, t^{-(S+2)}}{\dfrac{B(S+2)\alpha}{\rho_0^{\alpha+1}} t^{(S+2)(\alpha+1)-1} + \dfrac{\Pi_2(S+2)}{\rho_6 t} - \dfrac{1}{t}} \tag{66}$$

Evolution of Bulk Viscosity in full Causal Theory

With equations (57), (59) and (64) equation (7) becomes

$$\Pi + \frac{\eta}{\rho}\dot{\Pi} = -\eta\left(\frac{\dot{R}_1}{R_1} + 2\frac{\dot{R}_2}{R_2}\right) - \frac{\eta\Pi}{2\rho}\left[\left(\frac{\dot{R}_1}{R_1} + 2\frac{\dot{R}_2}{R_2}\right) + \frac{\dot{\tau}}{\tau} - \frac{\dot{\eta}}{\eta} - \frac{\dot{T}}{T}\right]$$

Which on simplification gives

$$\eta = \frac{-\dfrac{B}{\rho_6^{\alpha}}t^{(S+2)\alpha} + \Pi_2 t^{-(S+2)}}{\dfrac{B(S+2)\alpha}{\rho_6^{\alpha+1}}t^{(S+2)(\alpha+2)-1} + \dfrac{\Pi_2(S+2)}{\rho_6 t} + \dfrac{1}{t} + \left(\dfrac{B}{2\rho_6^{\alpha+1}}t^{(S+2)(\alpha+1)} - \dfrac{\Pi_2}{2\rho_6}\right)\left[\dfrac{S+3}{t} + \dfrac{B\alpha(S+2)}{\rho_6^{\alpha+1}}t^{(\alpha+1)(S+2)-1}\left(1 - \dfrac{B}{\rho_6^{\alpha+1}}t^{(S+2)(\alpha+1)}\right)^{-1}\right]} \tag{67}$$

2. DISCUSSION

In this paper, we have studied generalized Chaplygin gas model of Bianchi type I, Bianchi type III and Kantowski-Sachs space-time universe with time varying bulk viscosity, cosmological constant and gravitational constant. In first part of the paper, we have discussed non-causal cosmological models where as in the second part we have discussed causal cosmological models i. e. truncated theory and full causal theory, by considering power law relation between scale factor and cosmic time t. In the first part of the paper for $a + 2b > 3$, we are getting accelerating model of the universe. In both the parts shear dies out as t tends to infinity. In both parts of the paper energy density, bulk viscosity is decreasing with time. Where as gravitational constant G(t) is zero initially and gradually increases and tends to infinity at late times, which is consistent with observational results. Several relevant graphs of cosmological parameters have been plotted, all behave properly.

3. ACKNOWLEDGEMENTS

REFERENCES

1.   Singh, T. and Singh, G. P., *Astrophys. Space Sci*., **181**, 89, (1991).

2.   Singh, J. P., Tiwari, R. K. and Shukla P., *Chin. Phys. Lett*., **24**, 3325, (2007).

3.   Chakraborty, S. and Roy, A., *Astrophys. Space Sci.,* **313**, 389-392, (2008).

4.   Singh, G. P. and Kale, A. Y., *Int. J. Theor. Phys*., **48**, 1177-1185, (2009).

5.   Kalita, S., Dourah, H. L. and Dnorah, K., *Indian J. Phys.,* **84**, 629, (2010).

6.   Dey, S, Gewali, J. P., Jha, A. K., Chhaigte, L. and Jain Y. S., *Indian J. Phys*., **85**, 1309, (2011).

7.   Oli, S., *Indian J. Phys.*, **85**, 755, (2012).

8.   Nourinezhad, Z. and Mehdipour, S. H., *Indian J. Phys*., **86**, 919, (2012).

9.   El- Nabulsi A. R*., Indian J. Phys*., **87**, 195, (2013).

10.   Pradhan, A. Zia, R. and Singh, R. P., *Indian J. Phys*., **87**, 1157, (2013).

11.   Perlmatter, S. et al, *Astrophys. J*., 517-565 (1999).

12.   Riess, A. G. et al, *Astron J.,* **116**, 1009, (1998).

13.   W. J. Percival et al, *Mon. Not. R. Astron Soc*., **327**, 1297, (2001).

14.   D. Stern, R. Jimenez, L. Verde, M. Kamion Kowski and S. A Stanford, *J. cosmol, Astropart. Phys*., **2**, 8 (2010).

15.   R. Jimenez, L. Verde, T. Tren and D. Stern, *Asrophys. J.,* **593**, 622 (2003).

16.   Ratra and Peeble PJE *Phys. Rev*. , **D37**, 3406, (1988).

17.   Dolgov, A. D. *Phys. Rev*. **D 55**, 5881, (1997).

18.   Sahni, V. and Strarobinsky, A., *Int. J. Mod. Phys*. **D9**, 373 (2000).

19.   Padmanabhan, T., *Phys. Rept*. **380**, 235 (2003).

20.   Peebles PJE *Rev. Mod. Phys*. **75**, 599 (2003).

21.   Canuto, V. M. and Narlikar, J. V., *Astrophys. J*., **6**, 236, (1980).

22.   Singh, G. P., and Kotambkar, S. *Gen. Rel. Grav.,* **33,** 621, (2001).

23.   Verma, M. K. and Shri Ram, *Adv. Stud. Theor. Phys.,* **5,** 387,(2011).

24.   Pradhan, A., Bijan Saha and Rikhvitsky, V. , *Indian J. of Phys*., (2014)..

25.   Singh, C. P., Kumar, S. and Pradhan, A., *Class. Quant. Grav*., **24**, 455, (2007).

26.   Singh, J. P. and Tiwari, S. K., *Pramana*, **70**, 565, (2008).

27.   Singh, G. P. and Kale, A. Y., *Int. J. theor. Phys*., **48**, 17177, (2009).

28.   Bali, R. and Tinkar, S., *Chin. Phys. Lett*., **26**, 029802, (2009).

29.   Verma, M. K. and Shri Ram, *Ad. Stud. Theor. Phys.* **5**, 387-398, (2011).

30. Ellis GFR, In general relativity and cosmology, Enrico Fermi course, edited by R. Schas (Academic New- York, 1979) p47; Misner, C. W., *Astrophys. J.* **151**, 431, (1968); Hu, B. L., In advances in astrophysics edited by E. J.Fang and R. Ruttini (World Scientific, Songapore 1983).

31. Fabris, J. C., Concalves S. V. B. de Sa'Ribeiro, *Gen. Rel. Grav.*, **38**, 495, (2006).

32. Singh, C. P. , Kumar S. and Pradhan, A., *Class. Quant. Grav.,* **24**, 455, (2007).

33. Singh, T. and Chaubey, R*., Pramana*, **68,** 721, (2007).

34. Singh, J. P. and Baghel, P. S., *Int. J. theor. Phys*., **48**, 449, (2009).

35. Singh, J. P. and Baghel, P. S., *Electron J. Theor. Phys*., **6**, 85, (2009).

36. Kotambkar, S., Singh, G. P. and Kelkar, R. K., *Int. J. Theor. Phys*. **53,** 449, (2014).

37. Peebles, P. J. E. and Ratra, B., Rev. Mod. Phys., 75, 559, (2003).

38. Padmanabhan, T. Phys. Repts., 380, 235, (2003).

39. Benaoum, H. B., hep-th, 0205140; Dev, A., Alcaniz, J. S. and jain, D., Phys. Rev., D67, 023515, (2003).

40. Sen, A. A. and Scherrer, R. J., Phys. Rev., D72, 063511, (2005).

41. Debnath, U., Chin. Phys. Lett., 28, 19801, (2011).

42. Kamenshchik, A., Moschella, U., Pasquier, V., *Phys. Lett*. ,**511,** 265, (2001).

43. Bento, M. C., Bentilami, O. and Sen, A. A., *Phys. Lett*. **B575**, 172, (2003).

44. Paul B. C., Thakur, P. and Verma, M. K., *Pramana*, **81**, 691-718, (2013).

45. Maartens, R., *Class. Quant. Grav*., **12**, 1455, (1995).

46. Raychaodhuri, A. K., *Phys. Rev*., **98**, 1123, (1955).

INTERNATIONAL JOURNAL OF ENGINEERING SCIENCES AND MANAGEMENT (ISSN: 2231-3273)

International Journal of Engineering Sciences and Management is a bi-annual journal of Dronacharya Group of Institutions, Greater Noida, UP, India.

1. SCOPE OF THE JOURNAL

To publish full-length research papers in any one or more of the following disciplines:

Computer Science & Engineering, Information Technology, Electrical, Electronics & Communication Engineering, Mechanical Engineering, Civil Engineering, Physics, Mathematics, Economics, and Management.

2. PURPOSE OF THE JOURNAL

To keep the academic community abreast of the research and technical scenario in the stated disciplines in the world.

3. CHERISHED AIM OF THE JOURNAL

The aim of the Journal is to percolate latest information in the fields of Engineering, Technology and Management to aspiring minds to carryout meaningful research work and thereby benefit mankind in all possible ways. Knowledge shared on this common platform will immensely help researchers for gainful outputs.

4. GUIDELINES FOR AUTHORS

SUBMISSION OF MANUSCRIPTS: Soft copy of the manuscript for consideration of publication should be sent (as MS Word Windows 2007 attachment) by Email to the Executive Editor at advisor.r&d@gnindia.dronacharya.info

All papers, received for consideration of publication and complying with the below-mentioned format will be sent for review to at least two referees. In accepting the paper for publication, the Editors and reviewers will give special weight to readability and interest value for a wide readership besides the originality and the high-standard of its contents. The Executive Editor's decision is final in case of non-unanimity of opinion of referees. Under normal circumstances, the authors will be informed about the status of their papers by the Executive Editor within eight weeks of their submission.

PREPARATION OF MANUSCRIPTS:

- **Manuscript**: Manuscript should be in English, the preferred spelling being that of the Concise Oxford Dictionary. It should be in 'Times New Roman', single-spaced, and typed on 8.5" x 11" or A4-size paper with margins of 1" (25 mm) on each side. Manuscript should be typed in *single column* only (and not in double or triple columns).

- **Title of Paper**: Font size 16, ALL CAPITALS, bold, centered, and *not underlined*. The title must be 12.5 mm below the top of the page (in addition to the standard 25 mm margin). The Title should adequately describe the contents of the paper

- **Full names of all Authors**, with * as superscript with corresponding author's name and his/her Email ID (Font size 12, centered) and also the contact number. A blank line should be left between the title and the author's name(s).

- **Full postal address** along with affiliations (Font size 10, centered).

- **Abstract** (Font size 10, centered) All papers must have a non-mathematical abstract of not more than 200 words. The abstract should indicate the general scope of the paper, the important findings and the conclusions

drawn. The abstract should include only text. It should be specific about the methodologies used and the conclusion drawn of the work reported. Please avoid the use of abbreviations and references. (Text of the Abstract: Font size 9, single-space, justified).
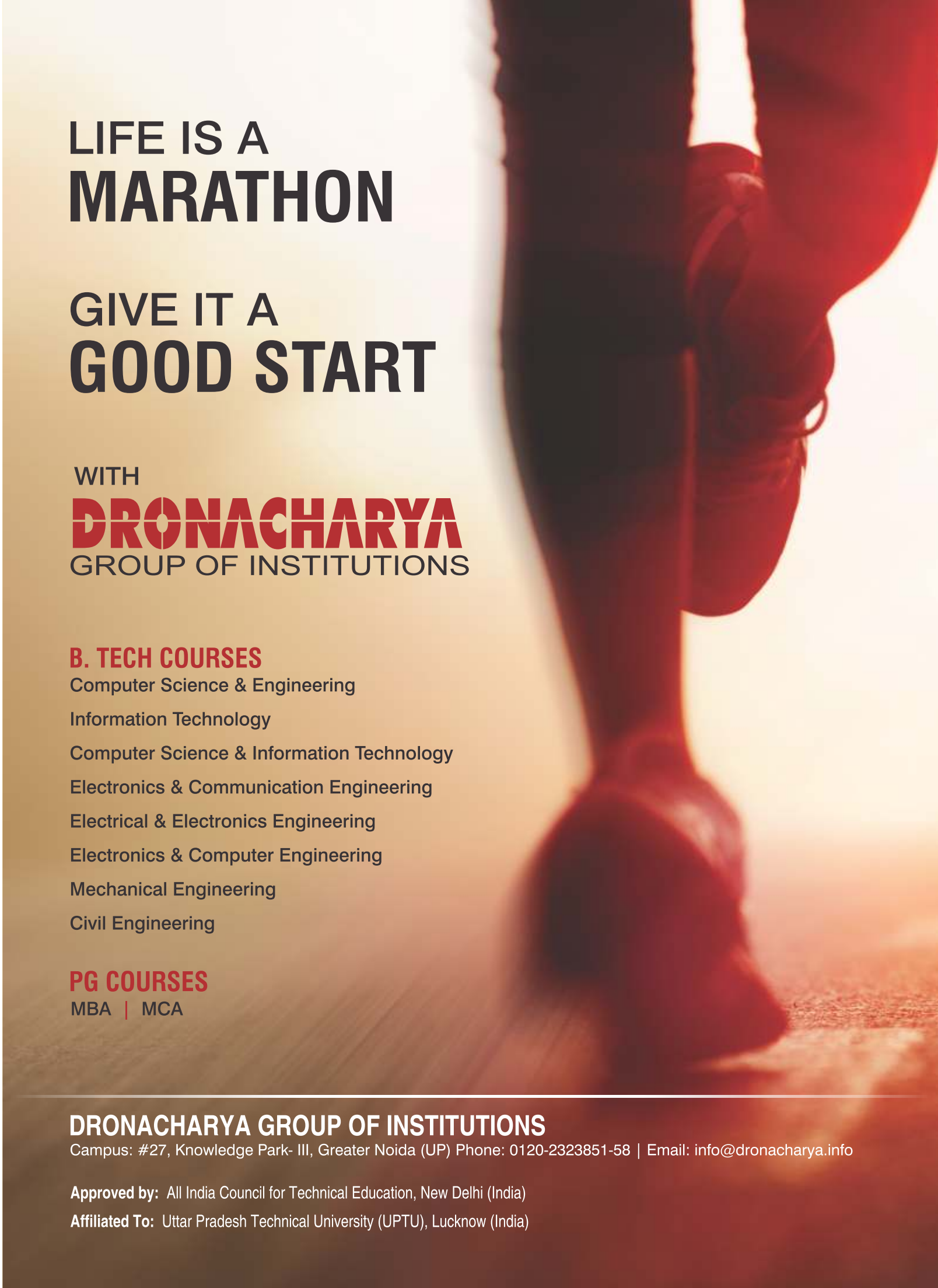
- **Keywords:** Include up to six keywords that describe your paper for indexing and for web searches. The more discriminating your keywords are, the greater is the likelihood that your article will be found and cited. (Font size 9, italics, left-justified).

- **Text:** (Font size 10, Justified). The paper must be divided into sections starting preferably with "Introduction" and ending with "Conclusion". The main sections should be numbered 1, 2, 3 etc and subsections as 2.1, 2.2 etc. Main headings should be typed in capitals, subheadings in lower case. Both types of heading should be underlined and left-justified. Footnotes should be avoided. Equations should be typewritten and with the equation number placed in parentheses at the right margin. Reference to the equation should use the form 'Eq. (3)'. Use extra line spacing between equations, illustrations, figures and tables. The use of SI units is strongly recommended

- **Tables and Figures**: Tables and Figures should be integrated with the text (and not sent separately at the end of the manuscript) and numbered consecutively in the order in which reference is made to them in the text of the paper. All captions must be centrally located above a Table and below a Figure (Font size 10). All tables and figures must be numbered consecutively in Arabic numerals (not Roman) (e.g., Table 3 or Fig. 3) in the order of appearance in the text. Tables & Figures should be reproduced in the exact format and at the exact place as desired to appear in the journal.

- **Conclusion:** A conclusion section must be included and should indicate clearly the advantages, limitations and possible applications of the paper. Authors may also discuss about the scope of future work.

- **Acknowledgements:** An acknowledgement section may be included after the 'Conclusion'.

- **References:** It is mandatory for references to be quoted in the text and be placed at the **end of the text.** They should be **numbered consecutively in order of their citation** in the text and be indicated by **superscripts** in the text of the manuscript. Examples of different citations as References are given below:

(i) **In case of referring to an Article in a Journal**

Kuebel, D.; Lahiri, M. & Wolf, E. *An Inverse Problem in the Theory of Stochastic*

Electromagnetic Beams, Opt. Commn., **282**, 2009, p.141.

(ii) **In case of referring to a Book/Monograph**
Rao, C.N.R. & Raveau, B. (Eds.). *Transition Metal Oxides*, Wiley-VCH, 2nd Edition, 1998, Ch. 2.

(iii) **In case of referring to a Conference Paper**
Ctvrtnickova, T.; Mateo, M; Yanez, A. & Nicolas, G. *Characterization of Coal Fly Ash Components by Laser-Induced Breakdown Spectroscopy*. Presented at the Fifth International Conf. on Laser-Induced Breakdown Spectroscopy, Berlin, Adlershof, Germany. Sep 22-26, 2008, CP-15, p. 67-68.

(iv) **In case of referring to a Report**
Marine, R.E. & Iliff, K.W. *Application of Parameter Estimation to Aircraft Stability and Control*. NASA, USA, 1986, Report No. NASA-RP-1168.

Papers quoting the LATEST references from the referred journals will be preferred for publication unless the original contribution from the author/s is of a very high standard.

UNDERTAKING

Authors must include, in the covering Email that their paper has not been published//accepted/submitted for publication/ presentation to any other journal/ book/conference in any form and the work submitted by them is their own and original. The same 'Undertaking' should also be attached, on a separate page, along with the manuscript. This ethical policy of the Journal will be strictly adhered to.

Note: Manuscripts not in conformity with these 'Guidelines' will not be forwarded to the experts for review.

IJESM SIGHTINGS

103 Different countries have visited this site

Others 10.9%
Taiwan 0.6%
Japan 0.6%
Spain 0.7%
Nigeria 0.7%
Pakistan 0.7%
Germany 0.7%
United Kingdom 0.8%
Malaysia 0.9%
Italy 1.0%
Iran 2.0%
China 2.0%
Brazil 4.9%

India 68.3%

United States 13.3%
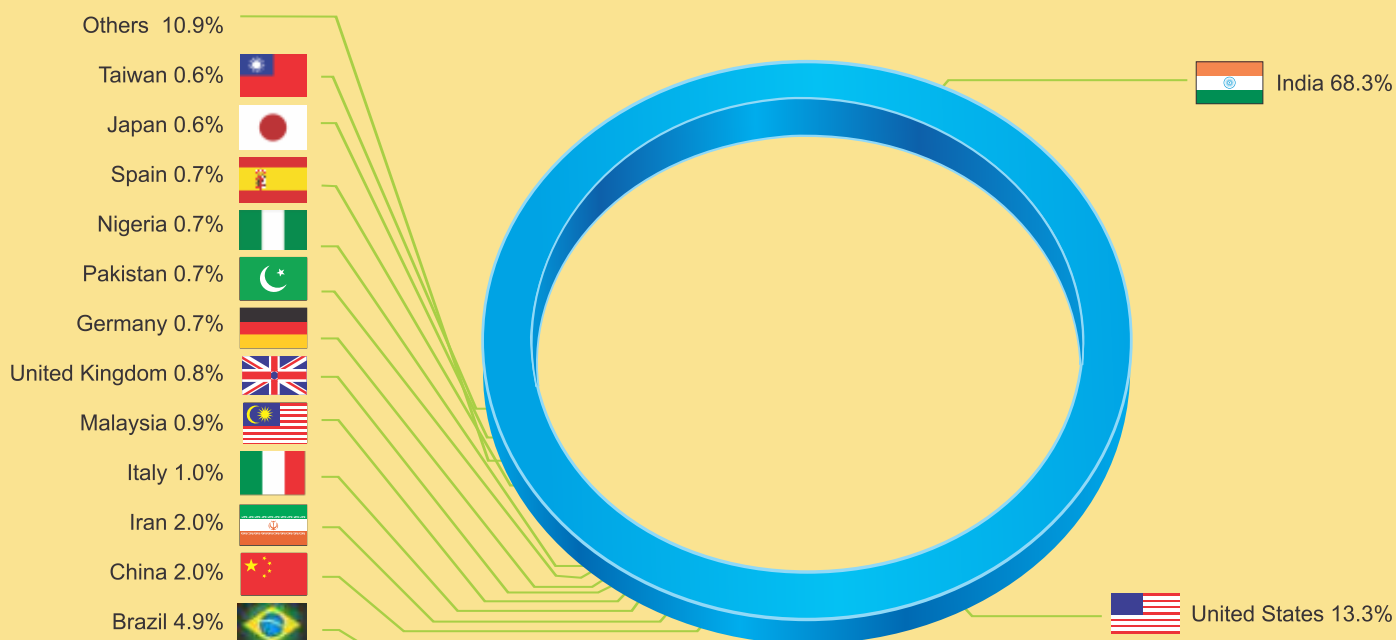
www.dronacharya.info

Approved by
All India Council for Technical Education, New Delhi (India)

Affiliated To:
Uttar Pradesh Technical University (UPTU), Lucknow (India)

Campus:
27, Knowledge Park-III, Greater Noida (U.P.) – 201308 (India)
Phone: 0120-2323854-58, Email: director@gnindia.dronacharya.info

Corporate Office:
76P, Part-III, Sector-5, Gurgaon, 122001, Haryana (India)
Phone: 0124-2251602, 2253144, Email: info@dronacharya.info